



**Preparation and Characterisation**  
**of**  
**Colour Converting Layers**  
**for**  
**OLEDs**

Thesis Presented for the Degree of Doctor of Philosophy

Andrea Mazzocut

Supervisors: Prof. Christopher S. Frampton and Dr. Paolo Coppo

# Table of Content

<b>LIST OF ABBREVIATIONS</b>	<b>1</b>
<b>ABSTRACT</b>	<b>3</b>
<b>CHAPTER 1 : INTRODUCTION</b>	<b>4</b>
1.1 The Light.Touch.Matters Project	4
1.2 Colour	4
1.3 Electroluminescence: the key principle of OLEDs	7
1.4 The structure of an OLED	8
1.5 Light generation in OLEDs	13
1.6 The colour of an OLED	14
1.7 AMOLEDs versus flexible and transparent OLEDs	16
1.8 Solutions to improve the range of colour in OLEDs	18
1.9 Colour converting layers (CCLs) for OLEDs	19
1.9.1 Luminescent materials for the fabrication of CCLs	24
1.9.1.1 Organic fluorescent molecules	24
1.9.1.2 Inorganic Phosphors	26
1.9.1.3 Quantum Dots	27
1.9.1.4 Nanodiamonds and other luminescent nanoparticles	28
1.10 Aim of the project	30
<b>CHAPTER 2 : MATERIALS AND METHODS</b>	<b>33</b>
<b>2.1 Materials</b>	<b>33</b>
2.1.1 Acrylic Coatings	33
2.1.2 Polyorganosiloxanes	35
2.1.3 Amorphous Silica	40
2.1.4 Faujasite Y	41
2.1.5 Organic fluorescent molecules	43
2.1.6 Ultra-fine Diamonds	49
<b>2.2 Techniques</b>	<b>58</b>
2.2.1 UV/Visible Spectroscopy	58
2.2.2 Fluorescence Spectroscopy	62
2.2.3 X-ray Powder Diffraction (XRPD)	65

2.2.4 Scanning Electron Microscopy (SEM)	69
2.2.5 Transmission Electron Microscopy (TEM)	71
2.2.6 Thermogravimetric analysis (TGA)	74
<b>CHAPTER 3 : ORGANIC FLUORESCENT MOLECULES IN POLYMERIC MATRICES</b>	<b>76</b>
<b>3.1 Introduction</b>	<b>76</b>
<b>3.2 Solid state CCLs</b>	<b>77</b>
3.2.1 Materials and Methods	77
3.2.2 Results	78
<b>3.3 Solution processed layers</b>	<b>80</b>
3.3.1 Materials and Methods	80
3.3.2 Results	81
<b>3.4 Discussion</b>	<b>89</b>
<b>3.5 Conclusions</b>	<b>90</b>
<b>CHAPTER 4 : FLUORESCENT SILICONE LAYERS</b>	<b>92</b>
<b>4.1 Introduction</b>	<b>92</b>
<b>4.2 Materials</b>	<b>94</b>
<b>4.3 Sample preparation</b>	<b>94</b>
<b>4.4 Results</b>	<b>95</b>
4.4.1 Rhodamine 6G	95
4.4.2 Fluorescein sodium salt	104
<b>4.5 Discussion</b>	<b>112</b>
<b>4.6 Conclusions</b>	<b>113</b>
<b>CHAPTER 5 : INVESTIGATION OF THE BLUE EMISSION OF FLUORESCENIN</b>	<b>114</b>
<b>5.1 Theories</b>	<b>114</b>
<b>5.2 Testing the theories</b>	<b>116</b>
5.2.1 Substitution of the hydrogen ions into zeolite	129
<b>5.3 Impregnation of HPTS into HY Zeolite</b>	<b>132</b>
<b>5.4 Recrystallisation of Fluorescein for single crystal analysis</b>	<b>136</b>
<b>5.5 Synthesis of large Faujasite-fluorescein crystals for single crystal X-ray diffraction</b>	<b>142</b>

5.5.1 Materials	143
5.5.2 Sample preparation	143
5.5.3 Results	143
<b>CHAPTER 6 : FLUORESCENT DIAMONDS</b>	<b>146</b>
<b>6.1 Introduction</b>	<b>146</b>
<b>6.2 Materials and methods</b>	<b>147</b>
6.2.1 Samples Preparation	147
6.2.2 Sample Irradiation	147
<b>6.3 Results</b>	<b>148</b>
6.3.1 Electron irradiated diamonds	148
6.3.2 Gamma irradiated diamonds	155
<b>6.4 Discussion</b>	<b>160</b>
<b>6.5 Conclusions</b>	<b>161</b>
<b>CHAPTER 7 : DISCUSSION</b>	<b>162</b>
<b>CHAPTER 8 : CONCLUSIONS</b>	<b>165</b>
<b>BIBLIOGRAPHY</b>	<b>167</b>

## List of Figures

Figure 1.1: Representation of the visible spectrum and table of the colours. ....	5
Figure 1.2: CIE 1931 chromaticity diagram. ....	7
Figure 1.3: Basic structure of an OLED. ....	8
Figure 1.4: Structure of a multi-layer OLED.....	9
Figure 1.5: Examples of small molecule and light-emitting polymer used in the fabrication of the emissive layer of OLEDs. ....	11
Figure 1.6: Schematic representation of the decay of an exciton. ....	13
Figure 1.7: Schematic representation of the HOMO-LUMO Band Gap. ....	15
Figure 1.8: The pixel and sub-pixel configuration in an AMOLED.....	17
Figure 1.9: The different approaches for the generation of new colour for OLEDs. (a) Deposition of multiple emitters following the RGB scheme; (b) Blue emitting OLED converted by application of colour converting layers.....	19
Figure 2.1: Chemical structure of methyl methacrylate and alkyl acrylate. ....	34
Figure 2.2: General chemical structure of polyorganosiloxane. ....	35
Figure 2.3; Reaction schemes to produce polyorganosiloxanes. ....	36
Figure 2.4: Chemical structure of dimethyldichlorosilane (a) and hexamethyldisiloxane (b). ....	37
Figure 2.5: Chemical structure of octamethylcyclotetrasiloxane. ....	37
Figure 2.6: Cross-linking reaction of silicone gum promote by peroxide radicals.....	38
Figure 2.7: Chemical structure of vinyl (a), phenyl (b) and nitrile (c) group. ....	38
Figure 2.8: Formation of silicil acid. ....	40
Figure 2.9: Schematic representation of the structure of zeolite. ....	42
Figure 2.10: Three dimensional structure of Faujasite. ....	43
Figure 2.11: Examples of fluorophores. ....	44

Figure 2.12: Chemical structure of Rhodamine 6G. ....	45
Figure 2.13: Chemical structure of fluorescein disodium salt. ....	46
Figure 2.14: Ionic forms of fluorescein. ....	48
Figure 2.15: Chemical structure of 8-Hydroxypyrene-1,3,6-Trisulfonic Acid Trisodium Salt (HPTS). ....	49
Figure 2.16: 3D representation of the diamond lattice. Grey spheres represent the carbon atoms. ....	50
Figure 2.17: Chemical structure of trinitrotoluene (left) and cyclotrimethyltrinitramine (right). ....	52
Figure 2.18: Schematic representation of the lattice of an impure diamond in presence of a defect. The black spheres represent the carbon atoms, the blue is the impurity and the light grey depicts the vacancy. ....	54
Figure 2.19: a) Schematic representation of a ZPL transition (Z), absorption sideband (AB) and emission sideband (CD). b) Energy of the ZPL and the sidebands. ....	55
Figure 2.20: Electron transition between the ground and excited state. ....	59
Figure 2.21: Absorption spectrum of Rhodamine 6G in water. ....	60
Figure 2.22: Schematic representation of a dual beam spectrophotometer. ....	61
Figure 2.23: Jablonski diagram showing the electronic transition related to the fluorescence phenomenon. ....	62
Figure 2.24: Optical design of a fluorimeter. ....	64
Figure 2.25: Mirror reflection illustration of an X-ray diffracted by crystal planes. ....	66
Figure 2.26: Schematic representation of a synchrotron ring. ....	69
Figure 2.27: Schematic diagram of a SEM. [50] ....	70
Figure 2.28: Schematic representation of a TEM microscope. [146] ....	72

Figure 3.1: Thermoplastic polymer discs containing 0.5% w/w of rhodamine 6G (from left to right: PMMA, PS and PC). .....	78
Figure 3.2: Pure emission of a green OLED at various voltages and the result obtained with the PC and PS layers. ....	79
Figure 3.3: Emission of rhodamine 6G dissolved in the acrylic varnish. ....	82
Figure 3.4: Emission of fluorescein sodium salt dispersed in the acrylic varnish. ....	83
Figure 3.5: Emission of pure blue OLED and the spectra obtain as a result of the down-conversion of the device with the fluorescein containing acrylic layers. ....	84
Figure 3.6: Down-conversion of a blue OLED with the acrylic layers containing rhodamine 6G. ....	85
Figure 3.7: Conversion of a blue OLED with the acrylic layers composed of fluorescein (middle) and rhodamine (right). ....	86
Figure 3.8: Emission spectra of a pure green OLED and the emission achieved by down-conversion with the rhodamine in the acrylic matrix. ....	87
Figure 3.9: Photographs of a pure green OLED (left) and the device down-converted with the 0.5% rhodamine layer. ....	87
Figure 3.10: Colour gradient effects on blue OLEDs achieved by brush painting the fluorescein (left) and rhodamine (right) acrylic layers. ....	88
Figure 3.11: MeLite by Pilotfish; luminescent headphone consisting of a green OLED down-converted with the acrylic-rhodamine coating. ....	89
Figure 4.1: Absorption of rhodamine encapsulated in silica gel and dispersed in silicone rubber versus the dye in ethanol solution. ....	96
Figure 4.2: Absorption spectra of rhodamine 6G in zeolite and silicone rubber versus a reference solution of dye in ethanol. ....	97

Figure 4.3: Normalised emission of rhodamine 6G absorbed in silica gel and embedded in silicone compared to the emission of the molecule in ethanol solution. ....	98
Figure 4.4: Normalised emission of rhodamine 6G in zeolite and silicone rubber versus the dye in ethanol solution.....	99
Figure 4.5: Emission spectra for a pristine blue OLED (black) and for the panel converted with the silicone layers containing rhodamine 6G.....	102
Figure 4.6: Photograph of pristine blue OLED (left) and converted by rhodamine containing silicone.....	103
Figure 4.7: Emission of the green OLEDs in pristine condition and the final emission achieved by using the rhodamine CCLs.....	104
Figure 4.8: Images of the pristine green OLED and the colour achieved by the addition of the layers with the 2% and 6% of supporting materials impregnated with rhodamine dispersed in silicone.....	104
Figure 4.9: Absorption spectra of fluorescein disodium salt impregnated in silica gel dispersed in silica versus the dye in ethanol solution. ....	105
Figure 4.10: Absorption spectra of fluorescein in ethanol, water and HY zeolite dispersed in silicone.....	106
Figure 4.11: Normalised emission of fluorescein disodium salt absorbed in silica gel and embedded in silicone compared to the emission of the molecule in ethanol solution. ....	107
Figure 4.12: Emission of fluorescein impregnated in HY zeolite against the molecule in solution of water and ethanol.....	108
Figure 4.13: Emission of blue OLEDs and the signal of the device converted with the fluorescein functionalised silicone layers. ....	111

Figure 4.14: Photo of the pristine emission of the blue OLEDs and the colours achieved converting the emission with the silicone layers composed by a 2% and 6% of fluorescein functionalised silica. ....	112
Figure 5.1: Chemical structures of the dianion form of fluorescein (left) and the cationic form (right) resulting from the dye's protonation.....	116
Figure 5.2: Absorption of fluorescein in HY zeolite with and without silicone against the dye in water or ethanol solution.....	117
Figure 5.3: Emission of fluorescein impregnated in zeolite before and after the dispersion in the silicone matrix against the dye in ethanol or water solution.....	118
Figure 5.4: Emission of the hybrid material (fluorescein-HY zeolite) dispersed in silicone over a period of 120 hours. ....	119
Figure 5.5: Thermogravimetric analysis of a pristine sample of HY zeolite and the aluminosilicate impregnated with fluorescein. ....	121
Figure 5.6: Emission of fluorescein in HY zeolite before (black) and after (red) the heat treatment at 50°C. ....	122
Figure 5.7: Emission spectra of fluorescein into HY zeolite without any treatment (black line), immediately after heating (red line) and one day after the thermal treatment (blue line). ....	123
Figure 5.8: Changes in the emission of the HY sample containing a 0.5% w/w of fluorescein within 18 hours after the thermal treatment.....	124
Figure 5.9: Intensity of the blue and green emissions of the sample HY_0.5F over the course of 18 from the thermal treatment. ....	125
Figure 5.10: XRD patterns of the pure Faujasite sample and the zeolite functionalised with 0.1, 0.5 and 1% w/w of fluorescein. ....	127
Figure 5.11: Shift in the position of the XRD peak as a consequence of the impregnation of the organic molecule in the zeolite. ....	128

Figure 5.12: 3D model of the zeolite supercage with the molecule of fluorescein. ....	129
Figure 5.13: Absorption spectra of the HY and NaY zeolite impregnated with fluorescein. ....	130
Figure 5.14: Emission spectra of the HY and NaY zeolite before and after the heat treatment. .....	131
Figure 5.15: Protonation of HPTS leading to the shift in the emission of the molecule. ....	133
Figure 5.16: Emission of HPTS in water solution and impregnated in Hy zeolite before and after the heat treatment.....	134
Figure 5.17: Emission of HPTS within a time-frame of 18 hours after the heat treatment. ..	135
Figure 5.18: Change in the intensity of the blue and green peaks during the 18 hours post the heat treatment.....	136
Figure 5.19: SEM micrograph of Faujasite zeolite.....	144
Figure 5.20: EXD analysis of a Faujasite crystal.....	145
Figure 6.1: SEM micrograph of the diamonds recovered from the polishing slurry. ....	149
Figure 6.2: Dark field TEM micrograph (left) and CL image (right) of TEM irradiated diamonds. ....	150
Figure 6.3: Cathodoluminescence spectrum of diamonds collected at the TEM. ....	151
Figure 6.4: UV-green region of the CL spectrum collected at the TEM. ....	153
Figure 6.5: CL emission from 560 to 860 nm of TEM irradiated diamonds. ....	154
Figure 6.6: EELS spectra of the diamonds recovered from the polishing slurry. The presence of nitrogen is confirmed by the small feature at 403 eV.....	155
Figure 6.7: XRD pattern of untreated and gamma treated diamonds. ....	156
Figure 6.8: Emission of pristine (black), low (red) and high (blue) dose irradiated diamonds upon excitation with UV light (365 nm).....	157
Figure 6.9: Emission of low (black) and high (red) dose irradiated diamonds upon excitation with blue light (480 nm). ....	159

Figure 6.10: Fluorescent microscopy images of diamonds excited by UV (left) and blue light (right). ..... 160

# List of Abbreviations

Alq <sub>3</sub>	Tris-(8-hydroxyquinoline) aluminium
AMOLED	Active Matrix Organic Light Emitting Device
AZO	Aluminium-doped Zinc Oxide
BSE	Back Scattered Electrons
CCD	Charge-Coupled Device
CCDC	Cambridge Crystallographic Data Centre
CCL	Colour Conversion Layer
CIE	Commission Internationale de l'Eclairage
CL	Cathodo Luminescence
CRI	Colour Rendering Index
CVD	Chemical Vapour Deposition
DCM	4-(dicyanomethylene)-2-methyl-6-(4-dime-thylaminostyryl)-4H-pyran
DPPO	3-(4-(diphenylamino)phenyl)-1-phenylprop-2-en-1-one
EDX	Energy Dispersive X-Ray analysis
EELS	Electron Energy Loss Spectroscopy
EL	Electroluminescence
ETL	Electron Transport Layer
FND	Fluorescent Nano Diamond
HIL	Hole Injection Layer
HOMO	Highest Occupied Molecular Orbital
HPHT	High Pressure High Temperature
HPTS	8-Hydroxypyrene-1,3,6-Trisulfonic Acid Trisodium Salt
HT	Heat-Treated
HTL	Hole Transport Layer
IR	Infra Red
ITO	Indium Tin Oxide
LED	Light Emitting Diode
LUMO	Lowest Unoccupied Molecular Orbital

LTM	Light.Touch.Matters
MEH-PPV	poly (2-methoxy-5-(2'-ethylhexoxy)-1,4-phenylene vinylene
ND	Nanodiamond
OLED	Organic Light Emitting Devices
OYSE	(N4,N410-bis-(4-tert-butyl-phenyl)-N4,N40-di-fluoranthen-3-yl- diphenylether-4,40-dia- mine
PC	Poly Carbonate
PDMS	Poly Dimethyl Siloxane
PL	Photoluminescence
PMMA	Poly Methyl Methacrylate
PMT	Photo Multiplier Tube
PS	Poly Styrene
PVAc	Poly Vinyl Acetate
QD	Quantum Dot
QY	Quantum Yield
RGB	Red Green Blue
SE	Secondary Electron
SEM	Scanning Electron Microscopy
SLS	Swiss Light Source
TCI	bis(2-hydroxyethyl) dimethylammonium chloride
TEA	triethanolamine
TEM	Transmission Electron Microscopy
TEOLED	Top Emitting Organic Light Emitting Devices
TFT	Thin Film Transistor
TGA	Thermogravimetric Analysis
UV	Ultraviolet
WOLED	White Organic Light Emitting Devices
XRPD	X-Ray Powder Diffraction
ZPL	Zero Phonon Line

# Abstract

In this work, three different classes of colour converting layers (CCLs) for the down-conversion of blue and green Organic Light Emitting Devices (OLEDs) have been developed. In Chapter 3, the dispersion of organic dyes into polymer matrices via solution processing and solid state methods is presented.

Application of hybrid organic-inorganic fluorescent particles, composed of organic fluorescent molecules absorbed into porous supporting materials, is discussed in Chapter 4. This solution allows for the dispersion of the organic molecule into an otherwise non-miscible polysiloxane matrix and resulted in the discovery of unusual optical properties of one of the organic dye (fluorescein disodium salt). This peculiar emission has been studied in more detail during Chapter 5.

In addition, the possible use of fluorescent nanodiamonds, produced by gamma radiation, as luminescent materials, has been investigated in Chapter 6.

# Chapter 1 : Introduction

## 1.1 The Light.Touch.Matters Project

Light.Touch.Matters (LTM) was a 7<sup>th</sup> Framework Programme project founded by the European Union which involved eight countries and a total of seventeen partners. During the project materials scientists and designers joined forces to develop new touch sensitive and luminescent smart products for healthcare and wellbeing based on the combination of flexible organic light emitting devices and piezo plastics materials.

To contain the cost of the final products and allow for the fabrication of thin, flexible and transparent prototypes, monochromatic OLEDs were selected as light sources. This type of organic light emitting devices present limitations due to their static appearance and the limited number of colour available.

The role of Brunel University within the LTM project, was to find solutions to these issues by developing colour conversion layers able to extend the range of colour of the OLEDs and create pleasant colour effects, without sacrifice the device's power efficiency or the physical characteristic of the final products.

## 1.2 Colour

From a physical point of view, a colour can be defined as electromagnetic radiation characterised by a specific interval of wavelengths. Such a definition made sense only after the work of Newton, Goethe and Young, which defined and characterised the six colours composing the visible spectrum as we know them today. (Figure 1.1) <sup>1</sup>

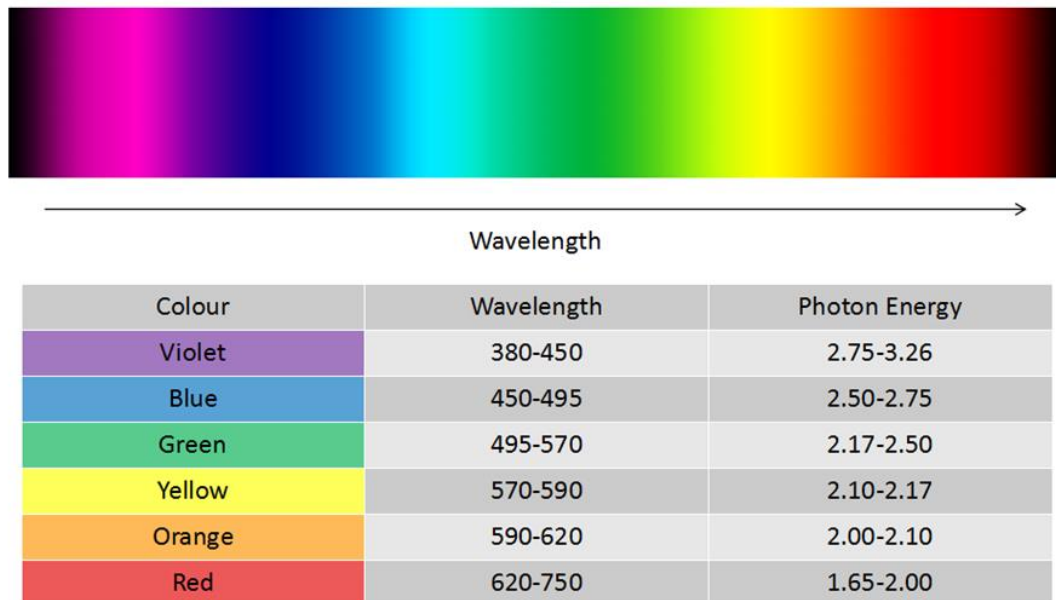


Figure 1.1: Representation of the visible spectrum and table of the colours.

In humans, the perception of colour is determined by photoreceptors, called cone cells, which are situated in the retina of the eye. <sup>2,3</sup> The human eye contains three types of cones which are sensitive to different ranges of wavelengths; these are named S, M and L in relation to their sensitivity to short (blue), medium (green) and long (red) wavelengths. S cone cells are lower in number than M and L cones and they are absent from the central fovea where the eye vision is optimal. In addition, the peak sensitivity and the absorption wavelengths of these photoreceptors are unevenly separated from each other with S cones presenting a maximum absorption at 420 nm whereas, M and L cones have their absorption maxima centred at 530 and 560 nm, respectively. These differences between the blue, green and red receptors are responsible for the higher sensitivity of the human eye to green and yellow colours. Such characteristics have been inherited by our primate ancestors who developed this ability to better distinguish the colour of the fruits from the foliage. <sup>2,3</sup> Perception of colour in humans is subjective from person to person, therefore, standard systems, called colour spaces were

developed to describe colours accurately. One of the most common standardisations currently used in display technology was created by the International Commission on Illumination (Commission internationale de l'éclairage, CIE) under the name CIE 1931. This colour scheme categorised colours based on the principle of chromaticity and luminance (or brightness). The CIE colour space diagram can be used to represent the chromaticity of a colour by use of two coordinate values, x and y (Figure 1.2). The x and y coordinates define the hue of the colour whereas the luminance is determined by a third parameter identified by the letter Y. <sup>4-6</sup>

The chromaticity diagram is often associated with a Planckian locus curve which represents the coordinates of the radiation emitted by an incandescence black body at different temperatures. <sup>5,6</sup> Another important parameter in colorimetry is the Colour Rendering Index, (CRI). The CRI is mainly used in lighting technology to measure the ability of a light source to reproduce a specific colour. CRI values of artificial light (fluorescent lamps, LEDs, OLEDs) are measured against an ideal light source, such as the black body radiation of the sun which is used as a reference for the colour white. If the two spectral outputs match perfectly, then the artificial light will have a CRI value of 100. <sup>6,7</sup>

Colours play a fundamental role in our life, they are used to indicate danger as well as the identity or the state of objects. The work presented in this thesis was completed as a part of the Light.Touch.Matters (LTM) project, (<http://www.light-touch-matters-project.eu/> Grant number: 310311 ) where colour and light manipulation are used to develop light emitting products for application in healthcare and well-being.

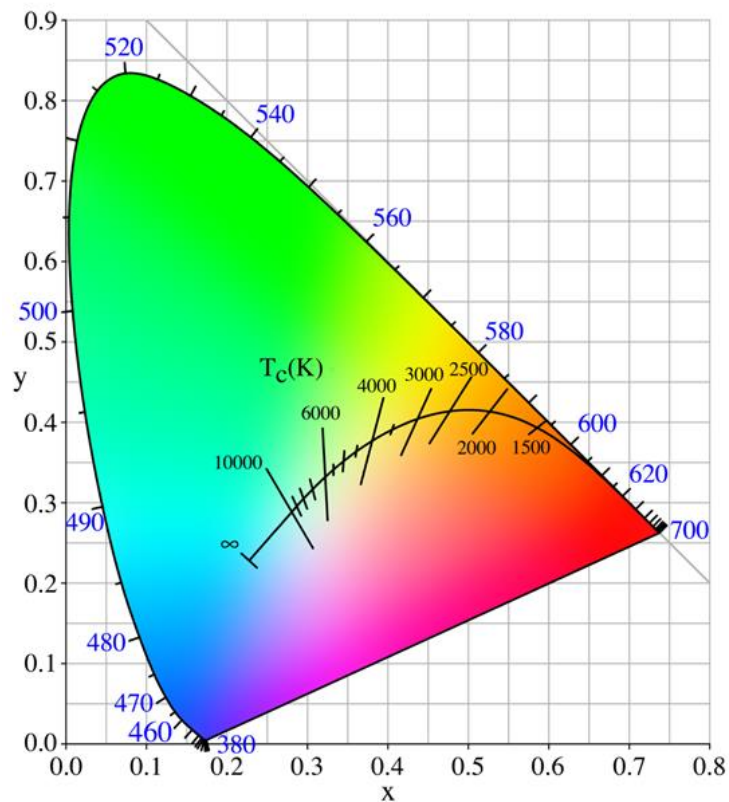


Figure 1.2: CIE 1931 chromaticity diagram.

### 1.3 Electroluminescence: the key principle of OLEDs

The phenomenon of electroluminescence (EL) can be defined as the direct transformation of an electrical signal into electromagnetic radiation (light), without involving any additional forms of energy. Electroluminescence is also referred as “cold emission” in order to differentiate it from its related counterpart which is incandescence.<sup>8,9</sup>

Electroluminescence was first reported, by Lossev in 1923<sup>10</sup>, and later by Destriau in 1936<sup>11</sup>.

During the course of their research, they discovered that certain inorganic materials were able

to emit light when an electrical current was applied to them. A similar observation in an organic compound was reported for the first time in 1953<sup>12</sup>, when a solution of acridine orange, upon stimulation with a high voltage electrical signal, was reported to emit light.<sup>5,13</sup> From a physical point of view, two different phenomena can lead to electroluminescence: the first is associated with the presence of accelerated electrons which are able to interact with the electroluminescent material. Such an interaction results in the promotion of the electrons of the electroluminescent compound to an excited state; these excited electrons will subsequently undergo relaxation falling back to the ground state and emitting the excess of energy in the form of photons. The second mechanism involves the recombination of subatomic particles; positively charged holes are paired with the negatively charged electrons leading to the formation of a high-energy state called exciton. This process is the principle on which Organic Light Emitting Devices (OLEDs) are based.<sup>5</sup>

## 1.4 The structure of an OLED

The basic structure of an OLED, generally called single layer OLED, is schematically represented in Figure 1.3. On a substrate, commonly made of glass or plastic, is deposited a stack of different functional layers. The stack consists of an emissive layer composed of an electroluminescent material sandwiched between two electrodes, an anode and a cathode.<sup>5,14,15</sup>

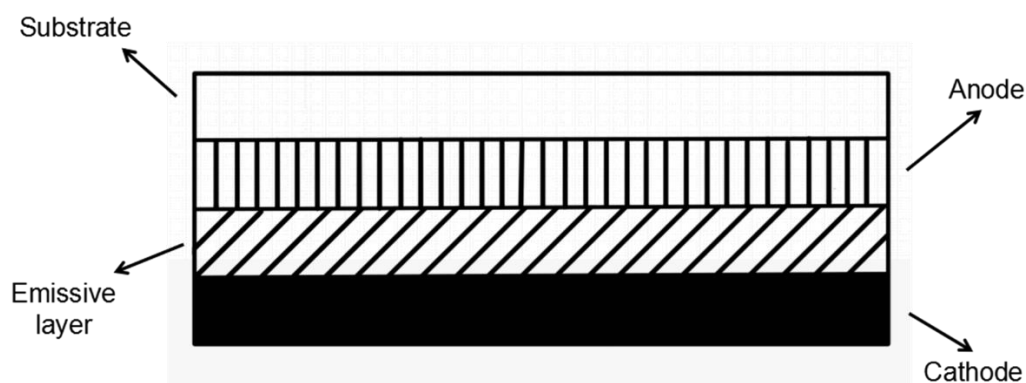


Figure 1.3: Basic structure of an OLED.

In virtue of their simple design, single-layer OLEDs are easy and inexpensive to produce, however, these advantages are counterbalanced by some limitations. In order for the electroluminescence phenomenon to be efficient, the electron-hole recombination has to occur within the emissive layer, therefore it is essential that the electroluminescent material possesses good carrier transport properties. This additional requirement limits the choice of materials that can be used during the device fabrication.<sup>14</sup> One solution is to adopt a more complex configuration, a multi-layer OLED, where dedicated layers for the charge transport are added to the OLED stack (Figure 1.4).<sup>5,14</sup>

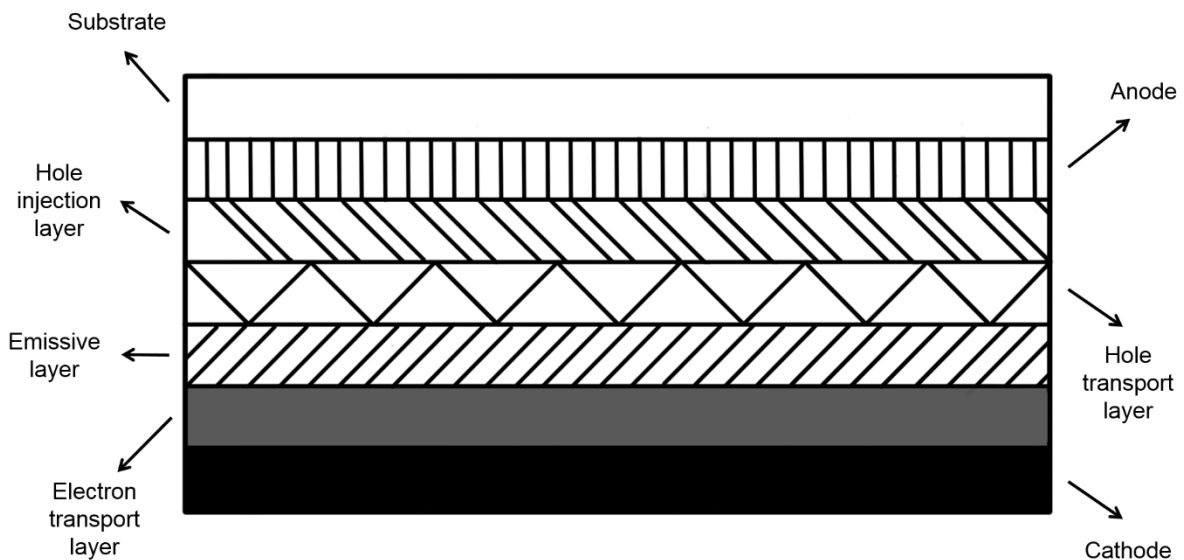


Figure 1.4: Structure of a multi-layer OLED.

The main components of a multi-layer OLED are:

- **The cathode:** the cathode is responsible for the injection of electrons. Generally reflective, except for transparent OLEDs, the cathode is made of metal alloys such as magnesium-silver or lithium-aluminium. Key requirements for the cathode are: high conductivity, low work function, suitable film forming properties and excellent stability.<sup>15,16</sup>

- **The electron transport layer (ETL):** is responsible for the transportation of electrons from the cathode to the emissive layer. The electron transport layer needs to possess a suitable work function, and a band gap wider than the band gap of the emissive layer, in order to facilitate the charge transportation, and simultaneously, block the migration of holes. In addition, the material used for the ETL needs to be transparent to permit the back-emitted light generated by the emissive layer, to be reflected by the cathode. Good film properties and compatibility with the cathode in terms of processing methods are also required.<sup>5,17</sup> Oxadiazole molecules and polymers, such as 2-(4-biphenyl)-5-(4-tert-butylphenyl)-1,3,4-oxadiazole, are the most common materials used as ETL in OLEDs.<sup>18</sup>
- **The emissive layer:** together with the anode and the cathode, the emissive layer is fundamental for the fabrication of an OLED. It is responsible for the light emission and is composed of an electroluminescent material with emission in the visible range of the electromagnetic spectrum. The most common electroluminescent materials used in OLEDs are small molecules or polymers, examples of which are shown in Figure 1.5. In the case of small molecules, the emissive layer is often combined with a charge transport material to facilitate the carrier mobility, and thus promote the encounter of electrons and holes leading to the formation of excitons. The materials used for the fabrication of the emissive layer have to possess elevated optical and chemical stability to produce long-lasting devices with high conversion efficiency of the excitons into photons, and excellent film-forming properties to ensure a uniform emission of light.<sup>17</sup>

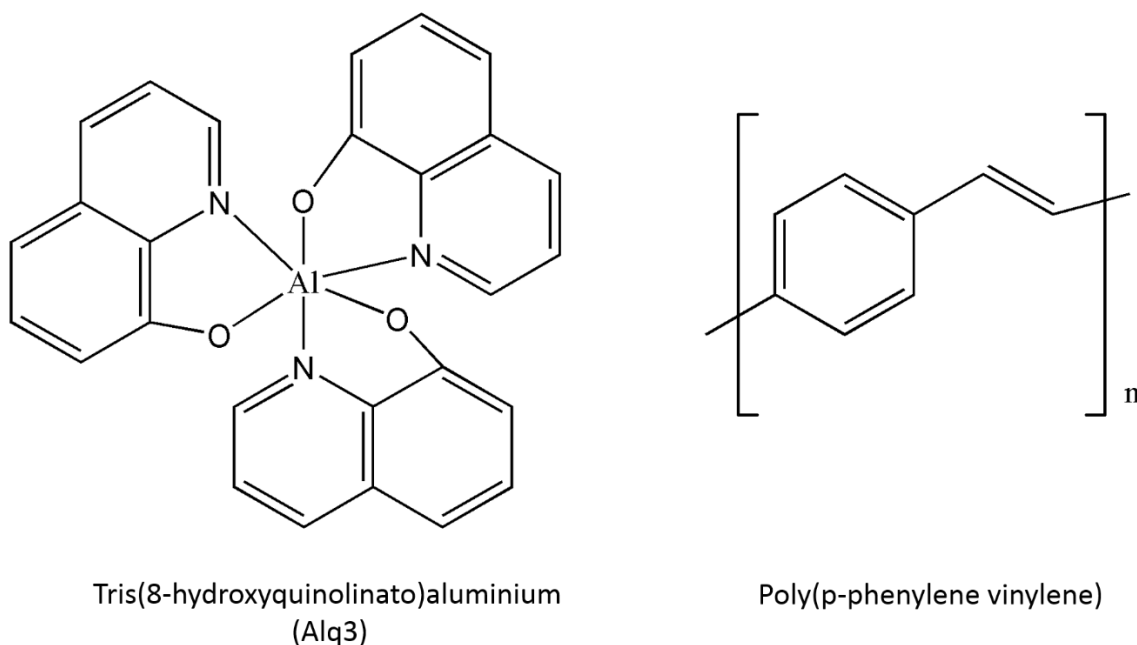


Figure 1.5: Examples of small molecule and light-emitting polymer used in the fabrication of the emissive layer of OLEDs.

- **The hole transport layer (HTL):** is used to transport holes into the emissive layer. These materials have to possess high mobility for the holes and also a wider band gap than the emissive layer. High transparency is fundamental for the hole transport layer to prevent any dissipation of the light emitted by the device.<sup>5,17</sup> One of the first and most common materials used for the hole transport layer is 4,4'-cyclohexylidenebis[N,N-bis(4-methylphenyl)benzenamine] (TAPC).
- **The hole injection layer (HIL):** is responsible for directing holes from the anode toward the EL. High mobility for holes and electron-blocking properties are mandatory for the materials used as hole injector along with elevated transparency.<sup>14</sup>
- **The anode:** is responsible for the injection of the holes into the device. High transparency is required to allow the transmission of light. Indium Tin Oxide (ITO) is the most common material for the production of the anode in virtue of its good semi-conductive properties, chemical stability, easy deposition and high transparency.<sup>5,14,17</sup> In recent years, due to the shortage in indium, alternatives such as aluminium-doped

zinc oxide (AZO), or thin metal films of gold, silver and nickel, have been developed.

<sup>17</sup> Moreover, ITO is not suitable for the next generation of flexible OLEDs due to the high temperature needed for its deposition which is not compatible with the plastic substrate of flexible OLEDs. <sup>17</sup>

The production of an OLED can be described as a top-to-bottom procedure, where the glass or plastic film at the top of the device is used as a substrate for the deposition of the subsequent layers.

Particular attention is required for the deposition of the emissive layer, this can be performed with different techniques. For OLEDs used in screens, ink jet printing is the most suitable process for the deposition of the emissive layers; this method allows for the production of devices with high resolution as a result of the small pitch size. However, such an approach presents limitations in terms of OLEDs' size and increase the cost of the final product.

Deposition by spin coating is generally used for research purposes since the technique is inexpensive and allows for easy application. The results obtained by this method, however, are poor and the device size is strongly limited. Dip coating is able to provide high homogeneity of the film, but the production time required is not compatible for large scale applications, and further cleaning procedures are needed to remove the excess material. The most common method of manufacture is screen printing which allows for the production of large devices in a reasonable time. One drawback of this method is the presence of creep, which has been observed as a result of the high dilution required by the technique. For small molecules, the thermal evaporation method represents the best technique, it ensures for excellent homogeneity, and allows for the deposition of multiple layers, but requires the use of vacuum equipment with high running and maintenance costs. <sup>19</sup>

## 1.5 Light generation in OLEDs

As previously discussed the light output from Organic Light Emitting Device (OLED) is generated by the electron-hole recombination phenomena. When a current is applied to the device, electrons and holes are injected into the system *via* the cathode and anode. As a consequence of the potential difference between the electrodes and the conductive properties of the materials used to fabricate the OLED, these subatomic particles are able to migrate through the device and recombine within the emissive layer, where they generate excitons.<sup>5,20</sup> Excitons can occur in different spin configurations, one with an anti-parallel orientation and three with parallel spin, resulting in a 25 % probability of singlet states and a 75 % probability of triplet state. The excess energy carried by the excited singlet and triplet states can be liberated via two distinct processes called fluorescence and phosphorescence (Figure 1.6).<sup>20,21</sup>

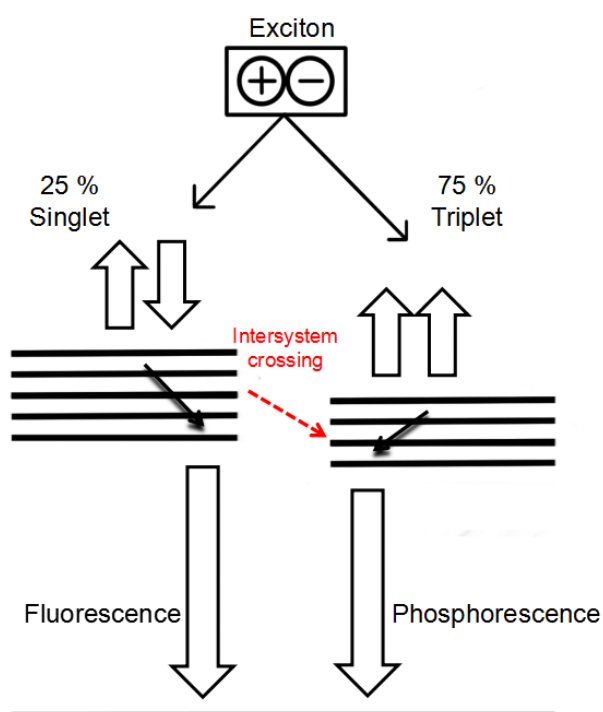


Figure 1.6: Schematic representation of the decay of an exciton.

The 3:1 ratio between the triplet and singlet excited states resulting from the electron-hole recombination is a primary factor for the choice of the electroluminescent materials used in the emission layer of the OLEDs. In order to achieve the maximum energy efficiency both the singlet and triplet states need to be converted into photons; this is generally realised by mixing different emitters in the emissive layer of the device. Luminescent materials, able to undergo fluorescence, are used to convert the singlet state formed by the excitons into photons as a result of the radiative decay from the excited state  $S_1$  to the ground state  $S_0$ , whereas phosphorescent species generate light from the triplet states as a consequence of the  $T_1-S_0$  transition.<sup>5</sup> Another possibility to efficiently convert all the excited states generated by the excitons into photons, involves the use of phosphorescent metal complexes, which as a result of their photo-physical properties, are able to achieve an intersystem crossing transfer (*i.e.* the transformation of the singlet states into triplet states) with an efficiency of nearly 100%, converting both the singlet and triplets into photons.<sup>20-22</sup>

## 1.6 The colour of an OLED

The colour of the light generated by an OLED is determined by the energy emitted as a result of the relaxation of the excitons. Such energy is liberated by the decay of the exciton in the form of photons, which have frequencies equal to the band gap of the electroluminescent species used in the emissive layer, *i.e.* the energy difference between the highest occupied molecular orbital (HOMO), and the lowest unoccupied molecular orbital (LUMO) of the emitter (Figure 1.7).<sup>5,15</sup>

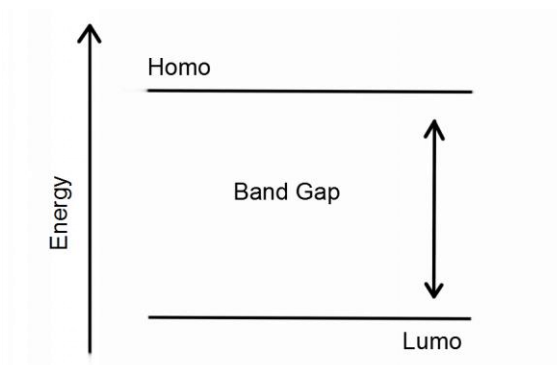


Figure 1.7: Schematic representation of the HOMO-LUMO Band Gap.

The correlation between the photo-physical properties of the emitter and the output colour of OLEDs introduce limitations in terms of the device appearance. Indeed, not all the species that are able to exhibit electroluminescence, possess the suitable physico-chemical properties that are required to be used in OLEDs. An ideal electroluminescent compound should demonstrate:

- Good chemical stability, particularly important for obtaining long lasting and reliable devices.
- Good semiconductor properties to facilitate the charge carrier flow, and enhance the recombination of the electrons and holes, leading to the formation of the excitons.
- Elevated quantum efficiency, *i.e.* the energy of the excitons needs to be fully converted into visible photons, and not dissipated in non-radiative decay such as heat.
- Good film forming properties and easy deposition techniques to allow the production of uniform layers, which will ensure a homogeneous emission of light.

As a result of the requirements listed above, the choice of electroluminescent materials, and consequently, the final colour of the device is limited. In recent years, a large number of researchers have devoted their attention to solve the issue of colour. New classes of emitters and alternative solutions have been developed, in order to extend the colour range of OLEDs, and in particular, to obtain the perfect white light that can mimic the spectra of the sun. These approaches will be discussed in more detail in section 1.8 of this thesis.

## 1.7 AMOLEDs versus flexible and transparent OLEDs

Although OLED technology has been known for years, only recently, have they found applications in day-to-day products, particularly in high-end displays for television, smartphones, tablets and cameras.<sup>23</sup> The reasons for the increasing popularity of OLEDs are related to the recent improvements in their stability, light efficiency and production costs, which along with the possibilities to create thin and flexible devices, allow for the development of new and innovative products. The advantages of using OLEDs include the possibility to produce devices with high brightness and contrast, fast response time and outstanding reliability in the reproduction of colours resulting from the absence of back-light illumination. OLEDs, moreover, are able to achieve an elevated energy efficiency as a consequence of their low level of energy dissipation in the form of heat and other non-radiative processes. This plays an important role in the battery life of portable products and will have high impact in the worldwide energy consumption. It has been calculated that as a result of the application of OLEDs as artificial light sources, the consumption of electricity could be cut by 62%.<sup>14,23</sup>

OLEDs used in display technology need to be able to change the output colour dynamically. As explained in section 1.6, however, the light emission of an OLED is generated by an electroluminescent material, and its colour is strictly related to the band gap between the excited state and the ground state. As a consequence, the spectral characteristics of conventional OLEDs are well defined and cannot be tuned easily. There is, nevertheless, a solution and it is represented by the combination of multiple emitters, red, green and blue, coupled with what is called an active matrix, hence the name Active Matrix OLEDs (AMOLEDs). The active matrix, composed of a thin-film-transistor (TFT) array, is responsible for the luminescence intensity of each red, green and blue sub-pixel, by varying the voltage applied to them. As a result of that, this system allows for the production of an RGB matrix,

where each pixel can be dynamically tuned to obtain an infinite number of colours (Figure 1.8).<sup>5</sup>

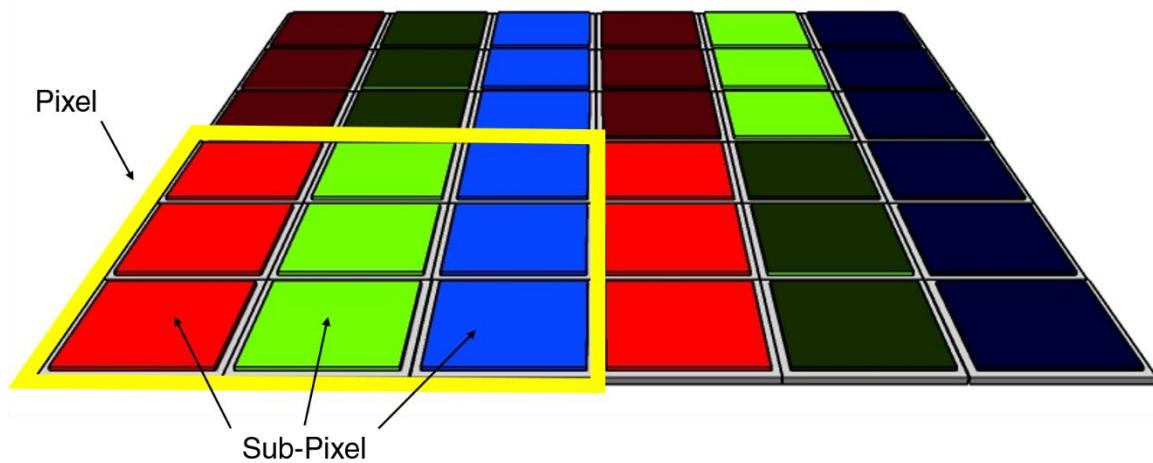


Figure 1.8: The pixel and sub-pixel configuration in an AMOLED.

The advantages of AMOLEDs, over conventional OLEDs, particularly in terms of colour capability are, however, counterbalanced by some drawbacks. These include the need for additional components such as the thin-film transistor (TFT) substrate (or backplane substrate), the driver integrated circuit, and for certain applications, a circular polariser. All these have a negative effect on the cost and complexity of the device restricting the use of these light panels to screens for high-end applications.<sup>5</sup> Furthermore, the supplementary components required to fabricate the active matrix introduce some limitations concerning the physical and mechanical properties of these luminescent devices. AMOLEDs, with both transparent and flexible properties, have not yet reached the market, and only recently, new materials with flexible or transparent characteristics have been developed to replace the components inside AMOLEDs.<sup>24-26</sup> Conventional OLEDs with high flexibility and transparency are currently available and their level of refinement (light stability, brightness and efficiency) allows for their use in common applications such as lighting and signage. These new class of emitting devices provide

designers with flat, transparent and flexible light sources, which can be easily modelled or embedded within other matrices, such as textiles, maintaining, in addition, high portability in virtue of their low power consumption and weight.

## **1.8 Solutions to improve the range of colour in OLEDs**

In recent years, various solutions to widen the range of colours available for OLEDs have been suggested. Novel emitters with the right physico-chemical properties and photo-physical characteristics, tailored to cover the gaps in the electromagnetic spectrum, were developed by several groups<sup>27-30</sup>, but this solution was soon abandoned, owing to difficulties in the design and development of electroluminescent species suitable for the OLEDs, and the attention was only focused on important colours such as blue, red, green and yellow. A more practical approach to overcome the colour limitation of conventional OLEDs has been found in the combination of existing emitters (Figure 1.9 a). Following the same principle used by the sub-pixel matrix in AMOLEDs, electroluminescent compounds with red, blue and green emission are combined within the same layer or are deposited in a stack configuration. By varying the amount of each primary colour, it is possible to fine tune the emission of the device, obtaining an infinite amount of tints able to cover the entire visible spectrum.<sup>15</sup> The multiple emitter approach provides a solution to the limited number of colours of OLEDs, but it again presents some major drawbacks that need to be addressed: the combination of various electroluminescent materials can result in devices that change their appearance overtime as a consequence of significant variations in the emitters efficiency due to the different ageing processes of the individual compounds. Colour shifting phenomena, as a consequence of the variation of the voltage applied to the OLED, have also been reported as a common problem in these devices. This is due to the discrepancies in the response of the various materials to

different currents. Moreover, the use of multiple emitters increases the production costs of the devices significantly since, deposition of multiple layers or the need of masking techniques and cleaning processes between different batches, are required. <sup>14,31–33</sup>

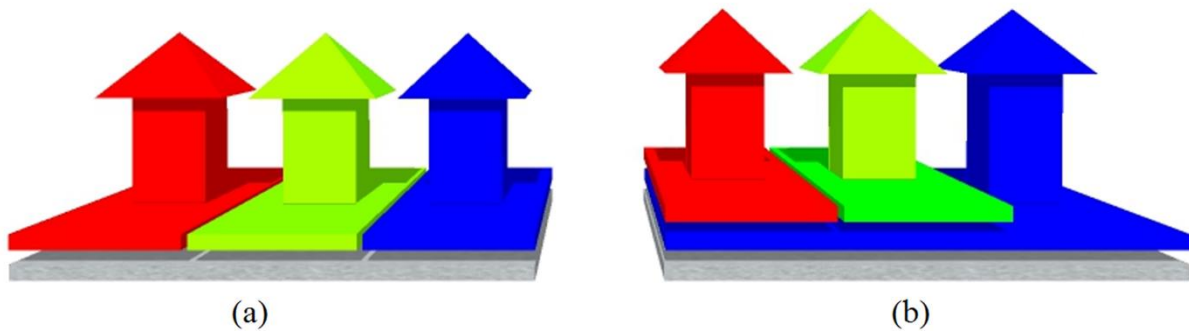


Figure 1.9: The different approaches for the generation of new colours for OLEDs. (a) Deposition of multiple emitters following the RGB scheme; (b) Blue emitting OLED converted by application of colour converting layers.

An alternative solution, aimed to widen the spectral response of OLEDs, is represented by the application of specific layers, commonly defined as Colour Converting Layers (CCLs), where luminescent species, which are able to down-convert the emission of the OLED panel, are used to fine tune the light output of a single emitter OLED (Figure 1.9 b). <sup>34</sup>

## 1.9 Colour converting layers (CCLs) for OLEDs

The approach represented by the use of colour converting layers for OLEDs can be compared to the application of phosphor colour converters widely used in inorganic light emitting diodes (LEDs). However, contrary to the phosphors in the LEDs, the number of articles, reported in the literature, concerning the development of CCLs for OLEDs is limited. This can be ascribed to the relatively recent appearance of OLEDs on the market, and the lack of standardisation in terms of electroluminescent species used for their fabrication, which consequently, results in the diverse emission characteristics discussed above.

Colour converting layers for OLEDs are based on the principle of photoluminescence, where luminescent materials are used to down-convert the light generated by the device *via* an absorption/emission mechanism regulated by the excitation/relaxation of electrons. These down-converting species can be embedded within the structure of the OLED (internal conversion) or applied as an external layer deposited on the device's substrate (external conversion).<sup>34</sup> The use of CCLs in OLEDs is mainly related to the fabrication of devices able to emit white light (WOLEDs). The fabrication of WOLEDs is generally achieved by functionalisation of a blue emitting OLED with a complementary down-converting material (*i.e.* yellow), or by the addition of green and red luminescent species, which combined with the residual blue emission of the OLED, leads to a white appearance.

Duggal and co-workers<sup>31</sup> were the first to report the successful application of an external colour converting layer to an OLED for the production of a white light emitting device, WOLED. In their work, the blue light originating from polymer-based OLED was down-converted to white by application of two separate colour converting layers. These CCLs were produced by a dispersion of organic dyes, namely lumogen F orange and lumogen F red, into a poly (methylmethacrylate) matrix, and a suspension of a yellow emitting inorganic phosphor, (Y(Gd)AG:Ce), into a polysiloxane matrix. The down converting layers were subsequently stacked on top of the glass substrate of the OLED using optical laminating tape. Their research resulted in a low conversion efficiency (1.3%), but, nonetheless, the approach attracted the interest of the scientific community. As a consequence of the simplicity of the method and the low cost involved, an increasing number of papers focused on the fabrication of CCLs for OLEDs were published. A summary of the most relevant publication in the field is shown in Table 1. This table has been redacted selecting the most innovative, original and interesting works which contribute to the development of materials for the downconversion of OLEDs.

Table 1: List of articles published in the literature concerning the colour conversion of OLEDs.

Authors (year)	Description
Swanson <i>et al.</i> <sup>34</sup> (2003)	Blue OLED downconverted with green and red organic dyes dispersed in poly(dimethylsiloxane) (PDMS) by solvent-assisted dissolution. Two novel derivatives of coumarin and benzophenxanone were specifically developed.
Li <i>et al.</i> <sup>35</sup> (2006)	Perylene based molecules (yellow, orange and red) used as a downconversion material to obtain with light from a blue emitting [tris-(8-hydroxyquinoline) aluminium] (Alq <sub>3</sub> ) OLED. The molecules were dispersed into silicone to produce lens-shaped layers in order to improve their conversion efficiency.
Krummacher <i>et al.</i> <sup>36</sup> (2008)	Yellow emitting nitridosilicate phosphor ([Sr,Ba,Ca] <sub>2</sub> Si <sub>5</sub> N <sub>8</sub> :Eu <sup>2+</sup> ) was dispersed in a silicone matrix to produce CCLs for the conversion of a blue phosphorescence-based OLED. White emission was achieved by combination of the blue light with the yellow light converted by the phosphor.
Li <i>et al.</i> <sup>17</sup> (2007)	A white emitting OLED was fabricated using the internal conversion. An aromatic red fluorescent material (P1) was deposited by vacuum on the hole injection layer of a blue-green emitting OLED.
Ji and co-workers <sup>37</sup> (2008)	Blue-yellow combination was used to obtain white emission form a top-emitting OLED (TEOLED). The yellow phosphor, 3-(4-(diphenylamino)phenyl)-1-phenylprop-2-en-1-one (DPPO), has been deposited on the external surface of the cathode by vacuum deposition.
Qi <i>et al.</i> <sup>38</sup> (2010)	A fluorescent-based blue OLED was converted into white by application of a red emitting polymer, poly (2-methoxy-5-(2'-ethylhexoxy)-1,4-phenylene vinylene (MEH-PPV). The polymer was spin coated on the ITO substrate; varying the amount of polymer they were able to fine tune the emission of the OLED and obtain the desired CIE coordinates.

<p>Bera <i>et al.</i><sup>39</sup> (2011)</p>	<p>Focus their attention on the optimisation of the CCLs for blue OLEDs. Yellow and red emitting phosphors were dispersed into silicone and poly (methyl methacrylate) matrices. They investigated the influence of the thickness of the layer, the nature of the matrix and the concentration of the luminescent species. A white OLED with a CRI index greater than 80 was produced by downconversion with a layer consisting of 30 mg of 2:1 ratio of red:yellow phosphors dispersed in 150 mg of silicone.</p>
<p>Kumar <i>et al.</i><sup>18</sup> (2011)</p>	<p>A blue emitting OLED was converted in to white using a yellow-emitting phosphor dispersed into poly (vinyl acetate) (PVAc). The layer was applied on the glass substrate by spin coating. In the process, they reported an enhancement of 60% in light extraction efficiency as a result of the light scattering produced by the phosphor's particles.</p>
<p>Gohri <i>et al.</i><sup>40</sup> (2011)</p>	<p>An hetero-system composed of a deep red emitter (4-dicyanomethylene-2-methyl-6-p-dimethylamino-2-styryl-4H-pyran (DCM)) and a yellow fluorescent dye (N4,N410-bis-(4-tert-butylphenyl)-N4,N40-di-fluoranthren-3-yl-diphenylether-4,40-diamine (OYSE)) was used to convert a blue emitting OLED into a white. The combined used of two luminescent species into the CLLs improved the light coordinates of the final colour as a result of the broad emission of the layer.</p>
<p>Lee and co-worker<sup>41</sup> (2011)</p>	<p>A microcavity structure, composed of alternate layers of SiO<sub>2</sub> and TiO<sub>2</sub> was used to tune the emission of a blue OLED to better match the absorption of the phosphors used in the down-conversion layer. The microcavity also acted as a waveguide to increase the out-coupling efficiency of the device. The CCL was produced by the combination of a yellow and red phosphor (2:1 ratio) dispersed into a silicone matrix.</p>
<p>Ahn <i>et al.</i><sup>42</sup> (2011)</p>	<p>A blue emitting OLED was converted into white by using the RGB approach. A 1:1 ratio of green (Zn<sub>2</sub>SiO<sub>4</sub>:Mn) and red</p>

	(CaAl <sub>12</sub> O <sub>19</sub> :Mn) phosphors were printed directly on the substrate of the device.
Ho <i>et al.</i> <sup>43</sup> (2012)	A light extraction system composed of latex nanospheres (polystyrene nanoparticles) was embedded into the CLLs to convert a blue OLED into white. The nanospheres were deposited by spin coating on the polycarbonate substrate of the device and coated with a red downconverting material (MEH-PPV). The presence of the nanosphere was reported to increase the conversion efficiency of the CCL by 137%.
Koh and co-workers <sup>44</sup> (2012)	CCLs with micro-lenses array were fabricated to enhance the downconversion efficiency. A phosphorescence-based blue OLED was converted into white following the RGB scheme. Green and red phosphors (2:1 ratio) were dispersed into silicone. The silicone was moulded in micro-lenses which were applied on the OLED substrate with an index matching fluid. The CCLs were reported to enhance the external quantum efficiency by 50%.
Kwon <i>et al.</i> <sup>45</sup> (2013)	Red emitting quantum dots (QDs) were used for the first time in a CCLs. The QDs (CdSe/ZnS) were mixed with a yellow phosphor (YAG:Ce) and dispersed into a poly (methyl methacrylate) matrix. The CCLs were used to convert a blue emitting OLED into white. The WOLED showed remarkable colour stability with only minor changes in the CIE coordinates as a consequence of changes in the applied voltage.
Lee <i>et al.</i> <sup>46</sup> (2015)	An organic CCL, composed of Alq <sub>3</sub> doped with a 2 wt% of 4-(dicyanomethylene)-2-methyl-6-(4-dimethylaminostyryl)-4H-pyran (DCM), was used to convert the blue light emitted by a transparent OLED. The CCL was applied only on one side of the device, allowing for the production of a double coloured OLED, with one face emitting blue light and the other emitting white light.

## 1.9.1 Luminescent materials for the fabrication of CCLs

In principle, all materials able to exhibit photoluminescence (PL), within the visible range, can be used in the production of colour conversion layers. However, in order for the down-conversion process to be efficient and produce good results, the down-converting material has to fulfil certain requirements in terms of optical and chemical properties. The first thing to consider for the selection of the luminescent species is a suitable absorption-emission pair. It is essential for the luminescent material to possess an excitation spectrum that will match the emission of the OLED, in order to capture the photons emitted by the device. At the same time, it is required that the emission of the down-converting material meets the requirement for the final colour. Fundamental for the choice of the photoluminescent material is also the quantum efficiency, (*quantum yield*), this quantity, defined by the number of photons emitted divided by the number of photons absorbed, need to be as close as possible to unity to ensure an efficient down-conversion. Finally, chemical and optical stability are required to ensure the production of long-lasting layers and prevent any losses in conversion as a result of bleaching or degradation processes. The luminescent materials for the production of CCLs can be categorised in different classes: small organic molecules, light emitting polymers, phosphors, quantum dots or nanodiamonds and other luminescent nanoparticles.

### 1.9.1.1 Organic fluorescent molecules

Organic molecules which are able to exhibit photoluminescence are widely used as probes in biological applications, as dyes in textile manufacture, as solar collectors in the photovoltaic industry, and for sensing or imaging probes in analytical tools.<sup>4,47</sup> As a consequence of their multiple uses, organic fluorescent molecules have attracted the interest of the scientific community leading to the development of hundreds of different compounds. Such widespread

popularity, resulted in the production of luminescent species with various absorption and emission pairs able to cover the entire electromagnetic spectrum from the ultraviolet (UV) to the infrared (IR).<sup>47,48</sup> These luminescent materials are generally characterised by broad absorption and emission spectra, moreover, they possess elevated quantum yield and absence of blinking phenomena (*i.e.* intermittent luminescence). These advantages are, however, counterbalanced by a relative poor optical and chemical stability, which might lead to photodegradation processes such as bleaching.<sup>4</sup>

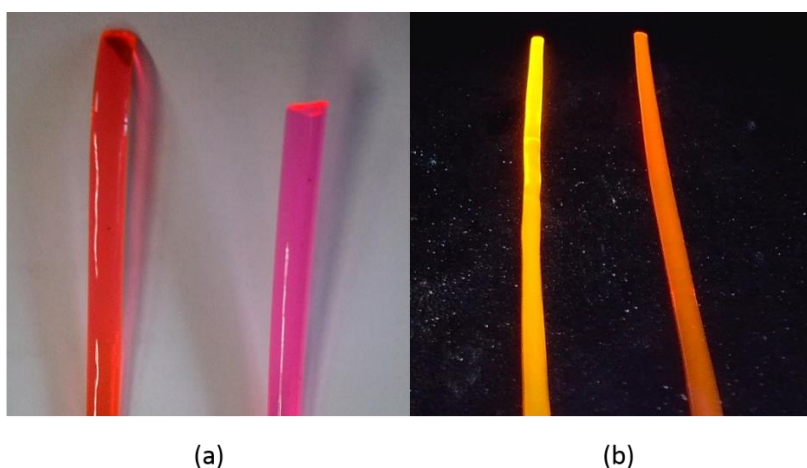


Figure 1.10: Polymers ribbon containing rhodamine 6G. Under (a) visible light and (b) UV light.

The use of organic fluorescent molecules as down-converting materials for the fabrication of colour conversion layers will be presented in Chapter 3, where rhodamine 6G and fluorescein sodium salt, have been solubilised into polymeric matrices. This allows for the production of transparent, flexible and thin layers specifically tailored for the conversion of blue and green OLEDs. Further investigation on the application of these organic dyes will also be discussed in the course of Chapter 4, where these molecules have been absorbed into supporting materials, zeolite and silica gel, to allow their dispersion into silicone-based layers.

### 1.9.1.2 Inorganic Phosphors

Inorganic phosphors are luminescent materials composed of a host material generally, an oxide, sulphide or nitrides of zinc or silicon, which is doped with luminescent centres called activators. The activators are often transitional metals like copper, silver and zinc or rare earth elements such as europium, cerium and yttrium.<sup>32</sup> Phosphors are a well-established class of materials which are used in several industrial applications involving lighting and displays. Phosphors can be found in LED bulbs as down-converting materials to transform the blue light emitted by the inorganic LEDs into a pleasant warm white.  $\text{Y}_3\text{Al}_5\text{O}_3:\text{Ce}^{3+}$  or more commonly  $\text{YAG}:\text{Ce}^{3+}$  was the first phosphor utilised for the production of white solid state lighting.<sup>32</sup>

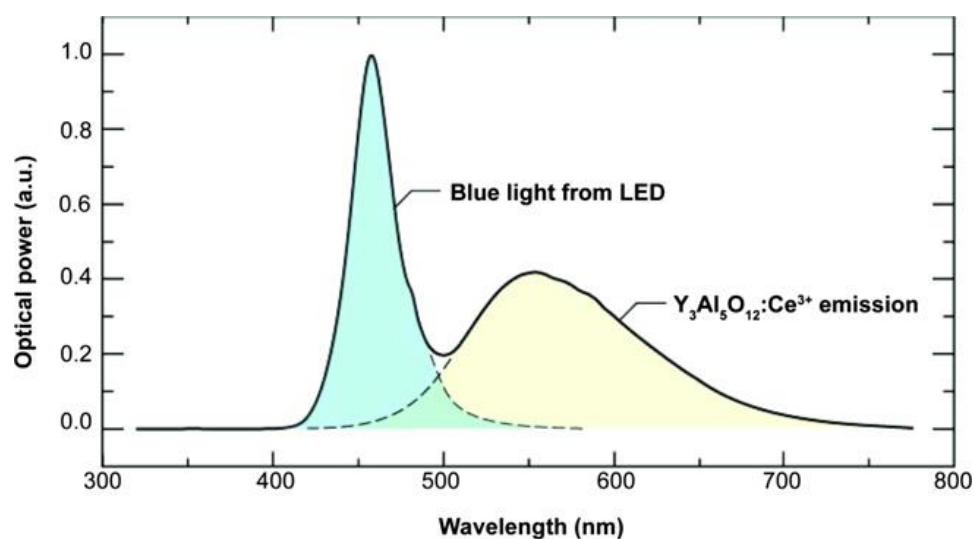


Figure 1.11: White light spectra obtained by the combination of a blue LED and the  $\text{YAG}:\text{Ce}^{3+}$ .<sup>32</sup>

Recently, phosphor technology was used for the down-conversion of OLEDs in virtue of their chemical and optical stability which outclass those of organic molecules. In addition, the luminescent properties of phosphors are not susceptible to the environment, therefore they can be easily dispersed in different matrices without incurring in alteration of their optical behaviour.<sup>4,7,32</sup>

The application of phosphors as down-converting materials in the CCLs for OLEDs was considered. However, since most of the common phosphors were specifically developed for application in LEDs, their optical properties often do not match the spectral characteristics required by the OLEDs.<sup>41</sup> In addition, the use of phosphors in the CCLs will result in layers which will not fulfil the requirements in terms of transparency as a consequence of the micrometer size of the particles size of the phosphors. The large particle size, moreover, can cause scattering phenomena which can lead to a substantial loss of light.<sup>32</sup> Nano-sized phosphors particles have been developed during the last decades to overcome these problems, but they have been found to suffer from low efficiency when compared to their micrometer counterpart.<sup>32</sup>

### 1.9.1.3 Quantum Dots

Quantum dots (QDs) can be defined as nanostructured semiconductors with a size between 1 and 30 nm. Quantum dots attracted significant interest as a result of their peculiar optical properties. The absorption and emission properties of QDs are strictly related to the size, shape and composition of the particles (Figure 1.12).<sup>49</sup>



Figure 1.12: Effect of the size on the luminescence properties of CdSe quantum dots (1.7 to 4.5 nm) excited by UV light.<sup>50</sup>

This behaviour is known as quantum confinement effect, a mechanism that can be observed when the size of the material is equal or less than the exciton Bohr radius (*i.e.* the distance between the electron-hole pairs), which for semiconductors is between 2 and 50 nm in relation with the nature of the materials.<sup>50</sup> As a result of that, the absorption and emission of quantum dots will shift towards the UV-blue region of the electromagnetic spectrum when the size of the particle is decreased, while increasing the size of the QDs will result in a red shift of the absorption and emission maxima.

Quantum dots are less prone to self-quenching phenomena at high concentrations than organic molecules and in addition, they possess high quantum yield.<sup>7</sup> These nanostructured semiconductors found application as down-converting materials in LEDs and OLEDs only recently<sup>45</sup>, but despite being promising candidates, their use is limited as a result of their poor stability and problems associated with the toxicity of these materials due to the use of heavy metals, particularly cadmium and tellurium.<sup>32</sup>

#### **1.9.1.4 Nanodiamonds and other luminescent nanoparticles**

Application of luminescent nanoparticles, such as nanodiamonds and carbon nanodots for the down-conversion of OLEDs has never been reported. Nevertheless, these luminescent materials found wide application in biology and medicine as imaging probes for the investigation of biochemical processes. They generally display elevated quantum yield, as well as high optical and chemical stabilities, which could make them potential candidates as down-converting materials in CCLs.<sup>51-55</sup> The drawbacks of these luminescent materials are related to poor availability and high cost. In addition, these nanomaterials are often difficult to produce, and they present aggregation phenomena at high concentration which might lead to a decrease in the optical properties.

The use of fluorescent diamonds as a luminescent material for the fabrication of CCLs, has been investigated in the course of this work and will be discussed in Chapter 6.

## 1.10 Aim of the project

The aim of the work presented in this thesis was to develop industrially scalable solutions, specifically designed to widening the spectral response of conventional blue and green OLEDs, used in day-to-day applications such as aesthetic signage, well-being and healthcare. One of the fundamental tasks in this project was to avoid as much as possible complex synthesis for the production of the down-conversion layers, as well as, modification of the internal structure of OLEDs, which might result in poor longevity of the devices and increase their production costs. As a result of that, the use of multiple emitters in the emissive layer or the addition of luminescent materials within the OLEDs stack were to be precluded. Attention was, therefore, to be focused on the development of external colour conversion layers that can easily be applied directly to the glass or plastic substrates of the devices. This solution was not only to provide advantages in terms of cost, due to the lack of additional steps required during the device fabrication, but it was also beneficial in terms of new design possibilities, allowing the final user to customise the device at his or her will and obtain colour effects virtually impossible to reproduce with other techniques.

Strict requirements regarding the mechanical, chemical and optical properties have been defined by the industrial partners and design agencies collaborating in the Light.Touch.Matters project. The CCLs had to be harmless (non-toxic) to allow the final user to interact with the device. They also needed to be transparent to ensure maximum light transmission and allow their application on transparent OLEDs. Moreover, they had to provide different tactile characteristic to the final user. Fundamental was also the production of layers that possess high efficiency in terms of light down-conversion in order to minimise as much as possible any energy dissipation. In addition, the CCLs needed to preserve the native flexibility of the

OLEDs, have a limited thickness, be compatible with the plastic substrate of the devices and, ideally, be self-adhesive to facilitate their application.

Fulfilling these requirements constrained the choice of luminescent materials and matrices that can be used in the fabrication of the CCLs.

For the matrix, polymers, such as polymethylmethacrylate (PMMA), polycarbonate (PC) and polystyrene (PS), as well as polyorganosiloxane have been considered, owing to their elevated transparency and flexibility.

Concerning the down-converting materials compromises had to be made. Fluorescent organic molecules have been selected over the phosphors, despite their poorer optical stability, in virtue of their higher availability, elevated quantum yield and their non-particulate nature which allow obtaining fully transparent layers. To allow the dispersion of the organic dye into the silicone supporting materials such as zeolite and silica gel can be used as carrier agents; these solutions will decrease the transparency of the layers but will provide a simple way to disperse the molecule into an otherwise non-miscible matrix and might have beneficial effects in terms of optical and chemical stability of the fluorescent molecules.

Fluorescent diamonds were also considered as an alternative down-converting material as a result of their high optical and chemical stability. In addition, the dispersion of the diamonds into the matrix could result in an increase of the mechanical properties of the layers.

The CCLs were optically characterised and have been tested on actual blue and green OLEDs, kindly provided by one of our partners in the project Light.Touch.Matters: the Holst Centre in The Netherlands (<https://www.holstcentre.com/>).

Some of these layers found practical application in the fabrication of the prototypes, developed by the design agencies involved in the project, showcased in conjunction with the final project meeting with the consortium that occurred in July 2016 in Delft.

# Chapter 2 : Materials and Methods

This chapter will provide background information about the different materials and characterisation techniques that have been used in the research carried out during this project.

## 2.1 Materials

### 2.1.1 Acrylic Coatings

The development of coatings based on the use of acrylic resins dates back to the 1930s but, the interest towards these types of protective layers remained limited until the introduction of acrylic paints in 1953. Nowadays, acrylic coatings are widely considered to be one of the best finishing layers due to their mechanical, chemical and thermal properties.<sup>56</sup> Originally, the term acrylic coating was used to indicate polymers produced exclusively by co-polymerisation of acrylic or methacrylic monomers, however, the current terminology has been extended to formulations which include vinyl monomers, such as styrene. Acrylic coatings can be divided into three main categories in relation to their compositions and production methods: thermosetting solution, thermoplastic solution and thermoplastic dispersion (latex).<sup>56</sup>

Thermosetting acrylics are formed by a mixture of acrylic monomers composing the backbone of the final product and other types of monomers, usually styrene, containing reactive groups. The polymerisation of these coatings occurs *via* cross-linking reaction promoted by thermal treatment (baking) or by the presence of a catalyst. Thermosetting acrylics are generally cheaper than other acrylic coatings and are characterised by elevated chemical stability, resistance to high temperature and glossy finishing.<sup>56</sup>

Thermoplastic acrylics are prepared by homo- or co-polymerisation of acrylic and methacrylic monomers (Figure 2.1). These coatings are synthesised by solution polymerisation; in a

reaction vessel, aromatic hydrocarbons, generally benzene and toluene, are heated to 90-110°C before proceeding with the gradual addition of the monomers and the initiator, benzoyl peroxide. After a period between 8 and 24 hours, the reaction is completed, and the final mixture is composed of a 40-60% polymer solution in the solvent. Thermoplastic acrylics are characterised by glass-like transparency, good resistance to UV degradation and high chemical stability.<sup>56,57</sup>

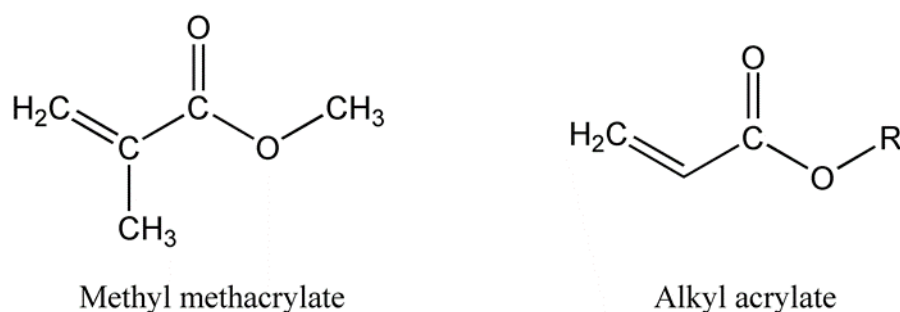


Figure 2.1: Chemical structure of methyl methacrylate and alkyl acrylate.

Thermoplastic dispersions, or more commonly acrylic latexes, are produced by emulsion polymerisation. A polymer emulsion can be defined as a colloidal solution in which the solid or semi-solid polymer particles are dispersed into water. A typical formulation for an acrylic latex includes: water, a mixture of acrylic and methacrylic monomers, a surfactant and an inhibitor. The monomers are the same used for the production of thermoplastic solutions and the surfactant is added to prevent their complete polymerisation and to promote the development of particles of polymer.<sup>56,57</sup> The film-formation mechanism for the acrylic latex is based on the evaporation of the solvent. When the emulsion is spread on a surface water starts to evaporate, as a result of that, the polymer particles suspended in the solution come into contact and coalesce leading to the formation of a thin and smooth layer.<sup>56,58</sup> The films formed by acrylic latexes are characterised by high refractive index and elevate gloss value as a result of the small size of the polymer particles dispersed in the solution. Moreover, as a result of their water based nature, acrylic latexes are more environmentally friendly than other coatings,

and as a consequence of the lack of organic solvents, they do not develop odours during the drying process.<sup>56,58-60</sup> In addition, the physico-chemical properties of these coatings can be further modified by the addition of additives, such as pigments to create coloured coatings, or plasticiser to improve the flexibility or enhance their adhesion.<sup>56,58-60</sup> Acrylic latexes are widely used in internal and external coatings, and they are the basis for acrylic paints used in artistic materials.

### 2.1.2 Polyorganosiloxanes

Polyorganosiloxanes or, more commonly silicones, are a class of polymer composed of chains of silicon and oxygen atoms with the addition of other organic groups (R). Silicones can occur in both linear and network structures, in relation to the type of silicon precursor used during their synthesis.<sup>57</sup>

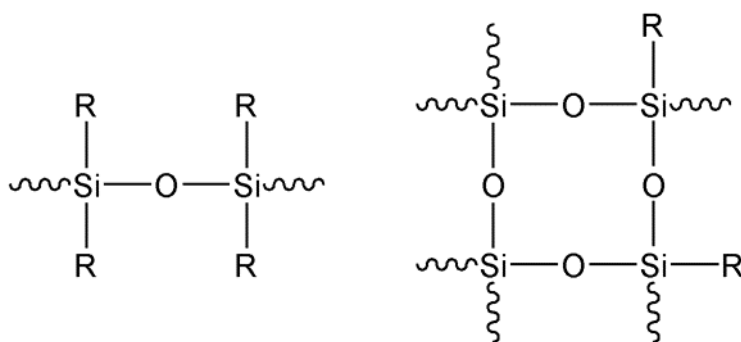


Figure 2.2: General chemical structure of polyorganosiloxane.

Compounds containing carbon-silicon bonds (organosilicon) were noted for the first time by Dumas in 1840 and subsequently synthesised by Friedel and Crafts in 1863. The major breakthroughs on this class of compounds are to ascribe to Kipping which, as a result of his work between 1899 and 1944, is considered to be the founder of organosilicon chemistry. His research, however, was focused on non-polymeric molecules and he often addressed the

accidental occurrence of polyorganosiloxane as a problem.<sup>57</sup> The industrial interest towards silicones began in the 1930s when there was the need for a material able to withstand elevated temperatures and which possess insulating properties. In the 1940s, the combined work of Corning Glass Work and General Electric Co. led to the development of silicone resins and, since then, silicones acquired popularity in several different areas.<sup>57</sup>

The production of silicones is based on the reaction of chlorosilanes with water, the process results in the formation of silanols (Figure 2.3 a). The silanols, being unstable, have a strong tendency to undergo condensation leading to the formation of siloxanes (Figure 2.3, b).

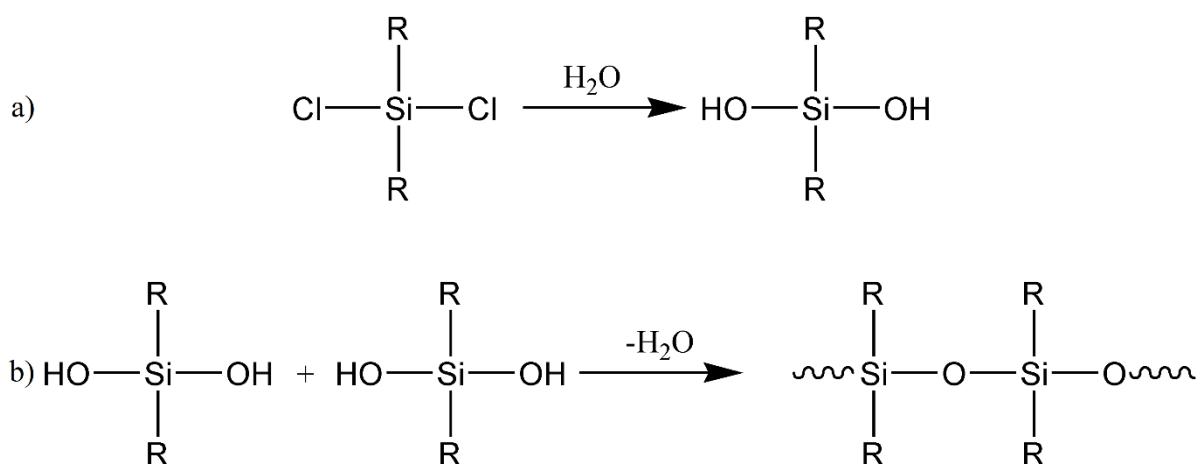


Figure 2.3; Reaction schemes to produce polyorganosiloxanes.

From a commercial point of view, silicones can be divided into three categories in relation to their mechanical and physical properties: fluids, elastomers and resins. Silicone fluids are composed of linear polymers with relatively low molecular weight (4,000-25,000). The silicon precursor used is dimethyldichlorosilane (Figure 2.4, a) which, when treated with low concentrated hydrochloric acid, forms short siloxane polymers. These chains are “capped” usually with hexamethyldisiloxane (Figure 2.4, b) to obtain the desired viscosity.<sup>57</sup>

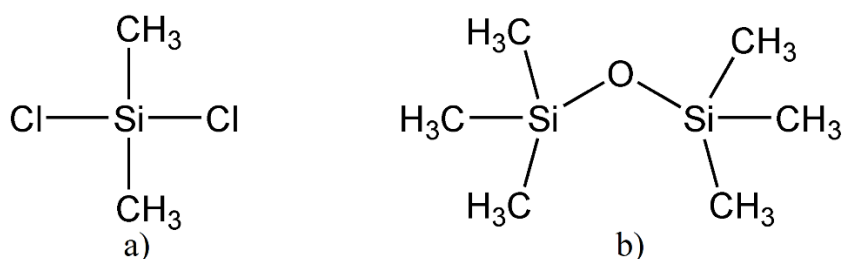


Figure 2.4: Chemical structure of dimethyldichlorosilane (a) and hexamethyldisiloxane (b).

The backbone of elastomers are linear macromolecules similar to those used in the fluids but, some modifications are performed in order to increase their molecular weight and promote cross-linking reactions to obtain elastic materials. Elastomers can be sub-categorised into two classes differentiated by the temperature required for the curing process. High temperature curing elastomers are based on the reaction of dimethyldichlorosilane, in presence of ether and water; the reaction leads to the production of cyclic monomers such as octamethylcyclotetrasiloxane (Figure 2.5).<sup>57</sup>

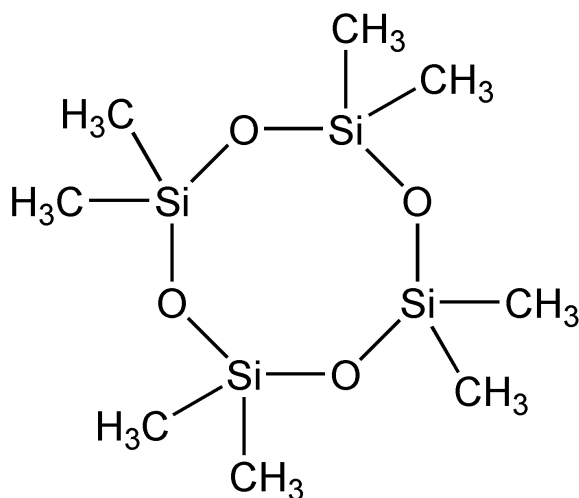


Figure 2.5: Chemical structure of octamethylcyclotetrasiloxane.

These newly formed heterocyclic molecules are then polymerised at 150-200 °C with a small amount of sodium hydroxide. The result is a highly viscous gum with no elastic properties, and

further thermal treatment at 110-175 °C in presence of peroxides is required to promote the cross-linking reaction (Figure 2.6). At this stage, the peroxide decomposes to form free radicals, that are able to attack the methyl group leading to ethylene cross-linkage.<sup>57,61</sup>

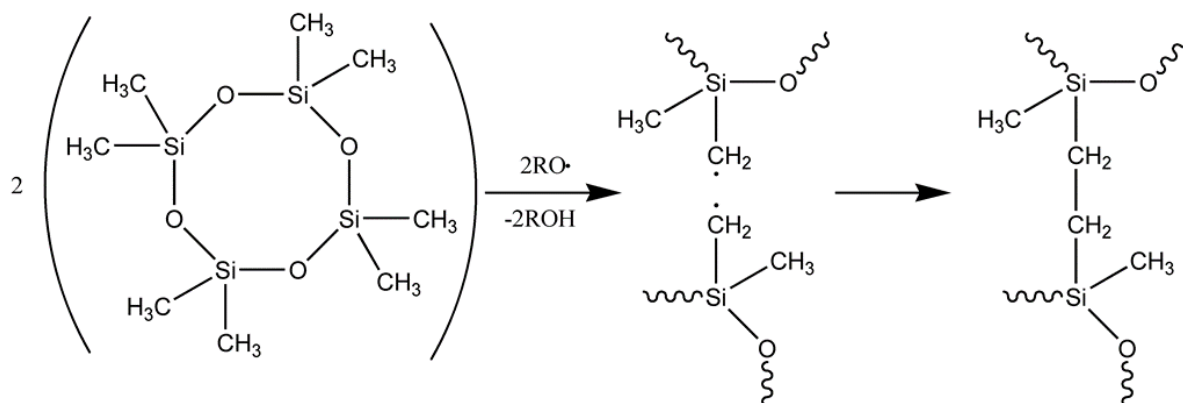


Figure 2.6: Cross-linking reaction of silicone gel promote by peroxide radicals.

The physical-chemical properties of the final materials can be modified by substitution of the methyl groups in the silicon precursor with vinyl, phenyl and nitrile groups.

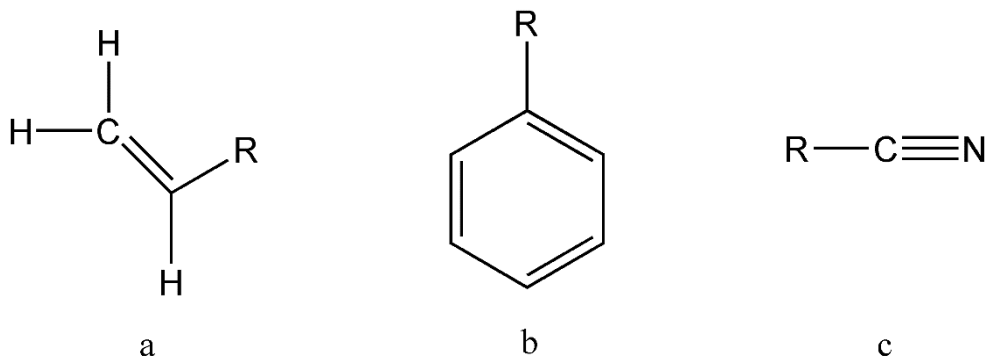


Figure 2.7: Chemical structure of vinyl (a), phenyl (b) and nitrile (c) group.

Room temperature curing elastomers are based on low molecular weight (10,000-100,000) polydimethylsiloxane with silanol groups, as chain terminators, to promote cross-linking. Their conversion to rubber occurs by reaction with alkoxy siloxanes (ROSi-) in the presence of a catalyst like stannous octoate, or by reaction with polysiloxanes, containing silanic hydrogen

(-SiH). This class of material is generally supplied in two separated components, which need to be mixed before the curing process can occur.<sup>57,61</sup>

Silicone resins are formed starting from a mixture of tri- and dichlorosilanes. This combination is defined by the R/Si ratio, which represents the amount of organic groups in relation to the silicon atoms. The R/Si ratio is normally kept between 1.2 and 1.6, to prevent extreme cross-linking, which will result in a material difficult to handle. Often the methyl groups are substituted with phenyl groups, to improve the heat resistance and flexibility of the resins. The tri- and dichlorosilane blend is initially dissolved in toluene or xylene before water is added, and the solution is stirred vigorously to promote hydrolysis. Once the reaction is completed, the solution separates into two layers, and the organic part is washed away from the hydrochloric acid residue. The organic mixture, at this point, consists of cross-linked and cyclic polymers as well as some silanol linear chains (10%); a further thermal treatment at 150 °C in presence of a catalyst is required to obtain the final product.<sup>57</sup>

The biggest advantages of silicones compared to other polymers is their thermal stability, within the temperature range, -50 to 200 °C, as they maintain their original physical properties. Such features, associated with their good electrical insulating properties, the ability to withstand most common organic solvents, their water repellent nature and the absence of ageing upon reaction with oxygen, make silicones the material of choice for various applications.<sup>57</sup> Silicones are, currently, used in cable insulation in aircraft components, as lubricants and greases, as a releasing agent for moulds, and in food-related products, in virtue of their non-stick and non-toxic nature.<sup>57</sup>

### 2.1.3 Amorphous Silica

Silicon dioxide (SiO<sub>2</sub>) is the most abundant component in the earth's crust. Silicon dioxide is more commonly referred to as *silica*; broadly used to identify all the crystalline forms of silicon dioxide such as quartz and cristobalite; as well as the amorphous forms, or all the chemical compounds composed of a silicon atom combined with four oxygen atoms arranged in a tetrahedral configuration. Industrial production of amorphous silica started in the 1940's. The process involves the reaction of sodium or potassium silicate solutions (X<sub>2</sub>SiO<sub>3</sub> where X=Na, K) with water and mineral acid, which lead to the formation of silicil acid (Figure 2.8).<sup>62,63</sup>



Figure 2.8: Formation of silicil acid.

Since the silicil acid is unstable in water, it tends to polymerise *via* condensation of silanol groups (Si-OH) to form the more stable siloxane bridges (Si-O-Si). This reaction is very sensitive to parameters such as feed rate, stirring, temperature, pH and alkali contents, which can be adjusted to match the desired characteristic of the final product. By varying the silicon precursor in the reaction solution, it is possible to obtain structures where the tetrahedra share two, three or four oxygen atoms with their neighbours, resulting in the formation of chains, planes or three-dimensional frameworks.<sup>62,63</sup> The polymerization is followed by the precipitation, filtration and drying of the material, which is then ground or compacted depending on the final applications.

Currently, silica is used as a reinforcement agent for elastomers, such as tyres, soles and mechanical rubber products; where it is able to increase the rolling resistance and wet traction of these products, without increasing their wear.<sup>62</sup> Silica is also employed in fire extinguishing

powders, in pigments or powder coatings, as a matting agent and in cosmetic products. As a consequence of its high absorption capabilities, it is used as a fast drying agent in inks, as a moisture absorber, and in the fabrication of apparatus for chromatography.<sup>62</sup> Moreover, in virtue of its hardness, structure and tunable particle size, silica is a perfect candidate for use as abrasive materials in toothpaste and fine polishing slurries. Another advantage of silica is its facile surface functionalisation, which allows tailoring of the physical properties of the material surface without altering the stability of the structure.<sup>62</sup>

#### **2.1.4 Faujasite Y**

Faujasite is one of more than two hundred types of minerals belonging to the class of zeolites. These are crystalline materials with a three-dimensional framework; characterised by a series of channels and cavities with sizes in the order of tens of Angstroms (Å). The term Zeolite has been coined from the Greek word *Zeo* and *Lithos* (*Zeo* = to boil and *Lithos* = stone), by Swedish mineralogist Alex Fredrik Cronstedt, when he observed that when heated, the material released a large amount of vapour, as a result of the high content of water trapped in its pores.<sup>64</sup> The structure of zeolites is composed of tetrahedra of silicon and oxygen atoms; the substitution of Si<sup>4+</sup> with Al<sup>3+</sup> in the material framework is common, and can occur in a wide range of Si/Al ratio that extends from 5:1 to 1:1. The presence of aluminium is responsible for the partial negative charge in the structure, which is counterbalanced by the existence of non-structural alkali cations such as Na<sup>+</sup>, K<sup>+</sup> or Ca<sup>2+</sup> located into the cavities.<sup>65-67</sup> The absence of a real chemical bond between the cations and the atoms composing the lattice of the zeolite, make possible and straightforward their substitution with other inorganic or organic ions, in a procedure commonly called *ion-exchange*.<sup>65-67</sup>

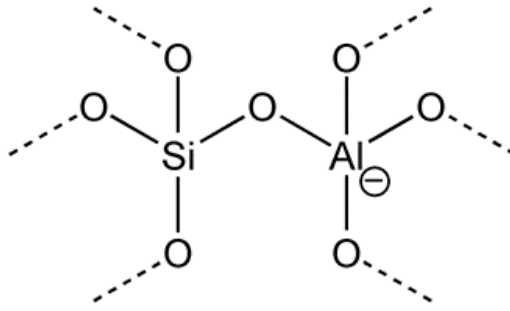


Figure 2.9: Schematic representation of the structure of the zeolite.

In Faujasite, the ratio between silicon and aluminium is used to classify the mineral into two subcategories called zeolite Y, where the Si/Al ratio is higher than 3, and zeolite X, where the ratio is between 2 and 3. Despite the different nomenclature and the difference in the content of silicon and aluminium, the structure of the material is maintained for both the X and Y type of Faujasite. The unique framework of Faujasite is characterised by the presence of two cavities with different size; the sodalite cage which presents a hexagonal window with an aperture of 8 Å and the supercage composed by 12 tetrahedra linked in a ring with an aperture of 12 Å (Figure 2.10).<sup>68</sup>

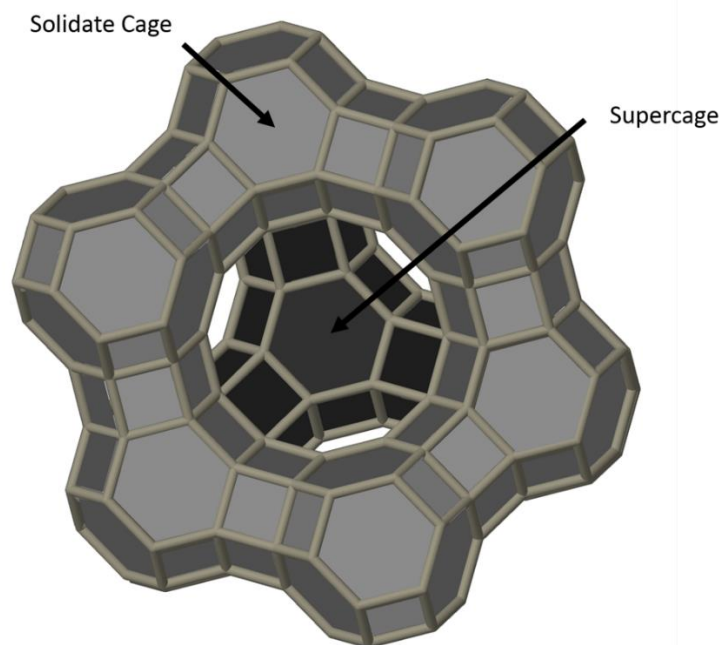


Figure 2.10: Three-dimensional structure of Faujasite.

The porous structure of zeolites is widely used for hydrocarbon conversion, gas separation and purification; as well as a desiccating agent and adsorbing material. Recently, with the advent of nanotechnology, this aluminosilicate found application as a scaffolding material for nanosynthesis processes for semiconductors, conductive polymers, inorganic clusters and organic molecules *via* a mechanism defined as *ship-in-a-bottle* synthesis.<sup>69-72</sup>

### 2.1.5 Organic fluorescent molecules

The emission of visible radiation from certain compounds, as a result of their exposure to the sunlight, has been discovered centuries ago. The first luminescence phenomenon ever reported dates back to 1565, when Nicolas Monardes, observed that a water solution of a particular wood, *lignum nephriticum*, glowed when exposed to sunlight.<sup>48,73</sup> Thirty-five years later an Italian shoemaker reported the discovery of phosphorescence when he noticed that a stone was able to glow in the dark after it was exposed to the sun. These light phenomena, however, remained a mystery until the second half of the 19th century, when Herschel observed that a

quinine sulphate solution emitted light when irradiated by the sun. He studied this phenomenon and concluded that it is not to be confused with light scattering but it must be of some other nature. A few years later, in 1852, Stokes investigated the emission of quinine, and he discovered that the light emitted from the molecule possess a different wavelength than the light absorbed by the compound. This discrepancy is, nowadays, a well-known phenomenon called *Stokes shift*, and represents one of the many characteristics of fluorescent materials.<sup>48,73</sup> In the following years, fluorescent molecules attracted the interest of the scientific community, and a large number of luminescent compounds were identified and characterised.<sup>48,73</sup> The first practical application of fluorescent molecules was ascribed to Victor Pierre in 1862. He devised a method to use these compounds as sensing materials in analytical tools, based on the fact that their emission is sensitive to changes in the environment such as pH and solvent.<sup>73</sup> Currently, the use of fluorescent molecules is widespread in various disciplines from chemistry, biology, medicine and physics; where these compounds are employed as tracers, pigments, and excitation sources in lasers.<sup>48,73</sup> In order for an organic molecule to undergo fluorescence, it has to possess specific atoms or groups of atoms defined as *fluorophores*. Common fluorophores include highly unsaturated aliphatic and aromatic configurations or chemical structures where nitrogen, oxygen and sulphur are present as substitutional groups or as heteroatoms in highly conjugated systems.<sup>74</sup>

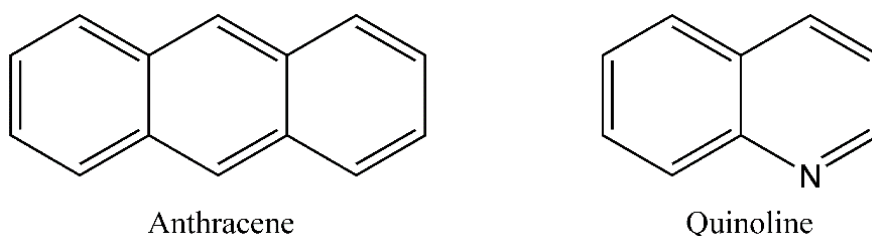


Figure 2.11: Examples of fluorophores.

Multiple factors can affect the optical behaviour of fluorescent molecules. The extension of the conjugate system is known to be directly proportional to the absorption and emission wavelengths of the species. The molecular structural rigidity is directly correlated with the fluorescence signal and this can strongly affect the efficiency of a compound. The presence of heavy atoms is often associated with a decrease in emission due to quenching mechanisms.<sup>73</sup>

### Rhodamine 6G

Rhodamine 6G, is a red-orange dye, belonging to the *aminoxanthenes* class. In its solid state, it appears as a brown-red crystalline material, which is highly soluble in common solvents such as water, ethanol and methanol.<sup>47</sup>

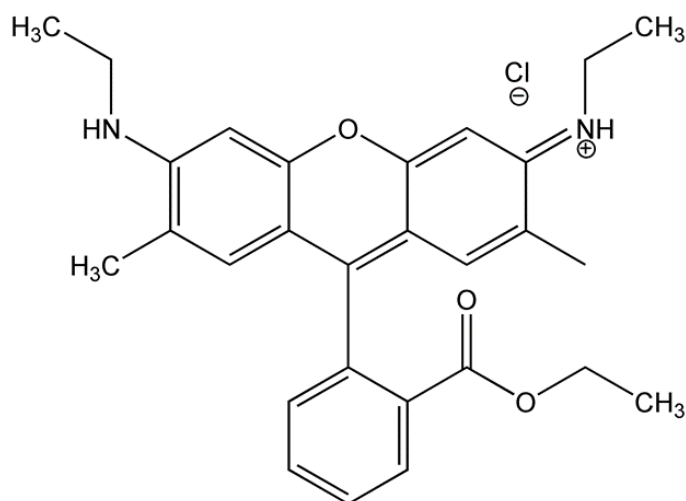


Figure 2.12: Chemical structure of Rhodamine 6G.

Rhodamine is produced by condensation of 3-ethylamino-*p*-cresol with phthalic anhydride, the reaction is followed by the esterification in presence of ethanol and a mineral acid, which results in the formation of the luminescent molecule.<sup>75</sup> Rhodamine 6G is characterised by elevated photostability and it possesses a quantum yield close to 100% when dissolved in water. These properties made Rhodamine 6G one of the most used and important commercially

available fluorescent dye.<sup>47,75</sup> Rhodamine is widely used in various applications; the molecule is added as a colour enhancer in particular ink-jet printing formulations, and it is often employed as a fluorescent probe to detect and trace biological processes. Rhodamine also found application as a chemosensor for the detection of other ions and molecules, and it has been one of the first fluorescent compounds employed in the production of dye lasers.<sup>73,75-77</sup>

### Fluorescein sodium salt

The sodium salt of fluorescein, also called *Uranine*, is an intense green fluorescent organic dye belonging to the class of xanthenes. Contrary to the free acid form, the sodium salt is highly soluble in water, as well as in common organic solvents such as ethanol and methanol.

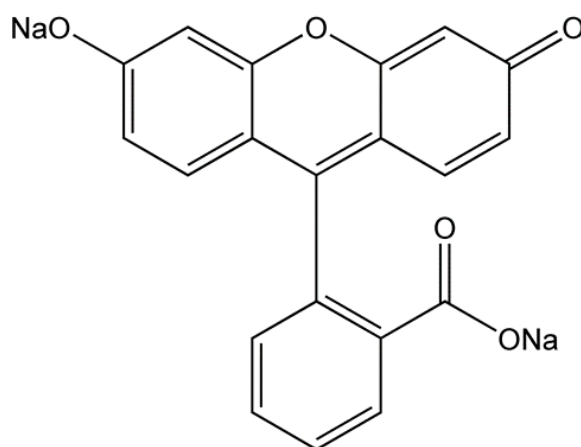


Figure 2.13: Chemical structure of fluorescein disodium salt.

Fluorescein was first synthesised by Von Baeyer in 1871. This was achieved by condensation of resorcinol with phthalic anhydride in presence of an acid catalyst; generally zinc chloride ( $ZnCl_2$ ).<sup>69,73,75</sup> Fluorescein is another important and widely used organic fluorophore. Its intense fluorescence signal is often used to trace water flow; in 1877 uranine was used to monitor the flow of the Danube river. In addition, the low toxicity of the dye makes the

molecule suitable for medical applications particularly in the field of ophthalmology; for the diagnosis of corneal diseases, or as a bio-labelling agent.<sup>73</sup>

Another interesting feature of fluorescein is its high sensitivity to pH. The optical properties of fluorescein are known to be related to the various ionic forms assumed by the dye at different pH values (Figure 2.14).

The absorption spectra of the cation, and the neutral forms (pH <5.5) of the molecule present a single peak, centred at 437 nm, whereas the anionic form (pH >5.5) is characterised by a double absorption at 437 and 475 nm. At pH ≥ 12, the dianion is formed and the absorption spectrum consists in a single peak with a maximum at 491 nm.

The emission spectrum of fluorescein is more consistent with the neutral, monoanion and dianion form presenting a maximum centred at ~515 nm. The exception is represented by the cation; this form, present only in strong acid conditions (10 M H<sub>2</sub>SO<sub>4</sub>), emits in the blue region of the visible spectrum at ~ 470-480 nm.<sup>78,79</sup>

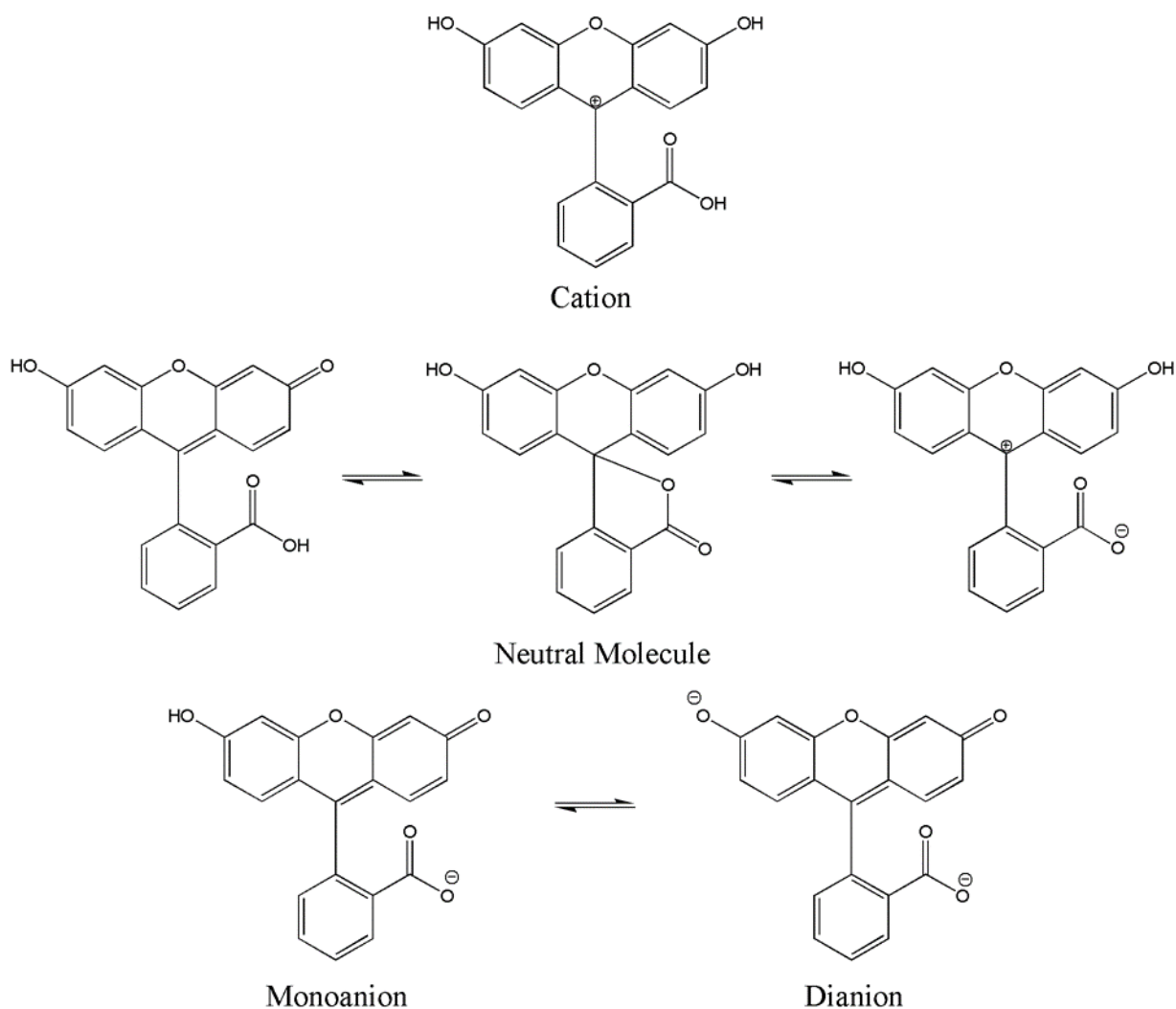


Figure 2.14: Ionic forms of fluorescein.

### 8-Hydroxypyrene-1,3,6-Trisulfonic Acid Trisodium Salt

8-Hydroxypyrene-1,3,6-Trisulfonic Acid Trisodium Salt, or more commonly known as HPTS, is an organic fluorescent dye, belonging to the class of pyrene. It was synthesised for the first time by Tietze and Bayer in 1939.<sup>80</sup> Its solid yellow crystals are soluble in water, *N,N*-dimethylformamide and glacial acetic acid but it is insoluble in common organic solvents such as methanol, ethanol or acetone.<sup>47</sup>

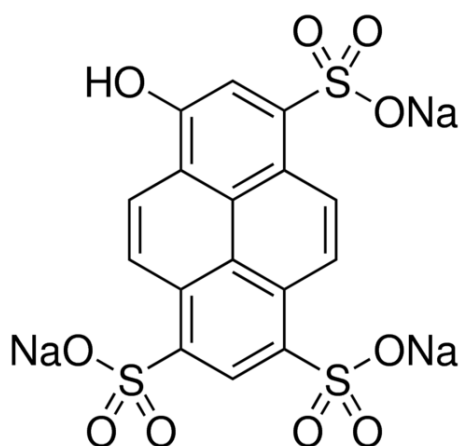


Figure 2.15: Chemical structure of 8-Hydroxypyrene-1,3,6-Trisulfonic Acid Trisodium Salt (HPTS).

HPTS is characterised by low toxicity, good solubility, large Stokes shift, and very strong pH-sensitive behaviour. It is therefore considered one of the best molecules for fluorescence acid-base titration, and pH determination. Moreover, in virtue of its  $pK_A$  value of 7.3, and its absorption spectra, that show a good match with the emission of blue LEDs; HPTS is one of the most suitable compounds for the production of carbon dioxide sensors.<sup>81</sup>

### 2.1.6 Ultra-fine Diamonds

Diamond is a metastable allotrope of carbon particularly known for its extreme hardness and thermal conductivity. The outstanding properties of diamonds arise from the strong covalent bond and the face-centred cubic structure (Figure 2.16).

A diamond lattice often presents impurities in the form of foreign elements that replace the carbon atoms in the structure or sit in the interstitial positions. These non-carbon elements are used for the classification of diamonds.

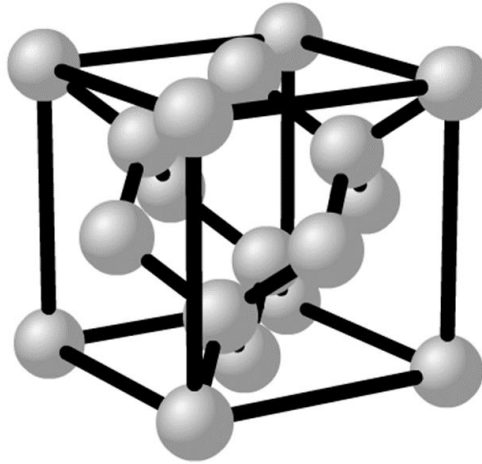


Figure 2.16: 3D representation of the diamond lattice. Grey spheres represent the carbon atoms.

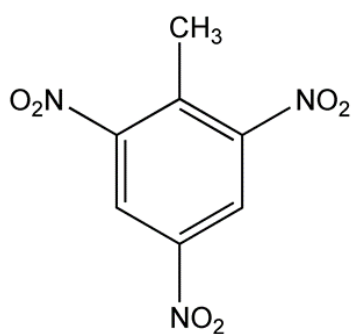
Two main categories defined as type I and type II diamonds, discern the crystals which contain nitrogen as impurities to those that incorporate other elements rather than nitrogen in the structure. Type I and type II diamonds are further divided into two sub-categories, denoted with the letter “a” and “b”, as follow:

- **Type Ia:** represents 98% of all natural diamond. They contain nitrogen impurities in cluster form at a concentration up to 3000 ppm. The elevated nitrogen content in these diamonds leads to sharp absorption lines in the blue region of the electromagnetic spectrum and emission under stimulation with UV light.<sup>82</sup>
- **Type Ib:** their natural occurrence is very rare (0.1%), but they are the most common type of synthetic crystals. Nitrogen is present up to 500 ppm, and it is in the form of single substitutional atoms. They are known to absorb green and blue light.<sup>83</sup>
- **Type IIa:** these diamonds present a negligible amount of impurities. As a consequence of that, they are colourless and possess the highest thermal conductivity of all diamonds. Only 1 or 2% of all the natural diamonds belong to this particular class.

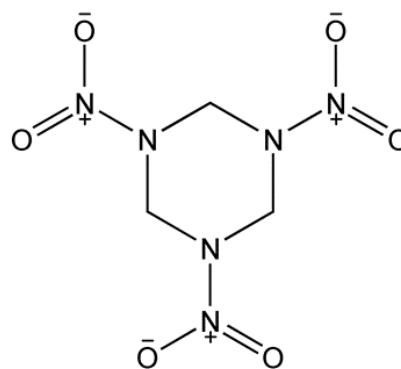
- **Type IIb:** are considered the rarest natural diamond. They present very low level of nitrogen impurities but contain a significant amount of boron atoms. The presence of this element is responsible for their p-type semiconducting nature and a blue-grey colour. They can be synthetically produced by doping type IIa diamonds with boron.<sup>83</sup>

Diamonds, nowadays, can be synthetically produced with different methodologies. High Pressure High Temperature method (HPHT) was the first ever reported working procedure for the synthesis of diamond crystals. The method was discovered in 1954 by Bundy *et al.*<sup>84</sup> while working for General Electric Company in the USA. The approach consists of heating amorphous carbon, derived from graphite, at a temperature higher than 1600° C in the presence of a metal catalyst such as chromium, manganese, cobalt, ruthenium or palladium. The reaction is carried out in a contained vessel pressurised at around 100,000 atm.<sup>85</sup>

In 1963, a group of Russian scientists, working for a nuclear armament research institute discovered the synthesis of nano-structured diamonds. However, due to strict security reasons in effect at the time, the procedure was kept secret, and in the next nineteen years, similar procedures for the synthesis of nanodiamonds (NDs) were re-discovered and reported by other research groups.<sup>86</sup> All these methods were based on the use of explosion energy, and therefore, were defined as a *detonation synthesis*. In this method, a sealed reaction vessel is loaded with powerful carbon-based explosives such as trinitrotoluene and cyclotrimethylenetrinitramine, non-oxidising agents and coolants. Upon ignition, the mixture generates the temperature and pressure needed for the formation of the diamonds, and the reaction results in the condensation of a carbon phase which contains nano-structured diamonds.<sup>86-88</sup>



Trinitrotoluene



Cyclotrimethylenetrinitramine

Figure 2.17: Chemical structure of trinitrotoluene (left) and cyclotrimethylenetrinitramine (right).

An alternative approach for the synthesis of diamond is represented by the use of a chemical vapour deposition (CVD) method. The procedure, described by Angus *et al.*<sup>89</sup>, involves the thermal decomposition of methane gas to form vaporised carbon atoms. These pure carbon atoms are deposited on diamond crystals acting as seeds, or on a non-carbon substrate such as silicon, generating diamonds. Contrary to the detonation synthesis, the CVD method allows the use of lower pressure, and as a result of the controlled chemical environment within the sample chamber, high purity diamonds can be obtained.<sup>89</sup>

Although nanodiamonds were discovered in the early 1960s, this class of materials gained attention and found practical applications, only at the beginning of the 1990s with the advent of nano-technology.<sup>86</sup> Ultra-fine diamonds are, currently, used for the fabrication of nanoscale magnetic sensors, in polishing or abrasive products, as additives in composite materials (polymeric fibres and rubbers) to enhance their mechanical properties, or in lubricants to improve anti-friction properties.<sup>52,86,87</sup>

Recently, the use of nanodiamonds was extended to the medical and biological fields. Researchers started to investigate the optical properties of fluorescent nanodiamonds (FNDs) and their possible application as fluorescent probes in biomedical imaging tools.

Nanodiamonds are considered valid alternatives to quantum dots and organic molecules, for the spectroscopic investigation of biological processes, on account of their non-toxic nature, high optical and chemical stability, elevated quantum efficiency and easy surface functionalisation.<sup>52,55,90-93</sup>

### **Fluorescent nanodiamonds (FNDs)**

The optical properties of nanodiamonds are the result of the formation of particular atomic configurations, within the material lattice, defined as colour centres. Colour centres are generally composed by impurities present in the structure of the diamonds as substitutional or interstitial atoms, but they can also originate by crystalline defects, such as vacancy and dislocation, or as a result of the combination of the two.<sup>94,95</sup> It has been estimated that more than 500 different colour centres can be present in diamonds. As a result of this large number, and variety in the optical properties; colour centres can cover the entire electromagnetic spectrum from the deep UV to the IR region.<sup>94</sup>

The most common atomic impurities, responsible for the generation of colour centres are nitrogen, silicon, nickel and chromium.<sup>94,95</sup> With the exception of nitrogen, no other atoms can be present inside the crystal lattice in a concentration higher than 100 ppm, without compromising the structural integrity of the material.<sup>83</sup> Such limitation is dictated by steric reasons, and in particular, by the small radius of the carbon atoms and their short bond length. The presence of impurities in the crystals can be introduced during the synthesis of the material. This occurs particularly in the case of diamonds produced by detonation synthesis, or by the high pressure high temperature method, where the impurities are carried by the reagents or are added intentionally into the reaction vessel along with the carbon precursors.<sup>83,95</sup> These techniques represent a straightforward method to produce doped diamonds, but they preclude the control over the concentration and location of the non-carbon atoms. More control over the

material's structure can be obtained with the use of the ion implantation methods. In this case, high purity diamonds, generally produced by chemical vapour deposition (CVD) method, are irradiated with high energy ion beams; by using this approach, it is possible to fine-tune the concentration, nature and location of the non-carbon atoms in the crystal lattice.<sup>96</sup>

The most interesting colour centres in diamonds are generated by the combination of substitutional atoms with lattice defects. The creation of defects is generally performed by irradiation with a high energy (MeV) electron, neutron or proton beams. These fast-accelerated sub-atomic particles are able to interact with the carbon atoms composing the diamond's structure, knocking them out from their original position and leaving an empty space in the structure called a *vacancy*. Subsequent heat treatment, usually above 600°C, is then performed to promote the migration of the vacancies towards the impurities to generate the colour centres (Figure 2.18).<sup>83,95</sup>

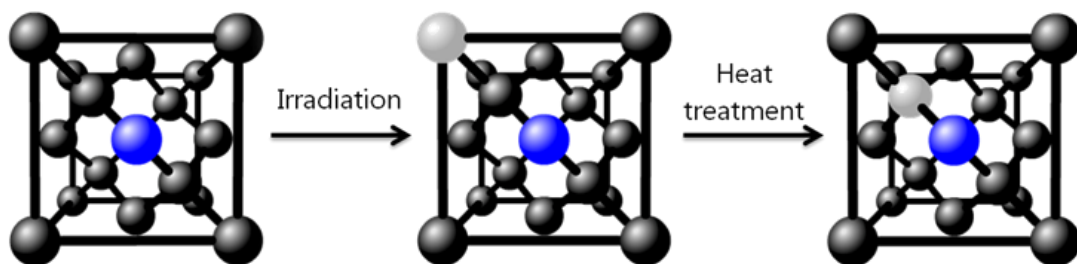


Figure 2.18: Schematic representation of the lattice of an impure diamond in presence of a defect. The black spheres represent the carbon atoms, the blue is the impurity and the light grey depicts the vacancy.

The spectral characterisation of the colour centres in diamonds is commonly performed by identification of the Zero Phonon Line (ZPL). ZPLs can be defined as a pure electronic transition between the ground state and the excited state as schematically represented in the Z transition of Figure 2.19, a.<sup>83</sup> ZPL transitions are very sharp lines due to the absence of phonons involved in the process. The spectral width of the ZPL gives an indication of the lifetime of the

excited state, and their splitting can be used to identify symmetry in the luminescent centres. In order to obtain well-defined ZPL bands, the spectral analysis of the diamonds should be performed at low temperature (77 K); since at such a low temperature the presence of the phonon-assisted emission sidebands is negligible.<sup>97</sup> ZPL peaks can be detected by absorption, photo-luminescence spectroscopy (PL) or cathodoluminescence (CL). When photo-luminescence is used to investigate the optical properties of diamonds, the ZPL bands are located in the middle between the absorption sideband and the emission sideband as represented in Figure 2.19, b.<sup>83</sup>

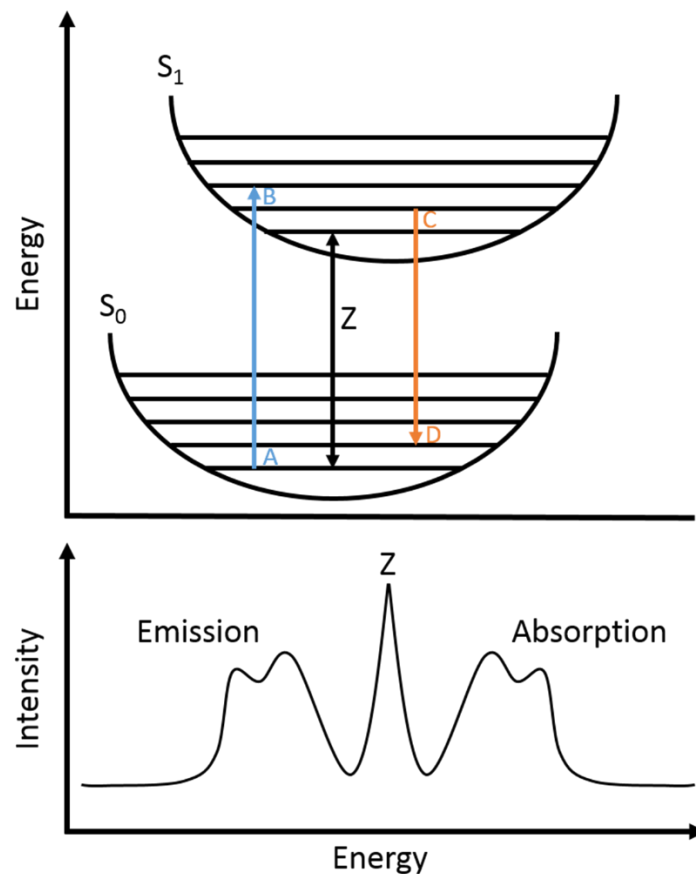


Figure 2.19: a) Schematic representation of a ZPL transition (Z), absorption sideband (AB) and emission sideband (CD). b) Energy of the ZPL and the sidebands.

## Displacement of carbon atoms from the diamond lattice

Electron beams are the most common form of high energy radiation used to produce point defects (vacancies) in diamonds. The interaction between the beam and the carbon atoms in the lattice can be described in terms of relativistic energy with the law of conservation of momentum:

$$T_m = \frac{2(E+2m_e c^2)}{M c^2} E \quad \text{Eq. 2.1}$$

Such an equation describes the energy transferred to a lattice atom of mass ( $M$ ) by an electron with a rest mass ( $m_e$ ), accelerated to an energy ( $E$ ), as a result of their collision. The atom will be knocked out only if the transferred energy ( $T_m$ ) is greater than the displacement energy ( $E_d$ ), which for a carbon in the diamond lattice has been reported to be between 30 and 40 eV.<sup>98-102</sup> Generation of defects in a diamond lattice can be also achieved by the use of gamma rays, however, due to the indirect ionising nature of this electromagnetic radiation, a completely different approach must be used to describe the displacement mechanism. When a gamma ray interacts with matter, the only energy transfer that can occur is via an electron. Gamma photons interact with the electrons or the nuclei of the target generating free electrons. These photon-created electrons transfer their excess energy to the atoms composing the lattice, knocking them out of position and leading to the creation of defects. The free electrons can be produced by three main mechanisms known as the photoelectric effect, Compton scattering and pair production.<sup>98,100,103</sup>

- *Photoelectric effect*: it is the dominant interaction mode in gamma rays with energy lower than 0.1 MeV. The photoelectric effect occurs when a gamma photon is absorbed by a core electron, which is excited to the conduction band. The excited electron can relax back emitting an X-Ray or an Auger electron. Generally, these electrons do not have enough energy to displace a carbon atom from the diamond's structure.<sup>98,100,103,104</sup>

- *Compton scattering*: occurs when the gamma ray has energy in the range between 0.1 and 10 MeV. The gamma ray photon is scattered by a valence electron, which then becomes a free electron capable of knocking out atoms.<sup>98,100,103,104</sup> The energy transfer from the  $\gamma$ -photon to the electron depends on the scattering angle  $\theta$ , and it is given by equation 2.2:<sup>102-104</sup>

$$E'_e = \frac{E_\gamma(1-\cos\theta)}{\left(\frac{E_e}{E_\gamma}\right)+(1-\cos\theta)} \quad \text{Eq. 2.2}$$

Where  $E_\gamma$  is the energy of the gamma ray and  $E_e$  is the electron's rest energy. The maximum energy that can be transferred to the electron can be calculated considering  $\theta=\pi$  so that the equation 2.2 becomes equation 2.3:

$$E_e^{max} = \frac{2E_\gamma^2}{E_e+2E_\gamma} \quad \text{Eq. 2.3}$$

- *Pair production*: this process is only possible when the incident gamma ray possess an energy higher than the double of the rest mass energy of an electron ( $E_\gamma > 1.02$  MeV). The radiation, in this case, will be entirely absorbed by the nucleus and an electron-positron pair will be created. The electron and positron will have equal energies and any excess of energy carried by the gamma ray will be converted into kinetic energy and shared by the newly formed sub-atomic particles which will contribute to the lattice damage.<sup>102-104</sup>

The use of gamma radiation for the creation of defects in diamonds carries several advantages, compared to electron and neutron beam. Gamma rays are more common, as a result of their application in the medical and food industries, where they are used as gamma knife, imaging technique and to sterilise food and medical instruments. Gamma radiation is known to have a higher penetration depth than electron or neutron beams, which results in a more uniform irradiation of a larger sample batch.<sup>104</sup>

## 2.2 Techniques

### 2.2.1 UV/Visible Spectroscopy

Ultraviolet-Visible spectroscopy, normally abbreviated UV/Vis spectroscopy, is a common technique used in analytical chemistry to identify and quantify different types of compounds, ranging from organic molecules to metal ions<sup>105</sup>. The working principle of this technique is based on the absorption of electromagnetic radiation, in the form of visible or ultraviolet light, by a specific compound or atom.<sup>105</sup> The interaction of the electromagnetic irradiation with matter results in a transfer of energy, which can be calculated in function of its frequency  $\nu$ , or its wavelength  $\lambda$  with the formula in equation 2.4.

$$E = h\nu = \frac{hc}{\lambda} \quad \text{Eq. 2.4}$$

Where  $h$  is the Planck's constant ( $= 6.62 \cdot 10^{-34} \text{ Js}$ ) and  $c$  is the speed of light ( $\approx 3 \cdot 10^8 \text{ m/s}$ ).

When the energy of the light matches the difference between two electronic levels of the compound (figure 2.20 $\uparrow$ ), electrons will be promoted to a higher state, and the corresponding wavelengths of light will be absorbed by the molecule in the sample.<sup>105</sup>

The amount of absorbed light is measured by the difference in intensity of the incident light ( $I_0$ ) and the transmitted light ( $I$ ); this is expressed in terms of transmittance ( $T$ ) or absorbance ( $A$ ) with the formulas in equation 2.5 and 2.6.

$$T = I/I_0 \quad \text{Eq. 2.5}$$

$$A = -\log T \quad \text{Eq. 2.6}$$

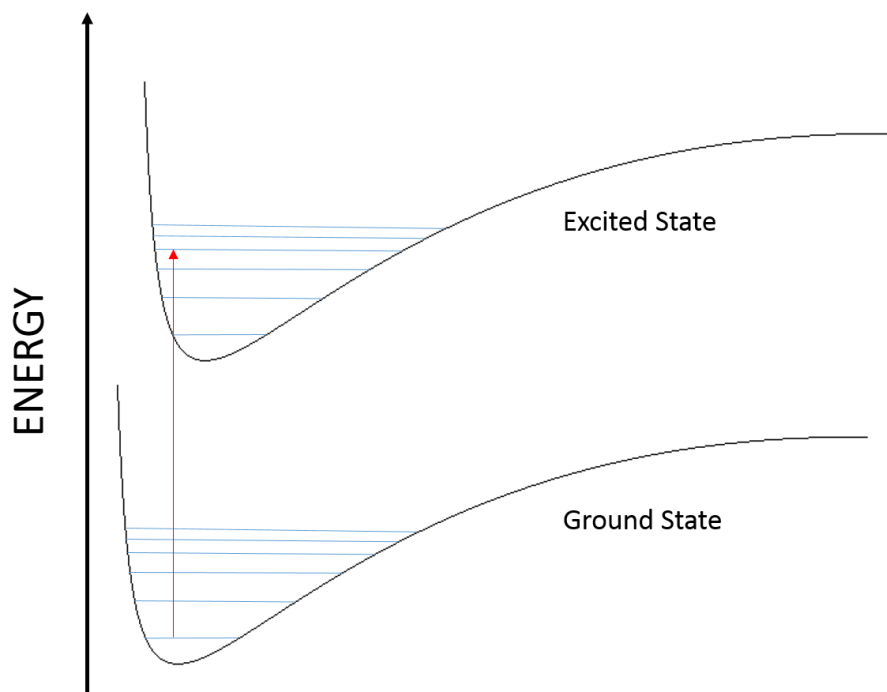


Figure 2.20: Electron transition between the ground and excited state.

Although UV/Vis spectra provide only a limited amount of information particularly regarding the molecular identification, the technique has been proved to be very useful in terms of quantitative analysis. The amount of light absorbed is indeed proportional to the concentration of the absorbing molecules in the sample.<sup>105</sup> The relationship that linked these two quantities is known as the Beer-Lambert's Law, shown in equation 2.7:

$$A = -\log T = \epsilon cl \quad \text{Eq. 2.7}$$

where  $\epsilon$  is defined as the extinction coefficient, which is a characteristic value determined by the measurement conditions (wavelength, temperature, solvent and analyte),  $l$  is the path length (normally fixed to 1 cm) and  $c$  is the concentration of the species under analysis. In order to obtain accurate results for the concentrations, the value of  $\epsilon$  is normally calculated with the use of a calibration or working curve, constructed by measuring standard solutions of known concentrations.<sup>105</sup>

A typical absorption spectrum is represented in Figure 2.21. The absorption curve for the specimen (Rhodamine 6G) is plotted on a two-dimensional coordinate system, where the ordinate axis represents the absorbance values (A) and the abscissa axis represents the scanned wavelengths of the incident light expressed in nanometre (nm).

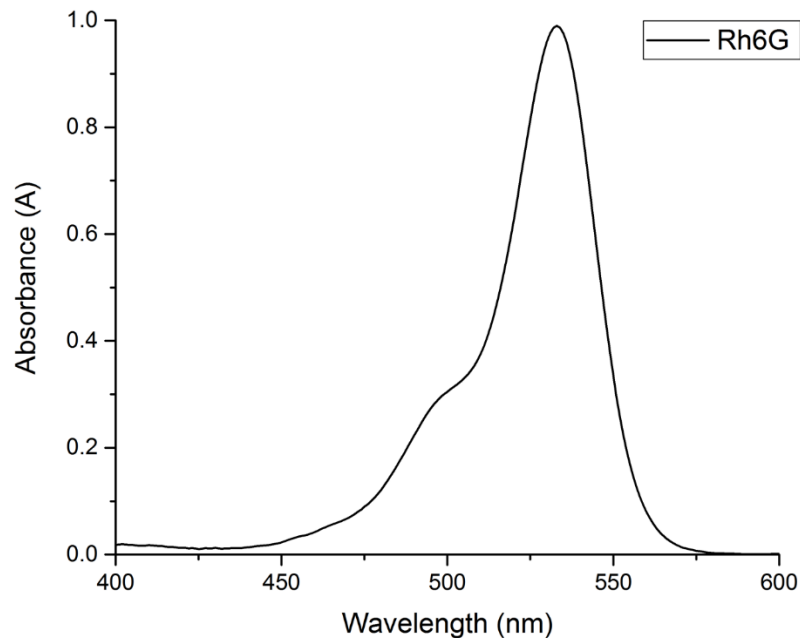


Figure 2.21: Absorption spectrum of Rhodamine 6G in water.

The instrument used to measure the absorbance is called a spectrophotometer; it consists of a light source, a monochromator, a sample chamber and a detector.<sup>105</sup>

- The light source should ideally provide a constant intensity for all the wavelengths from the UV to the near infrared (IR). Since this is practically impossible to achieve with a single lamp, most of the instruments adopt the use of two separate light sources; a deuterium arc lamp for the UV, and a tungsten-halogen lamp for the visible and IR.<sup>105</sup>
- The monochromator is the dispersion device responsible for the selection of a particular wavelength. In modern spectrophotometers, the monochromator is usually made of a

holographic grating. When hit by white light, produced by the lamps, the monochromator splits the entire radiation into single wavelengths and sends the selected wavelength to the sample chamber. <sup>105</sup>

- The detector is responsible for the conversion of the light signal into an electrical signal. Normally such a conversion is performed by a photomultiplier tube, a photodiode detector or a photodiode array. <sup>105</sup>

Spectrophotometers come in different design: single, dual and split beam. A schematic representation of a spectrophotometer is shown in Figure 2.22.

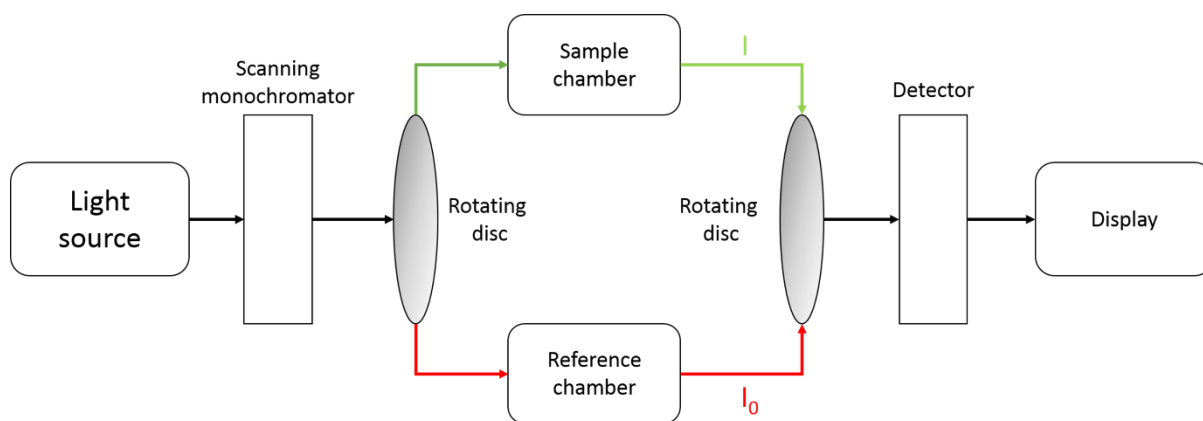


Figure 2.22: Schematic representation of a dual beam spectrophotometer.

Single beam spectrometers are the simplest, least expensive and most sensitive apparatus for the measurement of absorbance values. For this reason, they are normally used by national standard institutions. The single beam configuration, however, presents problems due to the time interval between the measurement of the sample and the reference, which might lead to lamp drift phenomena, resulting in significant readout errors. This drawback can be avoided with dual or split beam configurations. <sup>105</sup> These designs allow measurements of the absorbance of the blank and the sample, at the same time using a “chopper”, a rotating mirror that switches the light path between the sample chamber and the reference chamber; or a beam splitter, which

allows splitting of the incident beam into two parts with equal intensity. Dual or split beam configurations, however, require more complex mechanics, and the higher number of optical components leads to a decrease in their sensitivity, and ease of use.<sup>105</sup>

## 2.2.2 Fluorescence Spectroscopy

Fluorescence spectroscopy can be defined as a complementary technique to the UV/Vis absorption spectroscopy. The technique allows imaging, localise and identify compounds at a single molecule level. In virtue of its high sensitivity and absence of expensive or dangerous radioactive materials, fluorescence spectroscopy is widely used in biotechnology, medical applications, material science, forensics and genetic analysis. Fluorescence occurs when an excited electron in the molecule, relaxes back to the ground state emitting a photon of a certain frequency. Such a process can be schematically represented by the use of a Jablonski diagram (Figure 2.23).<sup>106</sup>

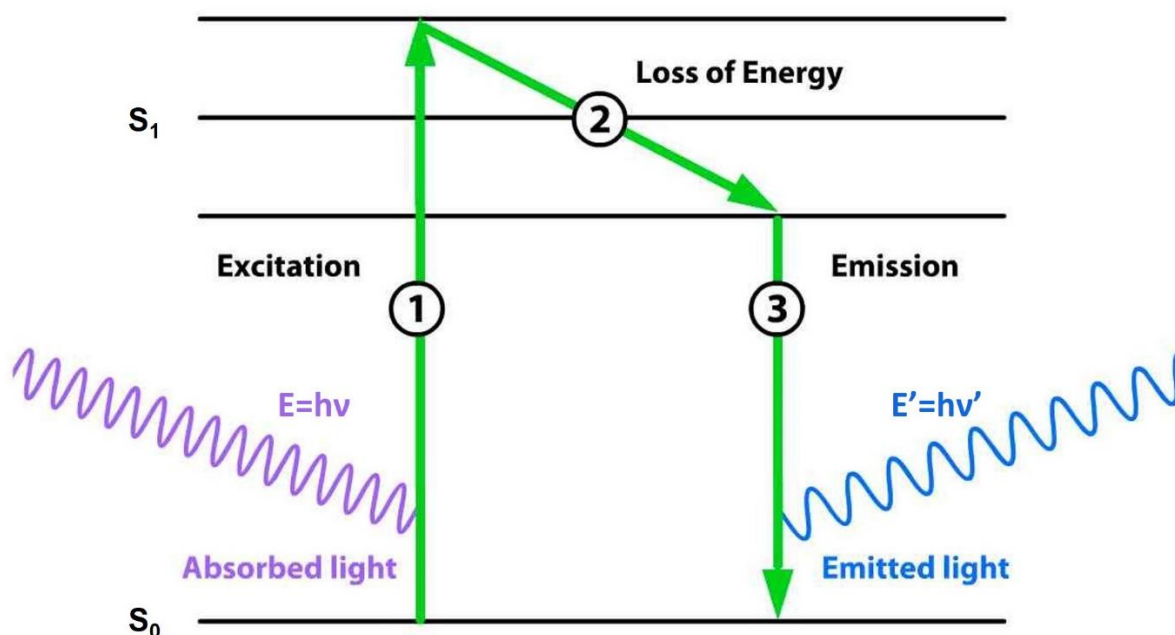


Figure 2.23: Jablonski diagram showing the electronic transition related to the fluorescence phenomenon.

The phenomenon can be described in three steps:

1. the incident light is absorbed by the fluorescent compound and the energy carried by the photon ( $E = h\nu$ ) is transferred to the ground state ( $S_0$ ) electron, which will be promoted into the excited state ( $S_1$ ).
2. The excited electron will fall from a higher vibrational level to a lower one, losing part of its energy, in a process called internal conversion.
3. The electron relaxes falling back to the ground state emitting a new photon with energy  $E' = h\nu'$ .

As a result of the energy loss during the internal conversion, the frequency of the emitted photon will be always lower than the frequency of the incident photon.<sup>106</sup> Such a difference is called *Stokes shift* and it is used to define the quality of a fluorescent compound, together with the *quantum yield* (QY), which represent the number of emitted photons relative to the number of the photons absorbed, and the *fluorescence lifetime* ( $\tau$ ), which indicates the average time that the molecule spend in the excited state.<sup>106</sup> The main advantage of fluorescence spectroscopy is its direct detection, *i.e.* the signal does not need to be measured by calculation as occurs for the absorption but it is directly readout by the detector. The direct detection allows for highly sensitive instrumentation. Only a limited number of molecules are able to undergo fluorescence, and in some cases, prolonged exposure to the exciting radiation can lead to irreversible chemical modifications resulting in the permanent disappearance of the signal (bleaching).<sup>106</sup>

The instrument used for fluorescence spectroscopy is known as a fluorimeter. A typical fluorimeter design is represented in Figure 2.24. Its design is similar to that already observed for the UV-Vis spectrophotometer. The main components are a light source with a broad emission, an excitation monochromator, which selects the wavelength of the incident light, a sample chamber, a second monochromator used to select the emission wavelength, and a

detector. Most fluorimeters allow the recording of emission and excitation spectra. In the first case the excitation monochromator is fixed on a single wavelength, while the emission monochromator performs a scan; in the latter case the situation is reversed with the emission monochromator fixed on a single wavelength, and the excitation monochromator responsible for performing the wavelength scan.<sup>106</sup>

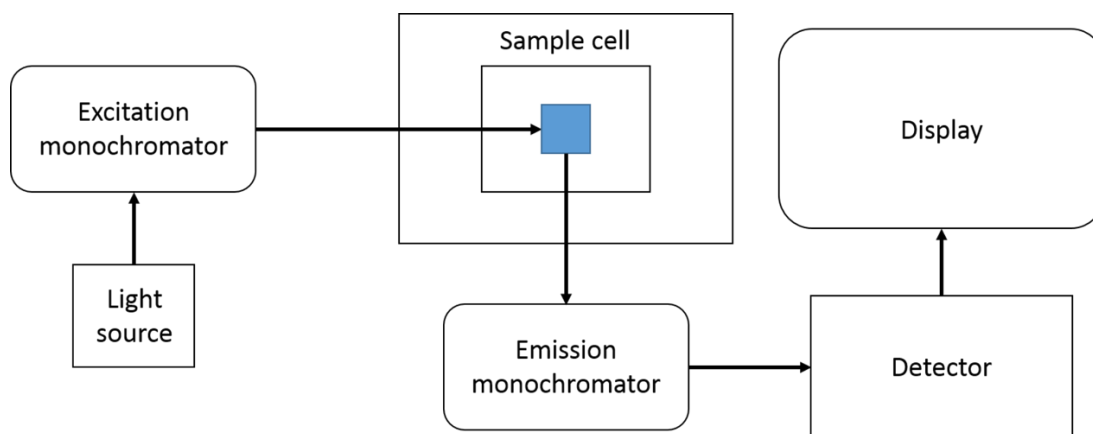


Figure 2.24: Optical design of a fluorimeter.

### Integrating sphere and QY measurement

From a mathematical point of view, the quantum yield ( $\Phi$ ) of a luminescent compound can be defined as the fraction between the emitted photons ( $N_{phem}$ ) versus the absorbed photons ( $N_{phabs}$ ).<sup>107</sup>

$$\Phi = \frac{N_{phem}}{N_{phabs}} \quad \text{Eq. 2.8}$$

The quantum yield is an important parameter for the characterisation of a luminescent compound since it gives an indication of its sensitivity and it allows to define electronic transitions.<sup>107,108</sup>

Two approaches can be used to determine the quantum yield of a substance; the first, called comparative or relative quantum yield, is based on the use of a known luminescent standard as

a reference. The intensities of the absorption and emission spectra of the standard and the luminescent sample under analysis are compared and the quantum yield can be calculated *via* Equation 2.9:<sup>107</sup>

$$\Phi_s = \Phi_{ref} \left( \frac{A_r}{A_s} \right) \left( \frac{I_r}{I_s} \right) \left( \frac{n_s^2}{n_r^2} \right) \left( \frac{D_s}{D_r} \right) \quad \text{Eq. 2.9}$$

In this equation  $\Phi$  represent the quantum yield, A is the absorbance value, I is the intensity of the exciting light, n is the refractive index and D is the area under the emission curve. The s and r subscripts represent the values for the unknown sample and the reference.<sup>107</sup>

This is the most common method to measure the QY of diluted solution, indeed, it does not require any specific apparatus, but the results obtained can often be inaccurate. Errors can be generated by variation in the spectral characteristics between the reference and the sample, as well as due to small changes in the environment which can have a significant effect on the QY.<sup>108</sup>

An alternative and more reliable approach consists in the use of an integrating sphere. The integrating sphere is an additional component available for most fluorimeter which allow to measure the absolute QY of a liquid or solid substance by collecting all the emission from the sample.<sup>108</sup> In this work the Quanta-phi accessory for the Horiba fluorolog has been used to measure the absolute quantum yield of the fluorescent silicone layers described in Chapter 4.

### **2.2.3 X-ray Powder Diffraction (XRPD)**

X-ray powder diffraction is an analytical technique for the characterization of solid materials based on their crystalline structure. The working principle of the technique consists in the detection of the constructive interference resulting from the diffraction of X-Rays, as a consequence of their interaction with the crystal planes in the lattice of the sample. A simplified

description of the phenomenon can be geometrically represented by the mirror reflection (Figure 2.25).<sup>109,110</sup>

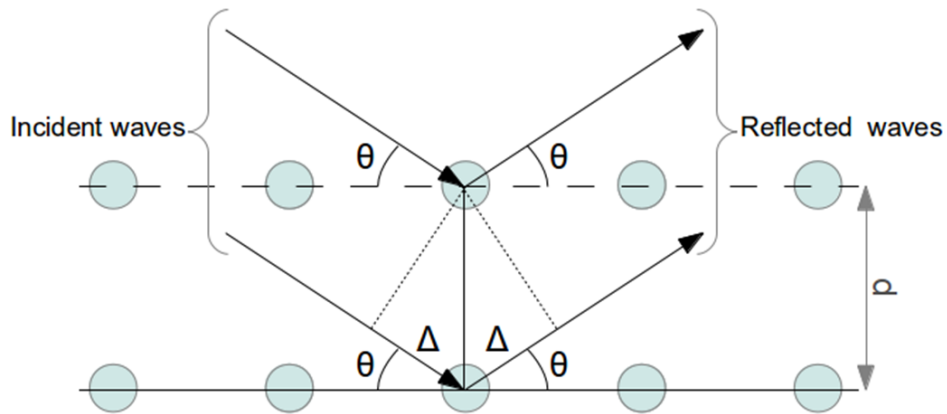


Figure 2.25: Mirror reflection illustration of an X-ray diffracted by crystal planes.

When X-rays interact with a material with an ordered array of atoms, the incident waves are reflected symmetrically (i.e. with the same incident angle  $\theta$ ) leading to a path difference equal to  $2\Delta$ .

The condition for a constructive interference to be generated is mathematically represented by the equation:  $2\Delta = n\lambda$ , where  $n$  is an integer number and  $\lambda$  is the wavelength radiation and the distance  $\Delta$  can be calculated with a trigonometrical function resulting in  $\Delta = d \sin\theta$ . Therefore, the condition for a constructive interference is given by the final equation:

$$2d \sin \theta = n\lambda \quad \text{Eq. 2.10}$$

This represents Bragg's law for diffraction and allows the computation of the distance between crystal planes  $d$  knowing the incident angle of the radiation  $\theta$ , and the wavelength  $\lambda$ . Extending this concept in three dimensions, it is possible to obtain detailed information on the crystal structure of a material.<sup>109,110</sup> Modern diffractometers equipped with rotational apparatus for the sample, and a movable detector, are able to collect all the constructive interferences created

by the interaction between the sample and the X-ray radiation. The results are presented in the form of a graph, called an X-ray powder diffraction pattern, where the  $2\theta$  angles are plotted against the diffraction intensities. <sup>109,110</sup>

Powder diffraction is one of the most commonly used techniques for the identification of the crystallinity of a material. The advantages of this technique are related to its relative speed of data collection; the simple procedure required for the preparation of the samples, and the considerable amount of obtainable information. <sup>109,110</sup> The interpretation of the data is straightforward, particularly when it is focused on the phase identification, phase transition or degree of crystallinity; a comprehensive database of patterns allows an easy comparison with a large amount of reference samples. Special care needs to be taken when the material to be analysed presents flat or needle-like crystals, since their tendency to arrange in preferred orientations can strongly affect the measurement, resulting in the absence of characteristic peaks in the diffraction pattern. <sup>109,110</sup>

The main components of a diffractometer are: the X-ray tube, the goniometer, the collimator, the monochromator and the detector. The X-ray tube is responsible for the generation of the incident radiation. It is composed of a cathode, generally made of tungsten, which when heated emits electrons. <sup>109,110</sup> These electrons are accelerated in the direction of the anode by a potential difference. Their impact with the metal plate composing the anode results in the generation of an X-ray with a specific wavelength, which depends on the chemical composition of the anode itself. The collimator is used to reduce the angular divergence of the X-rays. This is generally achieved by a metal slit that is able to block the waves non-parallel to the direction of propagation. <sup>109,110</sup> The monochromator is responsible for the selection of the wavelength; due to the monochromatic nature of the radiation produced by the X-ray tube used in common diffractometers, the monochromator simply results in a filter specific to the material of the anode. <sup>109,110</sup> The detectors used in modern instruments can be divided into point detector, i.e.

the detector is dedicated to measure the intensity of the diffracted beam, whereas the goniometer is responsible to determine the value of the Bragg angle, and an area detector, where every point is measured simultaneously due to the spatial resolution capability of the sensitive area.<sup>109,110</sup> The conversion of the X-ray into an electrical signal can be performed by ionization of the gas (Xe), which results in the formation of positive ions, and electron (gas proportional counter and position sensitive detector), by production of visible light photons as a result of the absorption of X-rays (scintillation, CCD and image plate detector) or by the generation of electron-hole pairs from the interaction of the X-ray beam (solid state detector).<sup>109,110</sup>

### **Synchrotron X-ray radiation source**

The synchrotron radiation source is considered the most powerful source of X-rays. Inside a synchrotron ring, electrons or positrons move, at relativistic speed, in circular orbits controlled by a magnetic field. X-ray and other electromagnetic radiations are produced by these accelerated subatomic particles and emitted along the tangent of their orbit (Figure 2.26).<sup>109,110</sup> X-ray radiation generated from the synchrotron has four to twelve times more brilliance than their counterpart obtained from X-ray tubes; as a result of the absence of cooling mechanism involved in their production. Moreover, the beams coming out from the storage ring are only weakly divergent, and particularly at the small distances used in powder diffraction analysis, they can be considered parallel providing a substantial improvement in terms of resolution.<sup>109,110</sup>

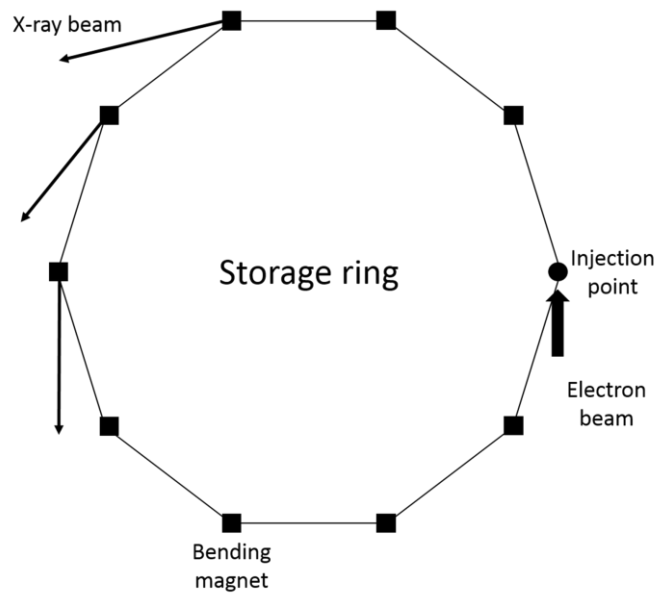


Figure 2.26: Schematic representation of a synchrotron ring.

## 2.2.4 Scanning Electron Microscopy (SEM)

Scanning electron microscopy is a powerful imaging technique based on the interaction of an electron beam with the surface layers of the sample. When these subatomic particles encounter a solid, they can be scattered elastically or inelastically as a result of their interaction with the atomic nuclei, or with atomic electrons. These scattering modes define the two most used imaging methods in SEM, which are defined as backscattered electron and secondary electron detection.<sup>111</sup> The signal from the backscattering electrons (BSEs) arises from the electrons composing the incident beam, that are elastically scattered by the atoms in the sample with an angle greater than  $90^\circ$ , and only a marginal loss in energy. Since the number of the backscattered electrons is proportional to the squared atomic number of the element they interact with (i.e. heavier element will produce more backscattered electrons), BSEs can provide information on the chemical composition of the materials.<sup>111</sup>

On the contrary, secondary electrons (SEs) are produced by the inelastic interaction of the microscope electron beam with the atoms composing the sample. The transfer of energy can

result in the excitation of the atoms which liberate the excess energy by emitting an electron. The secondary electrons mode is particularly indicated for the morphological analysis of the material's surface since the emission of the electrons is more probable from the atomic position next to the sample's surface. In addition, the emission of secondary electrons is strictly related to the angle between the incident beam and the surface of the sample, therefore, the images obtained with this mode appear to have three-dimensional features.<sup>111</sup>

Schematic representation of a scanning electron microscope is given in Figure 2.27. The main components of the microscope include the electron gun, normally a filament of tungsten or LaB<sub>6</sub>, placed at the top of the column. This is followed by a series of magnetic lenses to focus and direct the beam to the sample. Below there is the scanning mechanism for the x and y axes, the objective lens, which performance determines the final resolution of the microscope, and the sample chamber. A collector grid is used to discern the backscattered and secondary electrons, which are sent to the scintillator where they are converted into photons, and collected by a photomultiplier tube (PMT) detector.

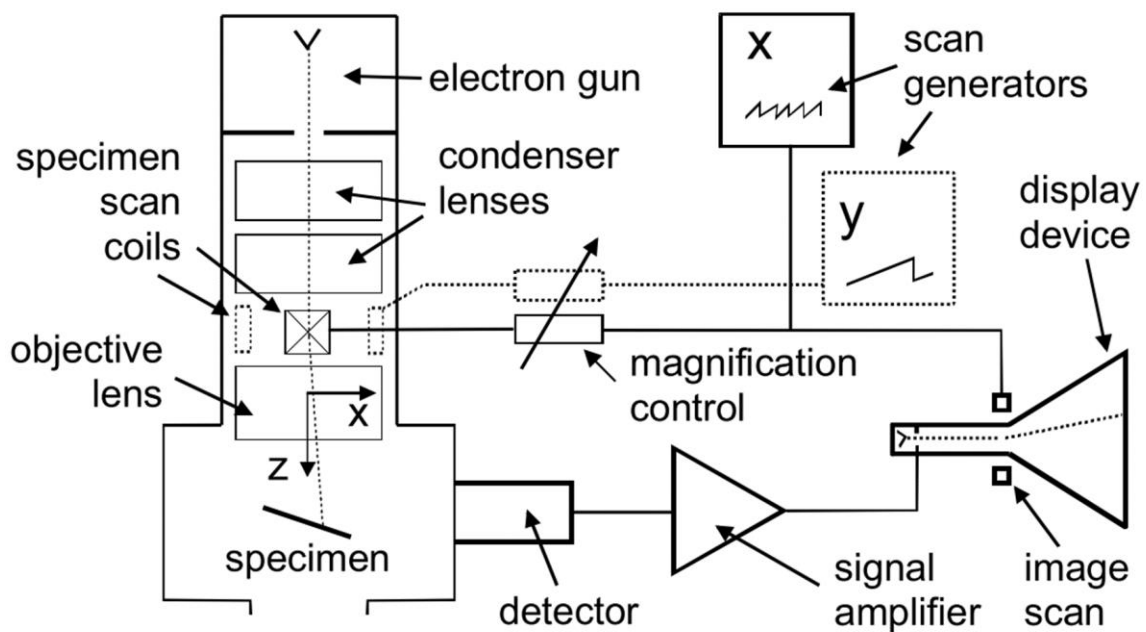
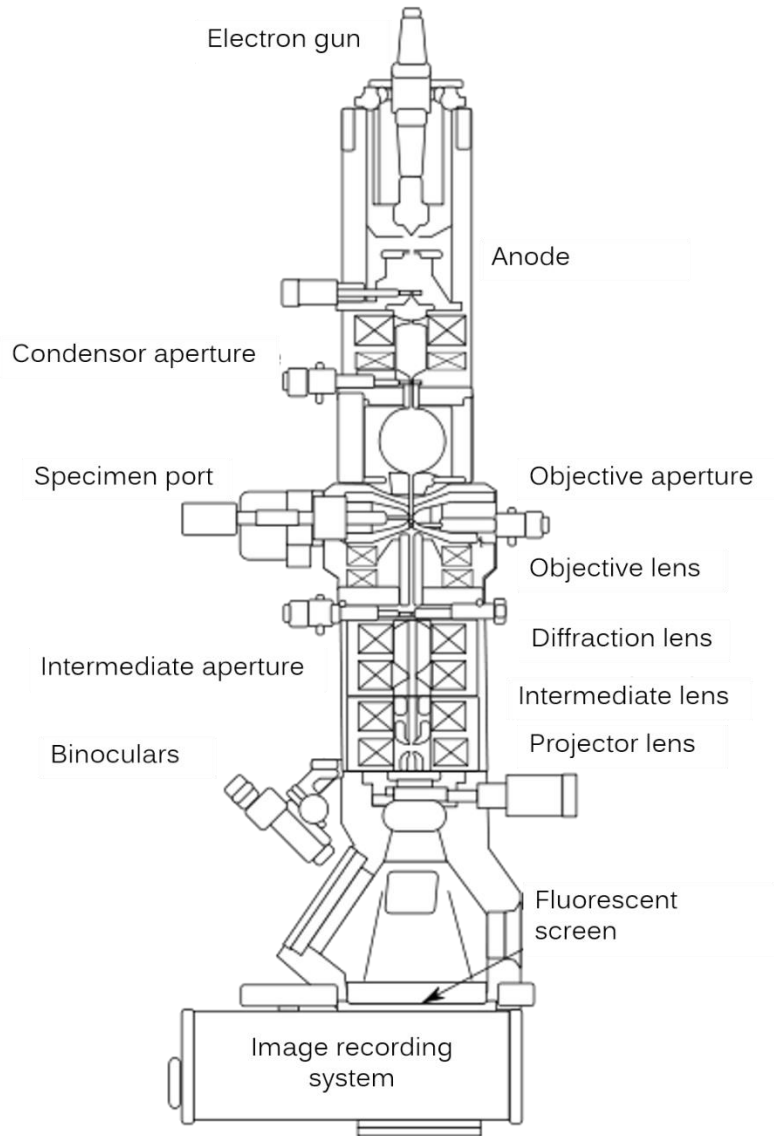


Figure 2.27: Schematic diagram of a SEM.<sup>111</sup>

### 2.2.5 Transmission Electron Microscopy (TEM)

Transmission electron microscopy is a powerful imaging technique used to investigate nanoscale samples based on the transmission of electrons throughout the sample. A schematic representation of a TEM microscope is depicted in Figure 2.28.<sup>111,112</sup> At the top of the vacuum column is placed the electron gun, this is commonly composed of a tungsten or a lanthanum hexaboride (LaB<sub>6</sub>) filament, that when heated by an electrical current, emits electrons via a process known as thermionic emission.<sup>111,112</sup> The electrons are then accelerated through a potential difference by a round anode plate through a series of electromagnetic lenses and apertures used to demagnify and control the beam diameter that hits the sample. The sample found space in the specimen chamber; a rod shaped sample holder, able to host the three millimetre TEM grid, is used to place the specimen in the path of the electrons.<sup>111,112</sup> The beam transmitted through the material is then focused and magnified by an objective lens, which forms a first intermediate image and a diffraction pattern; the switch between these two modes can be selected with the intermediate or the diffraction lens. Finally, the projector lenses are responsible for producing the final image on the TEM fluorescent screen, or in the CCD camera.<sup>111,112</sup>



The advantage Figure 2.28: Schematic representation of a TEM microscope.<sup>112</sup> in terms of resolution of the TEM with respect to a conventional optical microscope is attributed to the small wavelength of the electron.<sup>111,112</sup> Using an approximation of the De Broglie equation (Equation 2.11) is possible to compute the wavelength of the electron from their energy.

$$\lambda = 1.22/E^{1/2} \quad \text{Eq. 2.11}$$

Where  $E$  is the energy of the electrons that in a conventional TEM microscope can reach 200 KeV which results in a wavelength of  $2 \text{ pm} = 0.0002 \text{ nm}$ . Once this value is known it is possible, using the formula in equation 2.12, calculate the maximum achievable resolution ( $\delta$ ):

$$\delta = \frac{1.22\lambda}{\mu \sin \beta} \quad \text{Eq. 2.12}$$

Approximating the numerical aperture ( $\mu \cdot \sin \beta$ ) equal to one the maximum resolution becomes:

$$\delta = 1.22\lambda \cong 0.0024 \text{ nm} \quad \text{Eq. 2.13}$$

However, such small a resolution power is not really achievable, due to small imperfections of the electromagnetic lenses, used to focus the electron beam, as well as limitations attributed to the nature of the sample, its stability to the beam and its size. The major drawbacks of the TEM are the restrictions imposed on the nature of the sample and its size. Due to the necessity of a high vacuum within the column, and the presence of a high energy beam, conventional TEM are not suitable for the investigation of delicate samples, moreover, the transmission geometry limits the maximum thickness of the sample to 100 nm. <sup>111,112</sup>

### **Cathodoluminescence (CL)**

Cathodoluminescence is an electromagnetic phenomenon, which describes the emission of photons by a luminescent material upon interaction with electrons. Contrary to photoluminescence, in cathodoluminescence the luminescent centres are excited by the recombination of electron-hole pairs, and not by photons.<sup>113</sup> The consequence of this difference is reflected in the quantum efficiency of the techniques. Due to the incoming/outgoing photon mechanism, the maximum efficiency achievable with photo-luminescence is equal to 1; whereas for cathodoluminescence, the electron-photon mechanism allows a ratio between the emitted photon and the incident electron as high as  $10^3$ . <sup>113</sup>

### **Electron Energy Loss Spectroscopy (EELS)**

Electron energy loss spectroscopy is an analytical technique able to identify the chemical composition of a material, as a result of its interaction with an electron beam. The technique is

based on the detection of small differences in the kinetic energy of the transmitted electrons, generated by the inelastic scattering phenomena, arising from their encounter with the atoms in the specimen. A magnetic prism is used to divide the electrons in relation to their energy and focus them in the spectrometer where the signal is collected. Results are plotted in a graph which displays the number of electron versus their energy loss passing through the sample.<sup>111</sup>

### **2.2.6 Thermogravimetric analysis (TGA)**

The thermogravimetric analysis (TGA) is a thermal method used for the characterisation of the physio-chemical properties of materials. The analysis is based on changes of the sample weight as a function of increasing temperature.<sup>114</sup> A basic TGA instrument is composed of a precision balance and a furnace. The technique can provide useful information such as: vaporisation, decomposition, sublimation, absorption and desorption. The results are present in a graph, called thermogram, where the temperature is recorded against the weight of the sample or the percentage of weight loss.

# Experimental

# Chapter 3 : Organic Fluorescent Molecules in Polymeric Matrices

## 3.1 Introduction

Despite the recent development of novel optically active nanomaterials such as quantum dots, nanocrystals and metal nanoparticles which, led to efficient luminescent systems, organic fluorescent molecules are still the most used luminescent probes in numerous applications. The reason for their success is due to their physico-chemical properties, which include a broad range of absorption and emission wavelengths, low toxicity, high availability, and easy functionalisation.<sup>60,115</sup> Organic fluorescent molecules are mainly used in solution, but as several studies already demonstrated, these compounds can be dispersed into polymer matrices for the production of solid state lasers,<sup>116</sup> optical fibre amplifiers,<sup>117</sup> or biodegradable luminescent materials for bio-applications.<sup>118</sup>

In this chapter, the application of organic fluorescent molecules for the fabrication of colour conversion layers (CCLs), specifically designed for the conversion of blue and green OLEDs is presented. The organic dyes, Rhodamine 6G and fluorescein sodium salt, were dissolved into different polymeric matrices. Solid state, as well as solution processed methods, were used for the production of the fluorescent layers. The purpose was to fabricate flexible, thin and uniform optically active films with elevated transparency, and suitable luminescent properties for the conversion of the OLEDs emission. The spectral characteristics of these CCLs were studied by absorption and emission spectroscopy, and they were tested on top of blue and green OLEDs, that were kindly provided by the Holst Centre in The Netherlands.

## **3.2 Solid state CCLs**

Solid state colour conversion layers were produced using a three-step process, which included the extrusion, milling and compression moulding. Poly (methyl methacrylate) (PMMA), polystyrene (PS) and polycarbonate (PC) were chosen as matrices, by virtue of their optical and mechanical properties, particularly for their elevated transparency and flexibility. Rhodamine 6G was selected as a fluorescent molecule for the down-conversion, as a consequence of its high optical, chemical and thermal stability, suitable absorption and emission properties, as well as for its elevated quantum efficiency.

### **3.2.1 Materials and Methods**

Thermoplastic polymer granules of poly (methyl methacrylate) (PMMA), polystyrene (PS), and polycarbonate (PC) were obtained from Covestro (ex Bayer), and rhodamine 6G 95% (CAS: 989-38-8) was purchased from Sigma Aldrich. All the materials were used without any further purification. PMMA, PS or PC granules were mixed with rhodamine 6G using a 0.5% weight to weight ratios of dye into polymers. Once the fluorescent powder was suitably homogenised with the polymer, the mixture was processed by extrusion (Thermo Scientific Haake Minilab) at a temperature between 170 and 240°C; this being dependant of the type of polymer used. The fluorescent ribbons obtained from the extruder, were subsequently cut and milled in powder form, before being shaped into thin sheets by compression moulding (Moore & Son Birmingham).

### 3.2.2 Results

The solid state processed colour conversion layers containing rhodamine 6G are presented in Figure 3.1. A substantial difference in the solubility of the dye, and consequently, in the optical properties of the layers, were observed when the polymer matrices were exchanged between PMMA, PC and PS. The incorporation of the organic fluorescent molecule shows good compatibility with the polystyrene or polycarbonate matrices. The layers obtained from these combinations resulted in a uniform distribution of rhodamine with only minimal aggregation phenomena. Contrary results have been observed for the samples prepared with poly (methyl methacrylate). In this case, miscibility of the two organic components (PMMA and rhodamine) was poor, and the layers produced by this combination presented a dark red colouration, which suggested the preponderant presence of crystalline non-emissive aggregates of rhodamine (first disc in Figure 3.1).



Figure 3.1: Thermoplastic polymer discs containing 0.5% w/w of rhodamine 6G, (from left to right: PMMA, PS and PC).

With the help of the Holst Centre, the colour conversion capability of the CCLs produced by dispersion of rhodamine in the polystyrene or polycarbonate matrices were tested on top of green OLEDs (Figure 3.2). The results obtained, showed that both these layers were able to down-convert the light emitted by the electroluminescent device. However, despite the fluorescent molecule used for the conversion being the same, significant differences were

observed in the final colours of the OLED upon variation of the polymer matrix. Superimposing the luminescent polycarbonate disc on a green OLED, the colour of the device changed from the original green to a yellow-orange appearance (top-right image in Figure 3.2), whereas, applying the rhodamine-containing polystyrene layer, the final colour of the down-converted OLED resulted in an almost pure red (bottom image in Figure 3.2). These variations in the optical properties are attributed to the chemical differences between the polymer matrices, and in particular, to the miscibility of rhodamine in the polystyrene and polycarbonate. It is well known that shifts in the emission of rhodamine 6G toward the red region of the electroluminescent spectrum are an indication of the presence of dye aggregates or dimers, which are often associated with a decrease of the luminescence efficiency of the dyes as a result of self-quenching phenomena.<sup>119–121</sup>

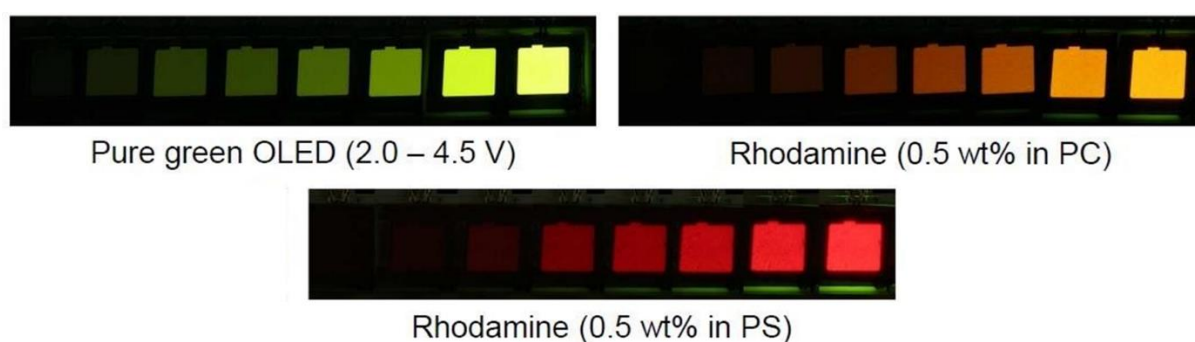


Figure 3.2: Pure emission of a green OLED at various voltages and the results obtained with the PC and PS layers.

The major drawback of these layers was represented by the low amount of rhodamine that can be solubilised in the polymer matrices, without incurring strong aggregation phenomena. Indeed, in order to efficiently down-convert the green emission generated by the OLEDs, thick layers had to be produced to incorporate a sufficient amount of fluorescent molecules. As a result of that, the polymer sheets showed problems in terms of mechanical properties,

particularly concerning their flexibility; their substantial size resulted in an excessive stiffness, which precluded their application as colour converting layers for flexible OLEDs.

### **3.3 Solution processed layers**

Solution processed CCLs, based on the use of acrylic latex as a matrix for the organic molecules, were developed to overcome the problem related to the lack of flexibility, which characterised the polymer layers produced by the solid state method. The change in the chemical nature of the layer's matrix was necessary to prevent damage to the surface of the flexible OLEDs. Indeed, despite the thermoplastic polymers employed previously (PMMA, PC and PS) that can be processed in solution, they require the use of strong solvents, such as tetrahydrofuran (THF), dichloromethane (DCM) and toluene, which can negatively affect the lifetime of the OLEDs thus damaging the protective layer of the devices, and consequently reducing its impermeability to oxygen and moisture.

On the contrary, the use of a water-based acrylic latex, not only prevents the development of such a problem, but it also allows for a facile dissolution of a larger number of organic dyes. In addition, acrylic latex can be directly applied on the OLEDs as a top layer by spray painting, brushing or screen printing techniques. In this section, the application of a commercially available acrylic latex as a matrix for the fabrication of CCLs is investigated. The layers produced by the combination of the latex with rhodamine 6G and fluorescein sodium salt were tested on actual OLEDs, and optically characterised by emission spectroscopy.

#### **3.3.1 Materials and Methods**

The water-based acrylic latex was produced by Vallejo under the name gloss acrylic varnish, rhodamine 6G 95% (CAS: 989-38-8) and Fluorescein sodium salt 98.5-100.5% (CAS: 518-47-

8) were bought from Sigma Aldrich. All the materials were used without further purification. The organic dyes were mixed with the acrylic latex solution in glass vials with ratios of 0.25, 0.5 and 0.75% w/w. The vials were then capped and hand-shaken to promote dissolution of the fluorescent molecules. The dye-containing latex was deposited on the surface of the OLEDs by screen printing to produce uniform layers. Paint brushing was also employed for the fabrication of layers with variable thickness designed to produce colour gradient effects.

### **3.3.2 Results**

The emission properties of the layers were analysed with a Horiba Fluorolog Jobin Yvon iHR320 fluorimeter. Those containing rhodamine were excited with blue light (488 nm) and the emission spectra were collected from 500 to 750 nm. The results are presented in Figure 3.3. The emission of rhodamine dispersed into the acrylic latex with the lowest concentration (0.25% w/w) resembles the fluorescent signal of rhodamine in solution; its spectrum is characterised by a main peak centred at ~555 nm followed by a shoulder at 600 nm. Increasing the dye concentration in the latex film (0.5% w/w) results in a red shift, and a broadening of the emission. The main signal for this sample is centred at 575 nm, and the shoulder appears more intense and shifted to 625 nm. These changes suggest that aggregation phenomena and formation of dimers are occurring as a result of the amount of rhodamine being doubled from 0.25% to 0.5% w/w. Such behaviour is even more evident for the acrylic layer containing a 0.75% w/w of the fluorescent molecule. The emission of this sample was significantly lower than those recorded for the 0.25 and 0.5% samples. The spectral positions of the main emission and the shoulder are the same as those observed for the sample with a 0.5% w/w of rhodamine, but the relative intensity of these two features appears changed with the shoulder almost equal in intensity to the main emission. The presence of aggregation phenomena in the highest

concentrated sample is evident, and can also be confirmed by a visual inspection of the sample, since the presence of dark spots scattered across the acrylic film is visible to the naked eye. These non-emissive crystalline aggregates, cannot be detected in the liquid suspension, and therefore, their formation has to occur during the drying process, as a result of the supersaturation of rhodamine, produced by the evaporation of the water.

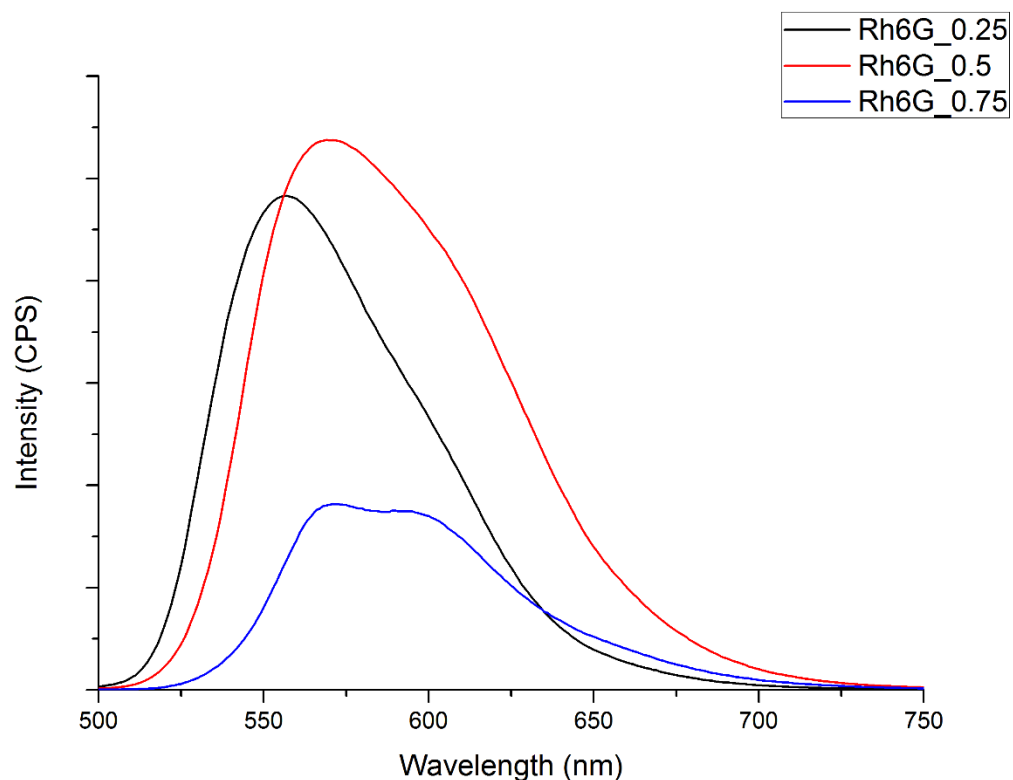


Figure 3.3: Emission of rhodamine 6G dissolved in the acrylic varnish.

The emission spectra obtained from the acrylic layers containing fluorescein are shown in Figure 3.4. In this case, the excitation monochromator of the fluorimeter was set to 460 nm, and the emission was collected from 475 to 700 nm. Similar to the rhodamine layers, changes in the optical properties, as a result of the increased concentration of dye in the acrylic matrix, were observed for fluorescein. The sample fabricated with a 0.25% of dye into the acrylic latex matrix presented an emission maximum centred at 519 nm, which closely resembles the

characteristic green signal at 515 nm of fluorescein in solution. Increasing the weight to weight ratio of fluorescein to 0.5%, resulted in a noticeable red shift in the emission of the dye, and a broadening of the peak. The shift is quantifiable to 6 nm with the 0.5% sample presenting the maximum at 525 nm. Further loading of fluorescein into the acrylic latex, as already observed for rhodamine, led to a steep decrease in the intensity of the signal due to self-quenching. However, no visible aggregates can be observed in the layer formed with fluorescein.

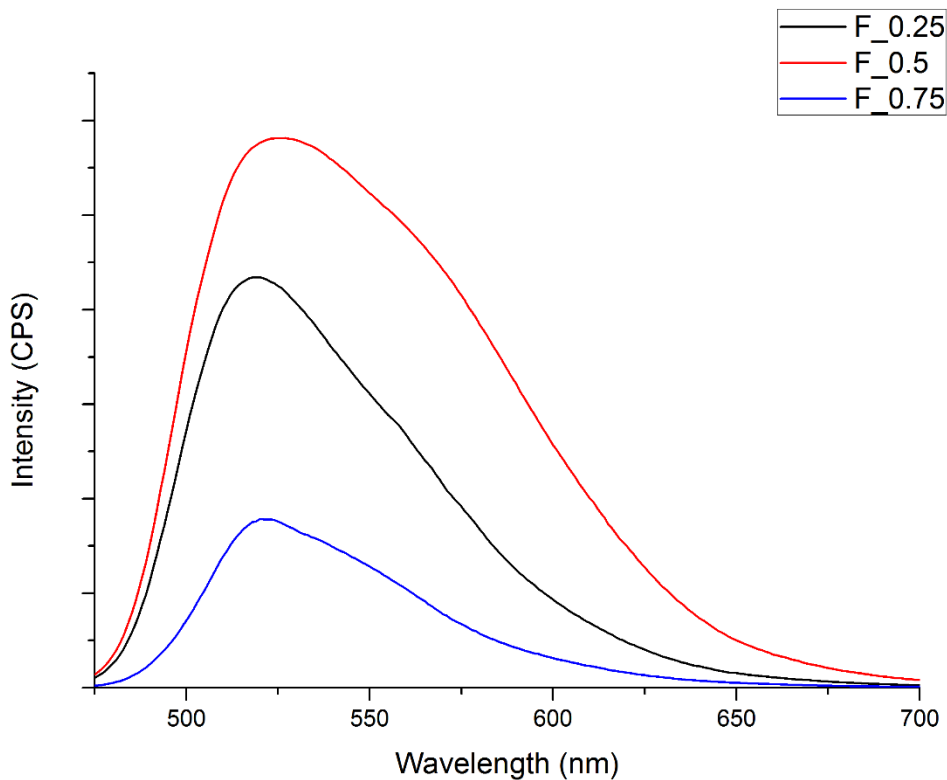


Figure 3.4: Emission of fluorescein sodium salt dispersed in the acrylic varnish.

The colour conversion capabilities of these layers were tested on top of blue and green OLEDs, kindly provided by one of our partners in the project: the Holst Centre in The Netherlands. The analysis was performed with a portable spectrophotometer Jeti specbos 1200 able to collect the emission spectra from 380 to 780 nm. The emission of the OLEDs, and the emission resulting from their down-conversion were collected with the same parameters, with the exception of

the exposure that was set in automatic mode by the spectrophotometer; the voltage applied to the OLED was set to 5V. The results for the unmodified blue OLED and the device converted with the layers containing fluorescein are presented in Figure 3.5.

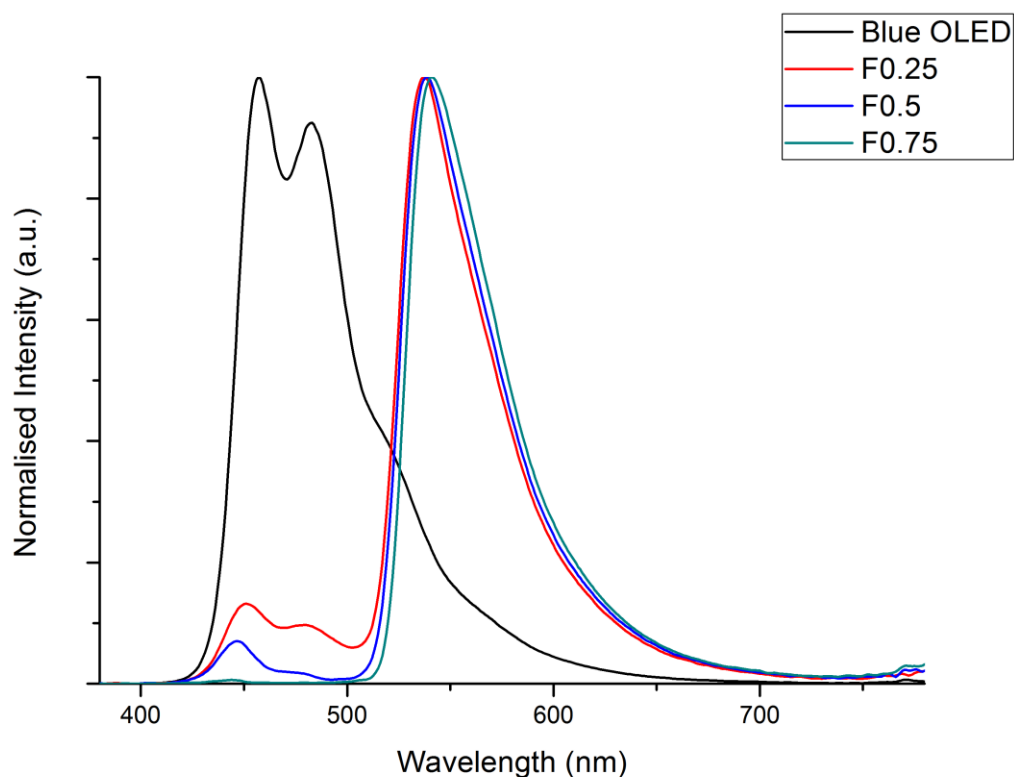


Figure 3.5: Emission of pure blue OLED and the spectra obtained as a result of the down-conversion of the device with the fluorescein containing acrylic layers.

The emission of the pristine OLED is characterised by the presence of two distinct peaks, with maxima at 457 and 482 nm, and the presence of a shoulder around 525 nm. Upon application of the acrylic layers containing fluorescein, the blue peaks native for the device disappear and a green signal, with a maximum at ~550 nm is observable. Some reminiscence of the blue light emitted by the OLED is, however, still visible in the spectra, particularly for the samples loaded with 0.25 and 0.5% w/w of fluorescein. The final emission of the down-converted device

differs slightly from the emission of the layers recorded on the fluorolog. The reason for such a discrepancy can be associated with variations in the calibration of the two instruments, or more probably, it is the result of the combination of colours between the OLED light and the down-converted light generated by the layers. The result obtained from the application of the rhodamine-containing layers on a blue OLED are visible in Figure 3.6. Despite rhodamine being more suitable for the conversion of green light, modifications of the blue light emitted by the OLED, are however, possible. As can be seen from the spectra, the rhodamine-acrylic layers were able to absorb the OLED emission at 482 nm and leave unaltered the peak at the lower wavelength (457 nm). This results in a double emission characterised by two distinct peaks in the blue and red region of the electromagnetic spectrum.

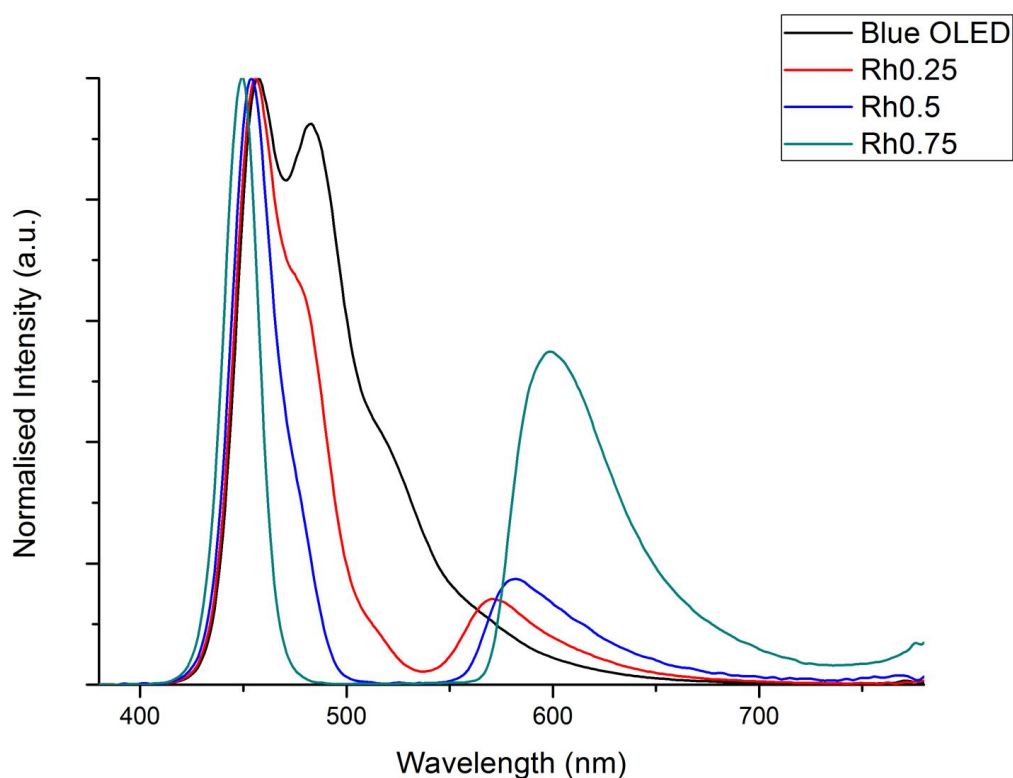


Figure 3.6: Down-conversion of a blue OLED with the acrylic layers containing rhodamine 6G.

A visual representation of the layers on top of the blue OLED is shown in Figure 3.7; in agreement with the result obtained with the portable spectrophotometer, the colour of the OLED, as a result of the application of the fluorescein layer is completely down-converted into an almost pure green. On the contrary, the rhodamine-containing layer applied on the blue device led to the production of a purple colour, as a result of the partial conversion of the OLED, and the combination of the residual blue emission with the orange-red emission, generated by the CCLs.



Figure 3.7: Conversion of a blue OLED (left) with the acrylic layers composed of fluorescein (middle) and rhodamine (right).

The acrylic CCLs with rhodamine were also used for the conversion of green OLEDs. The spectra of the pristine green device and the results obtained with the down-conversion are shown in Figure 3.8. The output of the pristine OLEDs is characterised by a broad emission with a maximum at 540 nm; as a result of the application of the dyed-layers, the emission of the device was converted into an orange-red appearance. Similarly, to that observed for the blue OLED, the layers with a dye content of 0.25 and 0.5% w/w let escape a small part of the original green emission of the OLED, but increasing the amount of rhodamine to 0.75%, resulted in a complete conversion.

The comparison between the appearance of the pristine emission of the OLED, and the result obtained by application of the CCLs is depicted in Figure 3.9. The change in colour as a consequence of the superimposition of the acrylic layer on the green OLED is evident, but less

drastic than the result obtained for the blue OLED due to the partial overlap between the emission of the device, and the emission of rhodamine.

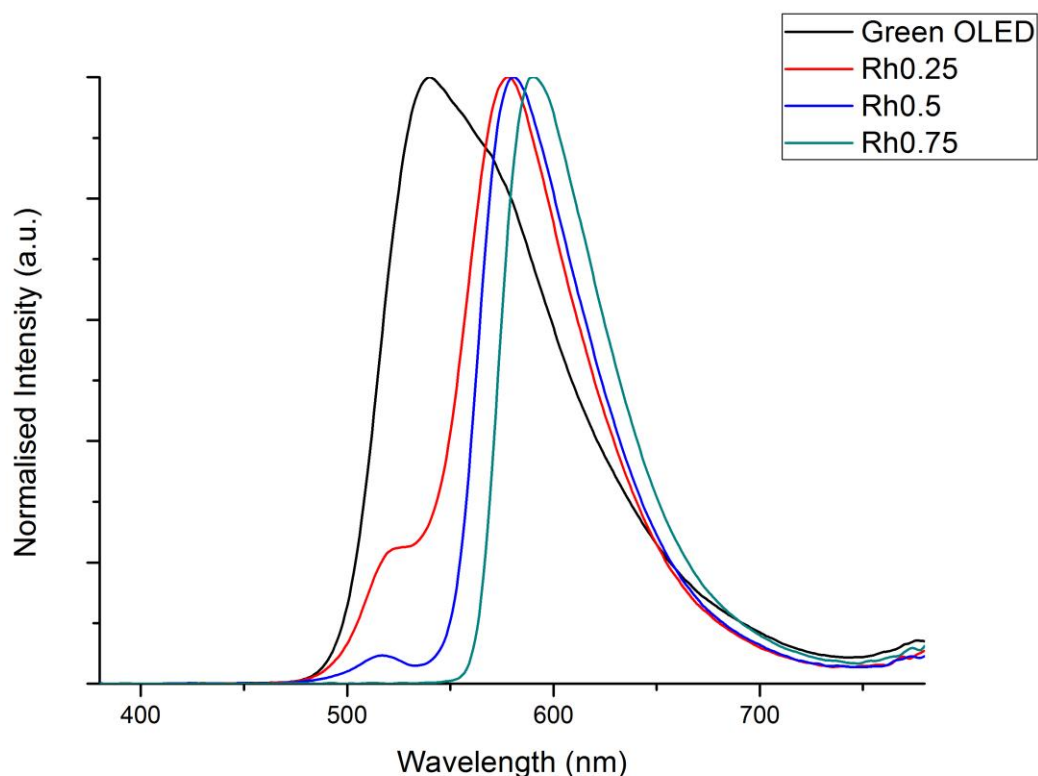


Figure 3.8: Emission spectra of a pure green OLED and the emission achieved by down-conversion with the rhodamine in the acrylic matrix.



Figure 3.9: Photographs of a pure green OLED (left) and the device down-converted with the 0.5% rhodamine layer (right).

The layers used for the characterisation of the optical properties were produced by screen printing, in order to ensure the maximum homogeneity in terms of thickness, however, deposition of these CCLs by paint brushing is also possible, and allow creation of colour effects

otherwise impossible to achieve with other techniques. An example of a colour gradient effect, obtained by brushing the dyed acrylic latex on the substrate of the OLEDs, is given in Figure 3.10.



Figure 3.10: Colour gradient effects on blue OLEDs achieved by brush painting the fluorescein (left) and rhodamine (right) acrylic layers.

The gradient effects on a blue OLED were created by varying the thickness of the films by application of multiple coatings of the acrylic latex containing respectively, fluorescein (left) or rhodamine (right). Similar results can also be achieved by spray painting; this alternative method has been considered, but the results obtained were not satisfactory. Drops of coating were formed as a result of the water-repellent properties of the OLED substrate, a phenomenon aggravated by the necessity to dilute the acrylic media with water in order to make it suitable for the use in the spray gun.

In addition to the suitable optical properties demonstrated above, these layers possess an elevated degree of flexibility, a key requirement for their application as colour converting layers. These advantages, along with the facile and direct application on the device's surface, made them the material of choice for the down-conversion of the OLEDs. Samples of this material were sent to the designers, and were used in the fabrication of prototypes. An example of a final product is shown in Figure 3.11, where the fluorescent acrylic coating was used to modify the emission of a green OLED used in the development of a pair of luminescent headphones (MeLite) designed by Pilotfish.



Figure 3.11: MeLite by Pilotfish; luminescent headphone consisting of a green OLED down-converted with the acrylic-rhodamine coating.

### 3.4 Discussion

The dispersion of fluorescent organic dye, rhodamine, in polymeric matrices, PMMA, PC and PS by solid state processing have been only partially successful. The results showed that despite rhodamine being able to withstand the temperature required for the process, its solubility is limited. This led to the production of layers with an excessive thickness, which compromised their use as colour conversion layers for flexible blue and green OLEDs. An alternative was found in the use of an acrylic coating and, specifically a water-based acrylic latex. The water-based nature was an ideal environment for the dissolution of fluorescent dyes, like fluorescein sodium salt and rhodamine 6G. The optical properties of the dye dispersed into the acrylic layers were investigated by fluorescence spectroscopy, and the colour conversion capabilities of the layers were tested on top of blue and green OLEDs. The results showed that the presence of the acrylic matrix has no effect on the emission of the dyes. The concentration, however, has to be limited, ideally to 0.5% for both fluorescein and rhodamine, in order to avoid the

occurrence of aggregation phenomena. The biggest advantage of these layers was the lack of aggressive solvents, which allows for the deposition of the coating directly on the surface of the OLEDs, without the need for any additional steps. Moreover, this approach allows for the production of layers with the required optical and mechanical properties; the flexibility and transparency of the acrylic latex are, indeed, ideal for the use of these materials as a matrix for the colour conversion layers. In addition, the dye-embedded acrylic solutions can be deposited by different techniques; screen printing was employed to obtain uniform and homogeneous layers, whereas paint brushing was used to create unique colour gradient effect by varying the layer thickness.

### **3.5 Conclusions**

In this section, the preparation and characterisation of colour conversion layers for blue and green OLEDs, based on the use of fluorescent dyes dispersed in polymer matrices, is presented. The best results were achieved by a combination of the organic molecules with a commercially available acrylic latex. The layers produced in this way have been demonstrated to be easy to apply and very effective in terms of down-conversion. The water-based nature of the acrylic matrix, not only was ideal for the dyes dissolution but, it also allows for the deposition of the coating directly on the surface of the OLEDs without the need for any additional steps. Moreover, the lack of organic solvents also prevents the development of odours. In addition, the matrix flexibility and transparency have been found to be ideal for their use as colour conversion layers. Finally, we investigated two approaches for the deposition of these acrylic layers. Screen printing was used to obtain uniform and homogeneous films, whereas brushing was employed to create unique colour gradient effects by varying the layer thickness. These layers were well received by the designer teams participating in the project, and they were used

for the fabrication of the prototype showcased during the final Light.Touch.Matters meeting in Delft.

# Chapter 4 : Fluorescent silicone layers

## 4.1 Introduction

Since their discovery polyorganosiloxanes (silicones) have been used in a wide range of applications as a consequence of their physico-chemical properties, which include high transparency, impermeability to water, and the absence of ageing upon reaction with oxygen.<sup>57</sup> These characteristics, along with an elevated flexibility and the absence of toxicity, make silicones ideal candidates as a material for the matrix in the fabrication of Colour Conversion Layers (CCLs) for OLEDs. These advantages are, however, counterbalanced by an important limitation: silicones are not compatible with organic dyes. Contrary to inorganic phosphors, quantum dots and nanodiamonds, the organic dyes need to be solubilised in order to be converted from their crystalline non-emissive form into the single molecule fluorescent form. Owing to the inert chemical nature of the silicones this is not possible, and consequently, the dispersion of the dye into the matrix will result in the production of layers, with limited or no optical properties. This problem can be overcome by the use of inorganic supporting materials, which act as a carrier for the organic molecules. The dye molecules can be solubilised and absorbed into the pores or cavities of the supporting materials. This will lead to the formation of fluorescent powders, that as a result of their organic-inorganic combination are commonly defined as hybrid organic-inorganic materials.<sup>122</sup> These fluorescent hybrids can be treated as luminescent particles, allowing the dispersion of the dyes into non-compatible matrices. Fluorescent hybrid materials have been proven to solve or limit most of the drawbacks of the organic dyes. Studies have demonstrated that impregnation of the fluorescent organic molecule into porous materials helped to prevent self-quenching phenomena. In addition, this

combination has beneficial effects on the chemical and optical stability of the dyes, and might result in an increase in the quantum efficiency of the luminescent species.<sup>123–126</sup>

The production of these hybrid organic-inorganic compounds can be achieved with several procedures; a common route, for silica-based hybrids, consists in the synthesis of silica particles within a solution containing the organic molecules. In this case, the fluorescent dyes need to be soluble in the synthesis media of the inorganic framework without affecting its formation or suffering from degradation itself. Once the synthesis is completed the organic molecules are trapped within the inorganic materials, and isolated from the external environment.<sup>127,128</sup> An alternative and opposite approach, consists in the synthesis of the fluorescent molecules within the pores of an existing supporting material, *via* a method called “*ship-in-a-bottle*”. The chemical precursors for the synthesis of the dye are initially absorbed in the porous material, where they react to form the final luminescent molecules.<sup>69</sup> Both these methods have been proven to work successfully, but they require relatively long synthesis and purification steps. A simpler and equally effective way to produce fluorescent hybrids is based on the impregnation of the organic dyes in the pores, or cavities of porous materials *via* solvent evaporation methods.<sup>121,124,126,129,130</sup> This procedure can be easily scaled-up, since contrary to the previously described approaches, it does not require any purification or synthetic procedures.

Hereafter, we investigate the impregnation approach to obtain hybrid fluorescent materials based on the absorption of organic dyes, specifically rhodamine 6G and fluorescein disodium salt, in amorphous silica gel and Faujasite type Y zeolite. The formation of these hybrid organic-inorganic composites allows for the dispersion of the fluorescent dyes into a thermosetting silicone rubber, chosen as the matrix for the production of the colour conversion layers (CCLs) for blue and green OLEDs. The optical properties of the CCLs were investigated by UV/Visible absorption and emission spectroscopy. In addition, the quantum yield of the

dyes in the inorganic matrix was measured and compared to the dye in solution, by use of the Quanta-Phi apparatus coupled with the fluorimeter. For some of the samples, we observed the development of peculiar optical properties, arising from the dye encapsulation inside the cavities of the Faujasite crystal, which will be discussed in a separate chapter of this thesis (Chapter 5).

## 4.2 Materials

Rhodamine 6G 95% (CAS: 989-38-8), fluorescein sodium salt 98.5-100.5% (CAS: 518-47-8), silica gel pore size 60 Å (CAS: 112926-00-8) and spectroscopic grade ethanol (CAS: 64-17-5) were purchased from Sigma Aldrich, hydrogen-containing Faujasite Y zeolite (CAS: 1318-02-1) was sourced from Alfa Aesar and the bi-component thermosetting silicone was produced and obtained by Wacker under the name Silgel 612. All the materials were used as received without any further purification.

## 4.3 Sample preparation

Rhodamine 6G and fluorescein disodium salt were absorbed inside the porous matrices via a solvent evaporation method; two stock solutions were initially prepared by dissolving the dyes in spectroscopic ethanol with a concentration of 1 mg/ml. Twenty glass vials each containing 250 mg of protonated Faujasite type Y zeolite (HY), or silica gel were set. To these were subsequently added 1, 0.8, 0.6, 0.4 and 0.2 ml of fluorescein, or rhodamine solutions, in order to obtain a loading of between 0.1 and 0.5% w/w of dye in the supporting material. The final volumes in the vials were made up to at 2 ml using spectroscopic ethanol, this was to ensure a uniform absorption of the organic molecules in the pores and cavities of the supporting materials. The solvent was allowed to evaporate at room temperature by leaving the vials open.

Once the solvent evaporated, 40 mg of dye-impregnated zeolite or silica were weighed in disposable plastic containers, and mixed with 8 g of previously blended bi-component (Silgel 612 A and B) thermosetting silicone. Samples were then homogenised with a spatula, poured inside fluorescence PMMA cuvettes and cured at 70° C on a hot plate for 2 hours. Blank samples of the supporting materials embedded in the siloxane matrix in absence of the fluorescent molecules were produced following the same procedure; reference solutions of the dyes in water, or spectroscopic ethanol, were prepared by diluting the stock solutions in order to obtain rhodamine or fluorescein concentrations comparable to the solid samples.

The samples were named starting with the initial of the supporting material (Si for silica and Y for Faujasite zeolite) followed by a number indicating the percentage of dye absorbed in the framework, and the initial of the dye, R for rhodamine 6G and F for fluorescein.

## **4.4 Results**

### **4.4.1 Rhodamine 6G**

The analysis of the absorption properties of rhodamine 6G impregnated in the supporting materials was conducted with a Perking Elmer Lambda 650s UV/VIS spectrophotometer; absorbance was recorded from 400 to 600 nm with a step size of 1 nm. The spectra of the dye impregnated in the supporting materials (silica gel and HY zeolite), and subsequently embedded in the silicone matrix were compared with those of the dye in a solution of spectroscopic ethanol or water.

The results of the dye in water or ethanol solutions, and impregnated into silica gel and dispersed in silicone are shown in Figure 4.1. The spectra for the liquid samples shows marginal differences in the absorption profile of rhodamine in water and ethanol. The difference in the position of the absorption maxima between the solvents is measurable in 6 nm; such

discrepancy is to ascribe to the nature of the solution in which the molecule is dissolved, as previously reported by Reisfeld *et al.*<sup>131</sup>. The absorption spectra of the dye impregnated into silica and subsequently dispersed in silicone, match the result obtained for the ethanol solution with the presence of two peaks: a maximum centred at 533 nm and a small shoulder around 500 nm.

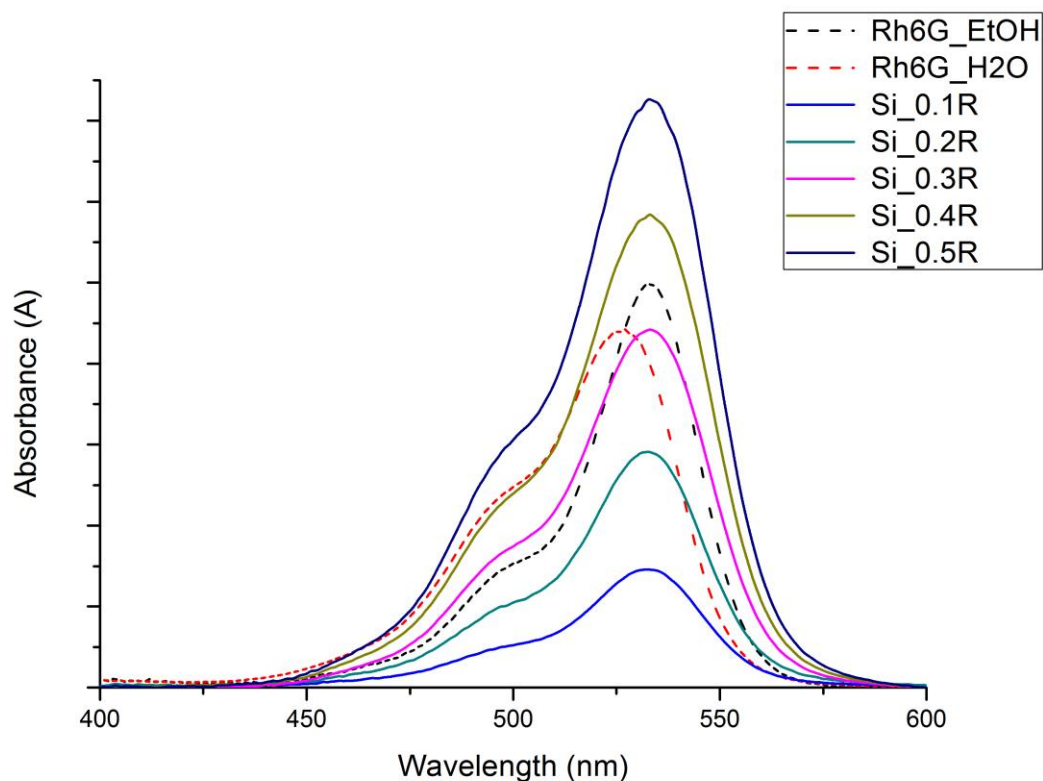


Figure 4.1: Absorption of rhodamine encapsulated in silica gel and dispersed in silicone rubber versus the dye in ethanol solution.

No significant modifications in the absorption spectra of rhodamine were encountered when the supporting material was changed from silica to Faujasite. The results for the dye impregnated into the zeolite (Figure 4.2) show similar optical characteristics to those observed for the dye contained in silica with only a marginal variation in the position of the maxima. The absorption for rhodamine into zeolite results in peaks with maxima centred at 530 nm,

their position between the spectra of the dye in water and ethanol solutions, suggests the coexistence of both solvents within the crystals structure of the zeolite. This can be explained by the high affinity of the aluminosilicate for water, which may have been absorbed within the crystals during the sample preparation.

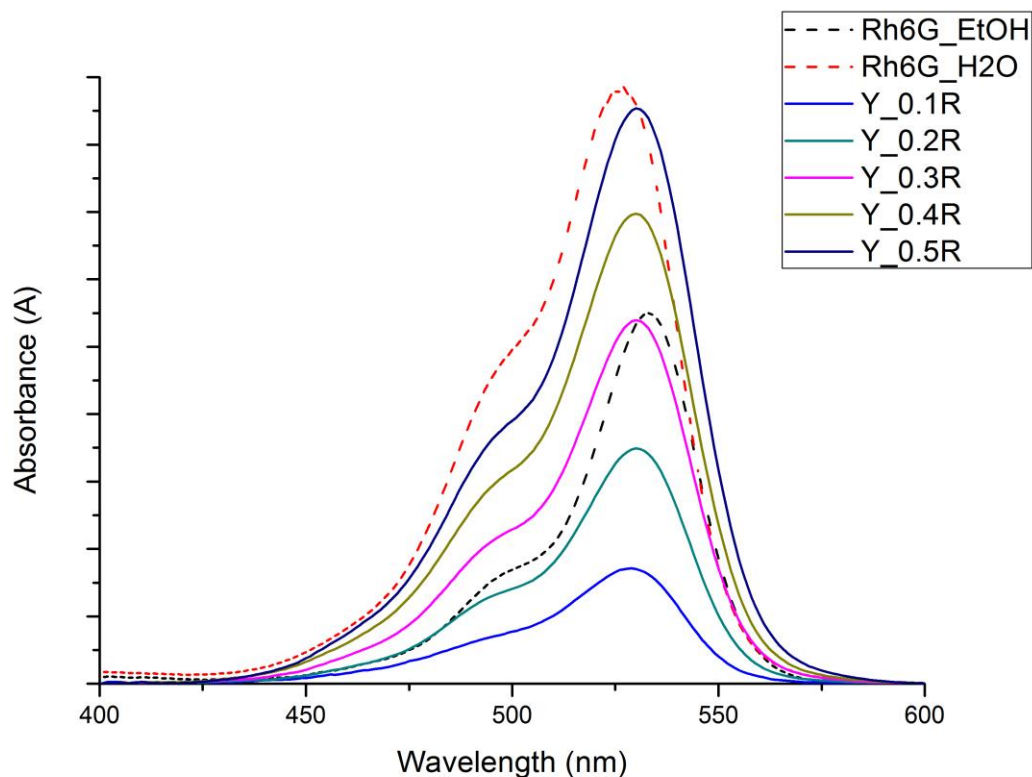


Figure 4.2: Absorption spectra of rhodamine 6G in zeolite and silicone rubber against reference solutions of the dye in water and ethanol.

The emission of rhodamine in the supporting materials was investigated with a Horiba Fluorolog Jobin Yvon iHR320 fluorimeter operating in front face mode. The excitation was set at 460 nm, and the emission was collected from 465 to 650 nm, with a step size of 1 nm, and an integration time of 0.1s. As for the absorption measurements, the emission spectra of the samples in solid form were compared to the fluorescence signals of the molecule in water or ethanol solutions.

Figure 4.3 represents the emission spectra for the dye trapped in silica. The data shows that, when a low concentration of rhodamine is impregnated into the pores of silica (0.1 and 0.2% w/w), the fluorescent signal of the hybrid materials match, almost perfectly, the emission of the dye in water or ethanol solutions with a maximum at 554 nm. Only when the amount of rhodamine was increased above 0.3 % w/w, did the spectra for of the solid sample show a red shift compared to the solutions. Such a discrepancy, between the solid and the liquid samples, reaches its maximum at the highest loading of dye (0.5 % w/w) with a difference of only 8 nm. Similar behaviours, have already been observed and reported in the literature for comparable systems, and they have been explained by various factors including the occurrence of re-absorption phenomena, caused by the high content of dye, or changes in the environment, due to the confinement effect, or as a consequence of the emission from aggregates.<sup>132–135</sup>

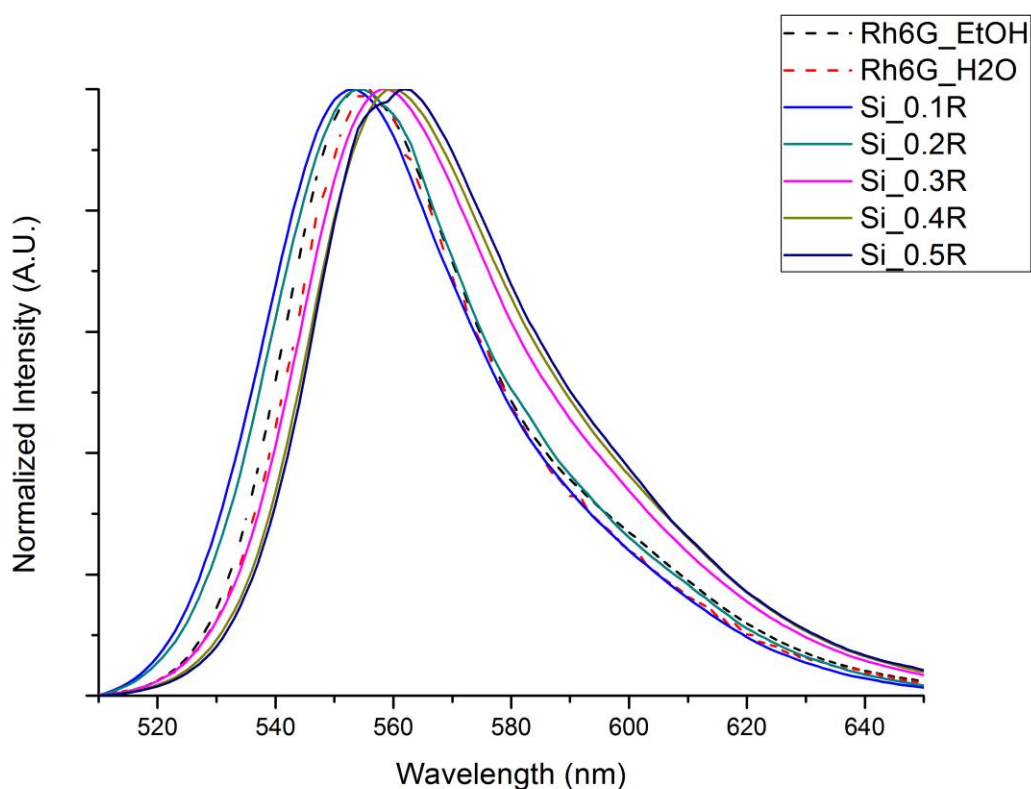


Figure 4.3: Normalised emission of rhodamine 6G absorbed in silica gel and embedded in silicone compared to the emission of the molecule in ethanol or water solutions.

The influence of the supporting material on the emission properties of the dye is further confirmed by the results obtained from the impregnation of rhodamine into the cavities of Faujasite (Figure 4.4). Contrary to what was observed for silica, when the dye is absorbed into the aluminosilicate, its emission resulted in being slightly blue shifted compared to those recorded for the ethanol or water solutions. The blue shift is more evident for the sample with the lowest content of dye (0.1 % w/w), and it attenuates when the amount of the dye into the zeolite is increased, matching the emission of the solution when the dye content is 0.5 % w/w.

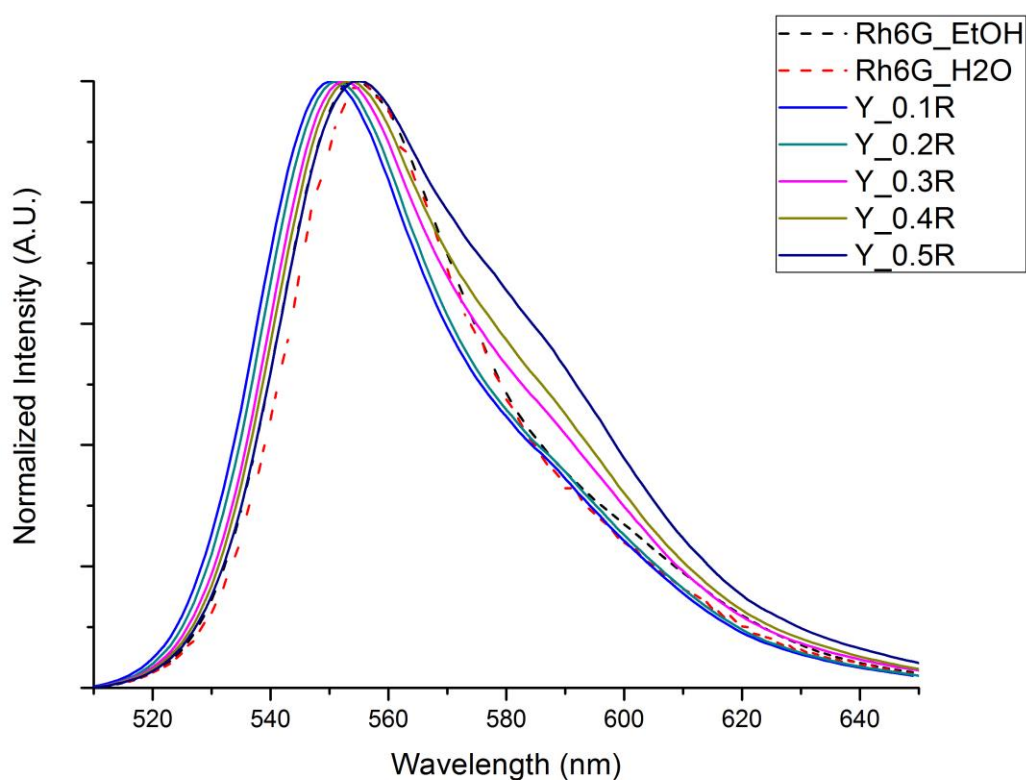


Figure 4.4: Normalised emission of rhodamine 6G in zeolite and silicone rubber against the dye in ethanol or water solutions.

The blue shift of rhodamine can be justified by taking into consideration the size of the organic molecule ( $\sim 1$  nm),<sup>136</sup> and the size of the cavities of the zeolite ( $\sim 1$  nm). This similarity might

prevent the formation of aggregates or dimers into the cavities of the supporting material, known to promote red shift in the emission of fluorescent organic molecules.<sup>132–135</sup>

The quantum yields (QYs) of these fluorescent silicone layers were investigated on the fluorimeter, using the integrating sphere produced by Horiba under the name Quanta-phi. Samples were excited at 480 nm and compared with blank samples of silica or zeolite. The results for the rhodamine 6G trapped into the silica gel and embedded into silicone are listed in Table 2. The QY values measured for the rhodamine layer resulted in being lower than the quantum yield, documented in the literature for rhodamine dissolved in a solution of ethanol (95 %).<sup>137</sup> The maximum value (76.30 %) was recorded for the sample containing 0.1 % of dye into silica, and this percentage dropped to 53.62 % when the amount of rhodamine was increased to 0.5 %.

Table 2: Quantum yield (QY) of rhodamine 6G impregnated in silica gel and embedded in silicone.

Sample	Quantum Yield (QY) (%)
Si_0.1R	76.30
Si_0.2R	76.14
Si_0.3R	59.33
Si_0.4R	54.78
Si_0.5R	53.62

A significantly lower quantum efficiency was observed for Rhodamine absorbed into the cavities of the HY zeolite (Table 3). The highest value, recorded for the sample with the lowest concentration of dye (0.1 % w/w), is only half of the quantum yield reported in the literature, for rhodamine 6G. Such a low efficiency might be attributable to the similarity between the size of the organic molecule and the cavities of the aluminosilicate. The steric reason might,

prevent the access of rhodamine within the zeolite framework; the excess dye is unable to be absorbed, and sitting on the surface of the crystals will be in contact with the non-miscible environment of the silicone; forming non-emissive aggregates which will affect the quantum yield of the hybrid material.

Table 3: Quantum yield of rhodamine 6G impregnated into the zeolite and embedded in silicone

Sample	Quantum Yield (%)
Y_0.1R	54.81
Y_0.2R	54.57
Y_0.3R	41.74
Y_0.4R	30.49
Y_0.5R	18.08

The colour conversion properties of the rhodamine-containing silicone layers were tested on top of blue and green OLEDs. These were kindly provided by one of our project partners; the Holst Centre. Preliminary investigations were performed placing the cuvettes on top of the OLEDs. These demonstrate that, although the best results in terms of quantum yield were obtained for the low concentration samples, the amount of dye in the porous materials need to be at least 0.5 % w/w, to achieve a noticeable down-conversion of the emission of the OLEDs. Moreover, a higher ratio of supporting material within the silicone matrix was needed to prevent the transmission of the device colour through the layers. New silicone layers, composed of silica gel impregnated with rhodamine, were therefore, produced. The dye/supporting materials ratio was fixed at 0.5%, and the silicone/silica gel ratio was incremented to 2, 4 and 6%; the casting and curing of the layers were performed directly on the same material used to fabricate the OLEDs.

The OLEDs were connected to a voltmeter set at 5V, and the spectral responses of the pristine and converted panels were collected with a portable spectrophotometer Jeti specbos 1200; able to record the output signal within a range of wavelength from 380 to 780 nm.

The results obtained for the blue OLED, with and without the layers, are depicted in Figure 4.5.

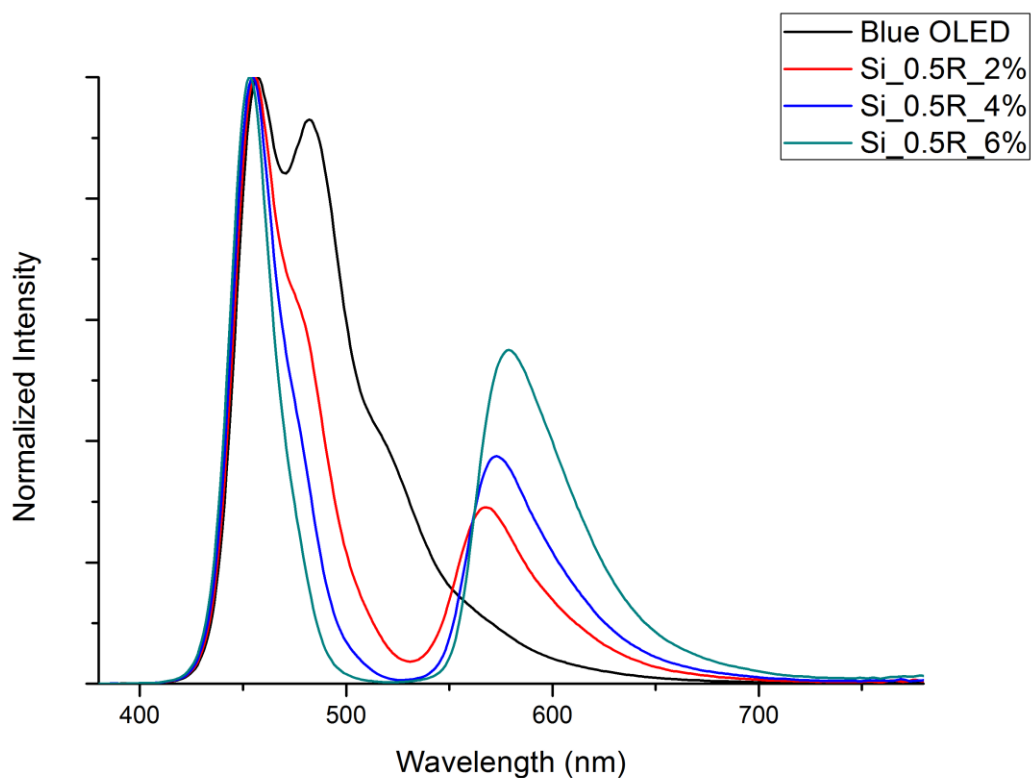


Figure 4.5: Emission spectra for a pristine blue OLED (black) and for the panel converted with the silicone layers containing rhodamine 6G.

Upon application of the silicone colour converting layers containing rhodamine, the results obtained were comparable to those observed for the rhodamine-containing acrylic layers, discussed previously (Chapter 3).

The double blue emission of the OLED (457 and 482 nm) is only partially converted by the organic dye dispersed into silicone. Rhodamine was only able to absorb the 482 nm signal, and

convert it into a yellow-orange emission (570-600 nm). The combination between the residual blue light (457 nm) and the yellow emission produced by the layer, led to a device characterised by a bright purple appearance, as demonstrated in the pictures in Figure 4.6.

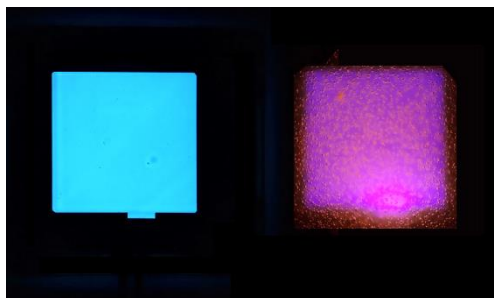


Figure 4.6: Images of the pristine blue OLED (left) and the converted device by rhodamine containing silicone (left).

The results obtained from the application of the CCLs on the green OLEDs are shown in Figure 4.7. The application of the silicone-based colour converting layers containing rhodamine resulted in the complete absorption of the original green signal, which is converted by the dye in a yellow-orange emission (~590 nm).

The colour of the pristine green OLED and the final appearance resulting from the down-conversion with the rhodamine-silicone layers are visible in Figure 4.8. Upon application of the layer containing a 2% w/w ratio of fluorescent hybrid materials in silicone, the original green emission of the device can be completely converted into a yellow colour. Increasing the loading percentage of supporting material to 6%, resulted in a further shift toward the red region of the visible spectrum leading to a final orange appearance.

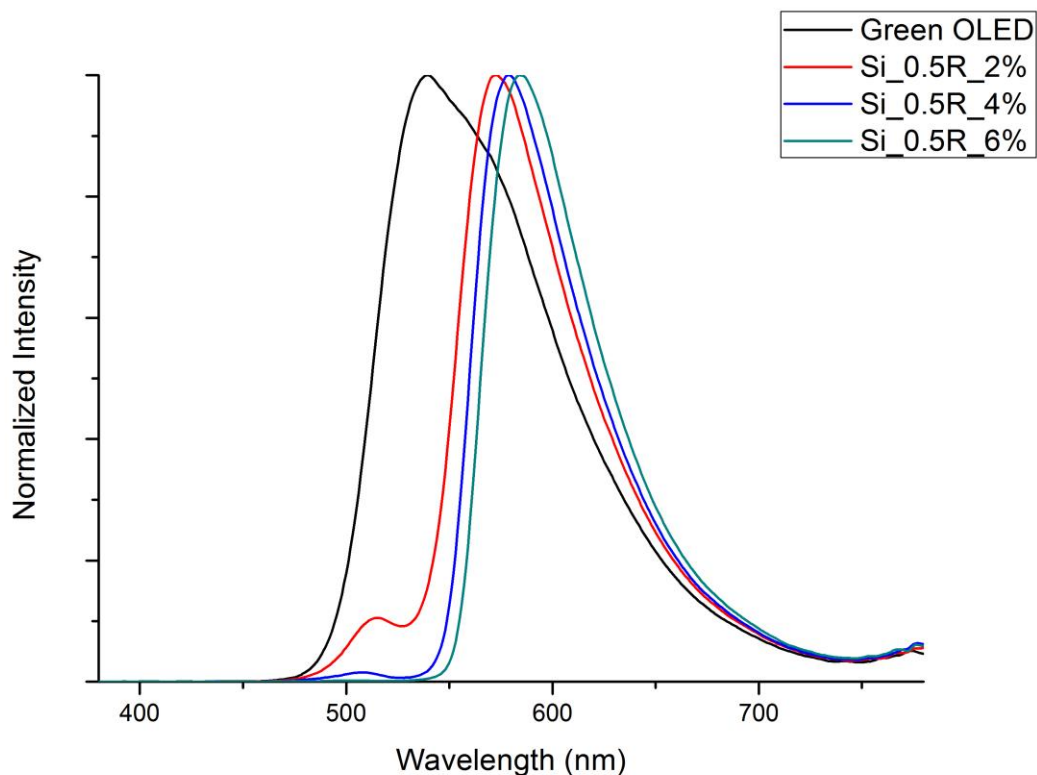


Figure 4.7: Emission of the green OLEDs in pristine condition and the final emission achieved by using the rhodamine CCLs.

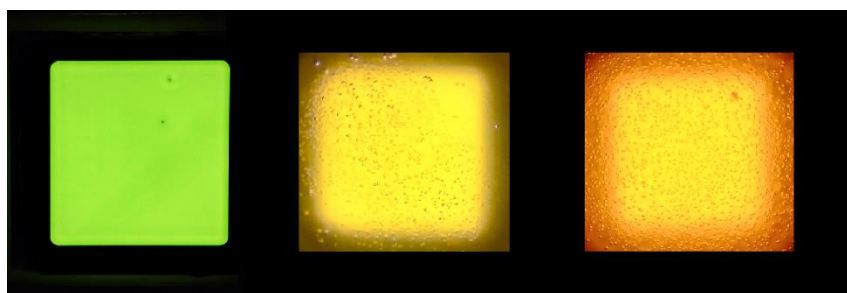


Figure 4.8: Images of the pristine green OLED (left) and the colour achieved by the addition of the layers with the 2% (middle) and 6% (right) of supporting materials impregnated with rhodamine dispersed in silicone.

#### 4.4.2 Fluorescein sodium salt

The absorption properties of fluorescein caged into the supporting materials were analysed with the same parameters used for the rhodamine samples. The spectra for the molecule impregnated

into silica gel are depicted in Figure 4.9; the well-known dependence of the optical properties of fluorescein in relation to the environment are clearly observable in the spectra.<sup>138</sup> While for rhodamine the difference between the absorption of the dye in a solution of water or ethanol was minimal, in the case of fluorescein, the discrepancy between the spectra in the two solvents is much more marked. The absorption profile for the alcohol solution presents two well defined peaks with a major feature at ~450 nm, and the second signal around 490 nm; whereas, for water, the spectra appear to be mirrored with a dominant peak centred at 485 nm, and only a small shoulder visible at lower wavelengths.

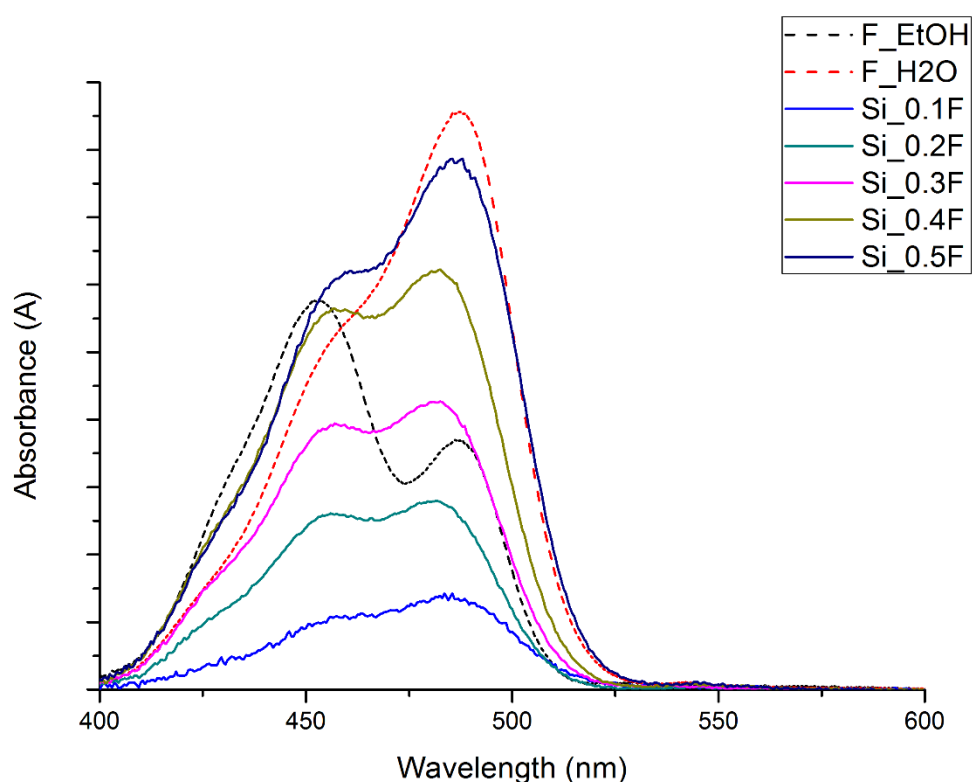


Figure 4.9: Absorption spectra of fluorescein disodium salt impregnated in silica gel dispersed in silica versus the dye in ethanol solution.

Further variation can be observed upon impregnation of the dye into the pores of the silica particles; in this case, the absorption spectra are characterised by the presence of two peaks

with comparable intensity. The profiles of these peaks partially resemble those of the dye in ethanol, but their spectral positions appear to be more similar to the result obtained for the fluorescent molecule dissolved in water.

The difference in the absorbance between the dye in the solutions, and the molecule absorbed into the supporting material, become even more evident when fluorescein is trapped into the cavities of hydrogen containing Faujasite (Figure 4.10). The spectra for the hybrid organic-inorganic samples show the presence of a single peak, at 445 nm, which results in a blue shift compared to the position of the peaks for the water or ethanol solutions.

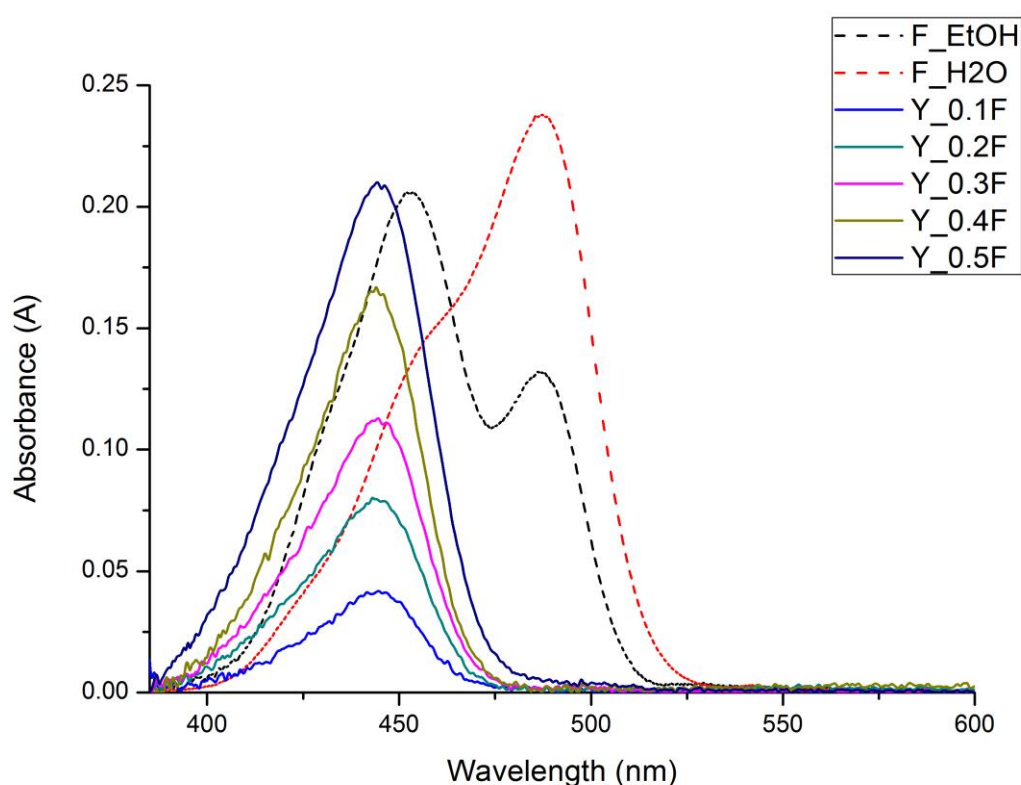


Figure 4.10: Absorption spectra of fluorescein in ethanol, water and HY zeolite dispersed in silicone.

Such results have been previously observed by Chrétien *et al.*<sup>69</sup> and Lukaska *et al.*<sup>139</sup> for fluorescein synthesized inside the cavities of Faujasite crystals; the phenomenon has been attributed to the presence of the non-framework hydrogen clusters used to counterbalance the

charge of the aluminosilicate structure, which can act as acid sites promoting the formation of the cationic derivative of the molecule.<sup>139</sup>

Due to the difference observed for the dye during the course of the UV-Visible spectroscopy, the analysis of the emissive properties of fluorescein in the inorganic scaffoldings was investigated using a different set of parameters. For the dye absorbed in silica, the excitation wavelength of the fluorimeter was set at 460 nm, and the fluorescence signal was collected in the range between 465 and 700 nm.

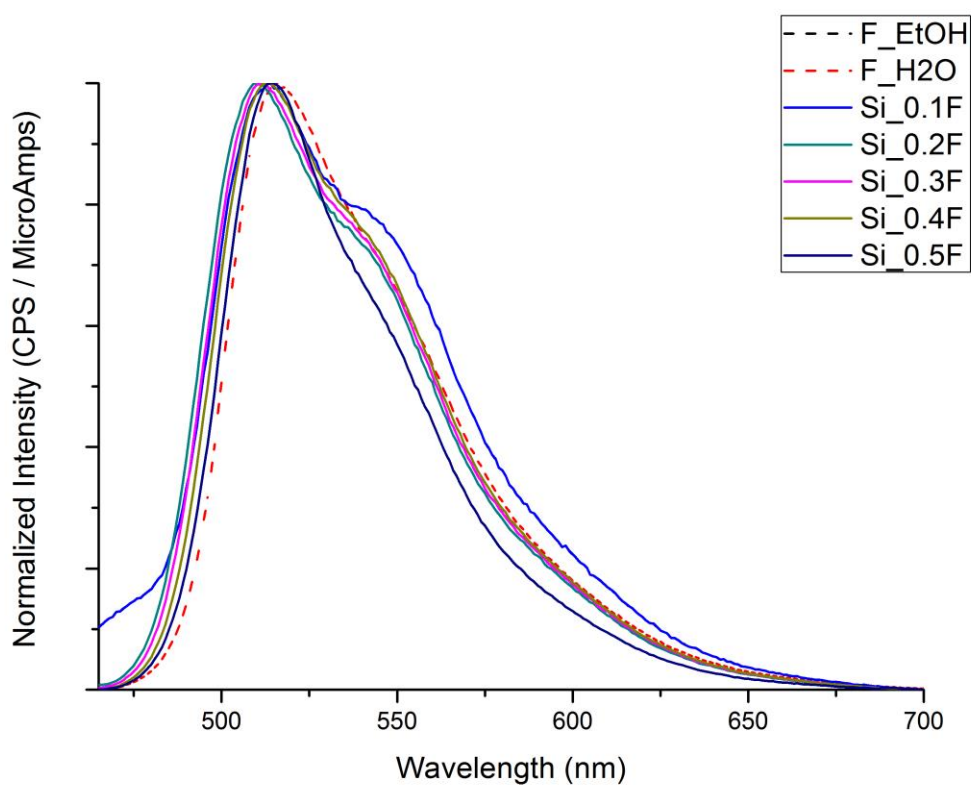


Figure 4.11: Normalised emission of fluorescein disodium salt absorbed in silica gel and embedded in silicone compared to the emission of the molecule in ethanol or water solutions.

As can be seen in Figure 4.11 no notable differences were observed between the emission of the dye dissolved in the water or ethanol solution, and the signal arising from the organic

molecule embedded in silica gel. The emission spectra for all the samples resemble the typical behaviour of fluorescein with a maximum centred at 515 nm.

In accordance with the spectra collected at the UV-Visible spectrophotometer, the emission of fluorescein, impregnated in HY zeolite, was investigated by setting the excitation wavelength at 430 nm and collecting the signal from 435 to 700 nm. As a consequence of the impregnation of fluorescein in the structure of the aluminosilicate, peculiar and unexpected optical properties were observed (Figure 4.12). The emission spectra of the dye impregnated into the zeolite differ significantly from the emission spectra for the organic molecule in water or ethanol solutions.

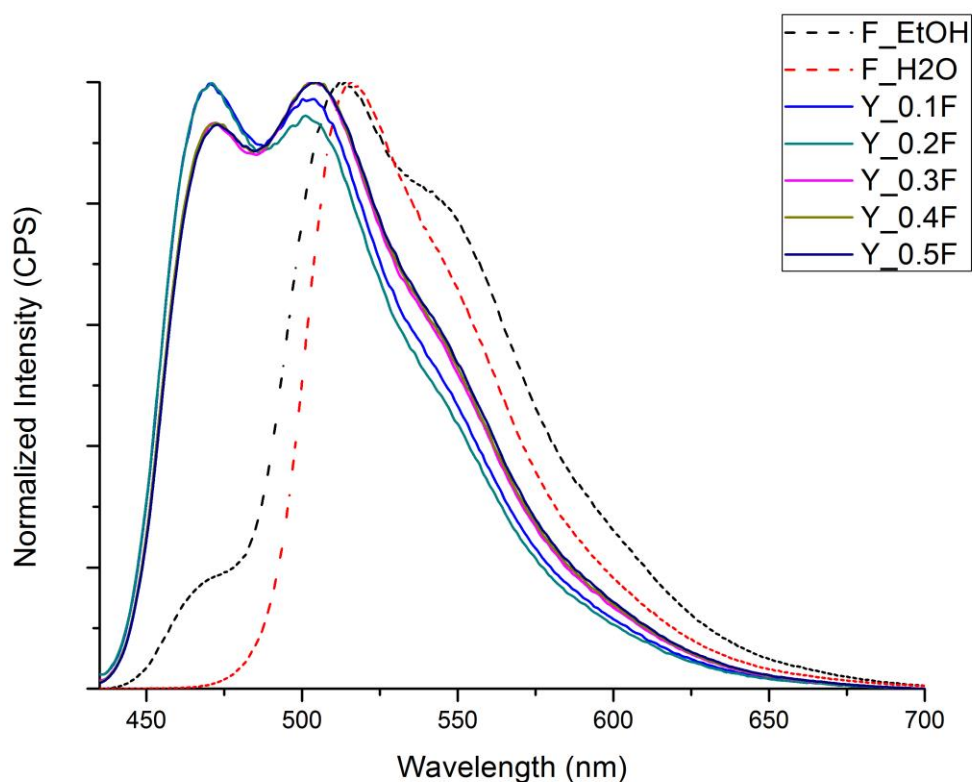


Figure 4.12: Emission of fluorescein impregnated in HY zeolite against the molecule in a solution of water and ethanol.

The spectra of the hybrid fluorescent material are characterised by the presence of a significant blue shift a double emission. Two maxima centred respectively at 470 and 506 nm were visible for the hybrid samples. If the emission at 506 nm could be interpreted as a consequence of the isolation of the molecule into the cavities of the crystalline material, then the same cannot be said for the blue emission at 470 nm. The discrepancy between this feature and the typical green emission of fluorescein is too accentuated to be taken as a result of the absence of aggregates or dimers, and it must be of other origins. Similar emission has been previously observed and reported by Martin and Lindqvist <sup>79</sup> during the course of their investigation about the dependence of the optical properties of fluorescein in relation to the pH of the solution in which the dye is dissolved. They discovered that the fluorescence signal of fluorescein shifted towards the blue region of the electromagnetic spectrum when the dye is subjected to a strong acid environment (10 M H<sub>2</sub>SO<sub>4</sub>). They associated the blue emission with the formation of the cation derivative of the molecule as a consequence of the reaction of the dye with the protons in solution. We have reason to believe that a similar phenomenon occurs in our system, in virtue of the intrinsic acidity of the zeolite framework, and the presence of the hydrogen clusters acting as non-structural cations. To our knowledge, however, the blue shift in the emission of fluorescein has never been observed in any systems comparable to ours. On the contrary, all the research published in the literature reported that the fluorescence signal of the fluorescein, when impregnated into the same supporting material, always matched the emission of fluorescein in solution. <sup>69,139</sup> The discrepancy between our results and previously collected data from similar samples was investigated further, and the results will be discussed in Chapter 5.

The quantum yield values for fluorescein in silica gel are reported in Table 4 and Table 5, for silica and zeolite respectively.

Table 4: Quantum yields of fluorescein impregnated into the silica gel and embedded in silicone.

Sample	Quantum Yield (QY) (%)
Si_0.1F	39.49
Si_0.2F	35.19
Si_0.3F	34.44
Si_0.4F	31.91
Si_0.5F	28.73

Contrary to what was observed for the rhodamine samples, the quantum yield of fluorescein appeared to be significantly affected by the presence of the supporting materials. The QY values measured for the both the hybrid materials never exceed 40%, whereas the value measured for fluorescein in ethanol solution was ~75%. Such a decrease in the efficiency of fluorescein can be attributed to the elevated susceptibility of the molecule to the environment, also confirmed by the shift in the emission recorded for the dye impregnated into the zeolite.

Table 5: Quantum yield of fluorescein impregnated into the zeolite and embedded in silicone.

Sample	Quantum Yield (QY) (%)
Y_0.1F	38.47
Y_0.2F	34.91
Y_0.3F	33.15
Y_0.4F	30.96
Y_0.5F	30.22

As for the rhodamine samples, the effectiveness of this material for the down-conversion of the OLEDs output was investigated, producing new layers respectively with 2, 4 and 6% weight ratio between the silicone matrix and the supporting material, and keeping constant the

percentage (0.5%) between the dye and the scaffolding. As a result of the blue emission of fluorescein impregnated into the zeolite, only the layers produced with silica gel were suitable for the down-conversion of the luminescent device. The results obtained with the portable spectrophotometer are depicted in Figure 4.13. From the spectra it is evident that the fluorescent silicon layer with the lowest content (2%) of fluorescent hybrid material is not able to fully convert the emission of the OLED, and some of the blue light of the device is transmitted through the layer. Increasing the amount of silica gel to 4 and 6% resulted in a complete down-conversion of the OLED output, leading to a green emission centred at 515 nm. This is also visible in the photographs of the pristine and down-converted device depicted in Figure 4.14.

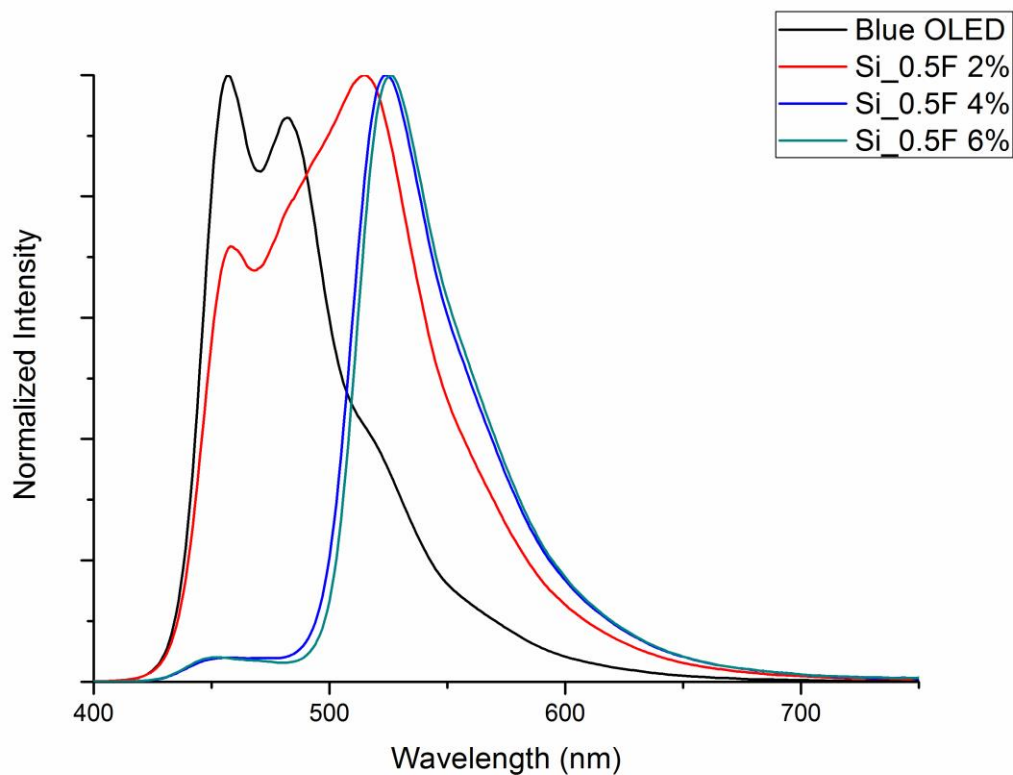


Figure 4.13: Emission of the blue OLEDs and the signal of the device down-converted with the silicone layers containing fluorescein.

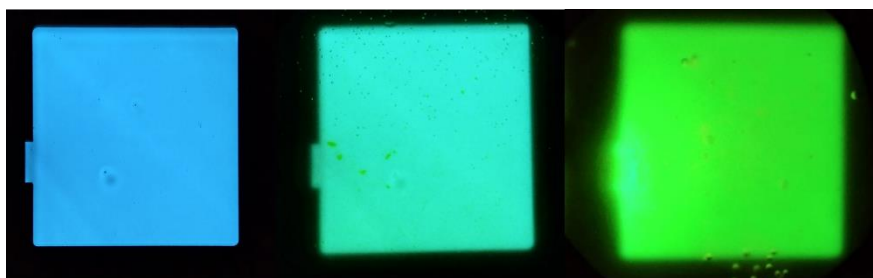


Figure 4.14: Photographs of the pristine emission of the blue OLED (left) and the colours achieved converting the emission with the silicone layers composed by a 2% (middle) and 6% (right) of fluorescein absorbed into silica.

## 4.5 Discussion

The impregnation of fluorescent molecules into the pores and cavities of inorganic supporting materials has been proven to be an effective and simple method to disperse organic dyes in an otherwise immiscible matrix such as silicone rubber. In the course of our study, we demonstrated the primary importance of the supporting material, which not only needs to possess an appropriate morphology to allow absorption of the fluorescent molecule within the pores, but it also plays an important role concerning the optical properties and quantum efficiency of the organic compounds. Such a relationship is particularly evident in the results reported for the system fluorescein-zeolite-silicone, where a significant shift in the emission (from 515 nm to 470 nm) was observed for the first time in what can be considered a non-acidic solution.

The method here described does not require any modification of the chemical structure of the dye in order to make it soluble in the polyorganosiloxane matrix, neither does it involve complex synthetic procedures which can lead to low yields and time-demanding purification steps. As a result of that, we have reason to believe that such a procedure can be easily scaled up and extended to a wider range of fluorescent species.

## 4.6 Conclusions

Fluorescent silicone layers, based on the impregnation of organic dye in supporting materials, were developed and characterised. We demonstrated that they can represent optimal candidates as colour conversion layers (CCLs) for monochromatic organic light emitting devices (OLEDs). As a result of their optical properties, they are able to modify the emission of the OLEDs without significantly impacting the power efficiency of these luminescent devices. The low curing temperature, and the lack of aggressive solvents allow the ability to cast these layers directly on top of the substrate of OLED, ensuring good adhesion and preventing the use of external glueing agents. In virtue of the silicone nature of the matrix, injection moulding or other industrial technique can be employed for large scale production. The range of colours achievable with this method is almost infinite since the OLEDs emission can be tuned by varying the concentration as well as the nature of the dyes in the supporting materials, and modifying the ratio between the inorganic scaffolding and the polysiloxane matrix. In addition, the increased flexibility of the matrix makes these colour conversion layers excellent candidates for the next generation of flexible and transparent light emitting devices.

# Chapter 5 : Investigation of the blue emission of fluorescein

The phenomenon of the blue emission of fluorescein, as a result of the dye impregnation into the hydrogen containing zeolite, deserved further investigation. In the course of this chapter, several theories are outlined and tested, to understand the peculiar optical behaviour of the molecule, which has never before been observed in comparable systems.

## 5.1 Theories

In order to explain the behaviour of fluorescein once impregnated into the zeolite and dispersed into the silicone matrix, three theories were developed based on the structural, chemical and physical characteristics of the hybrid materials produced. These theories, listed and explained below, include the presence of a chemical reaction, the configurational change of the dye and the protonation of the molecule.

- *Chemical reaction*: since previous research on comparable hybrid materials without the presence of silicone did not show any change in the optical properties of the molecule, it is plausible to assume that the shift, observed by us, is the result of a chemical reaction between the dye and the polysiloxane matrix. However, considering the well-known chemically inert properties of the silicone, as well as the fact that the blue emission is only visible when fluorescein is combined with the zeolite and the silicone, such a possibility is very unlikely.
- *Configurational change*: changes in the optical properties can be related to modifications in the electronic structure of the molecule. Modification of the electronic

structure can occur as a consequence of a chemical reaction or as a result of a change in the atomic structure of the molecules (i.e. modifications in bond length, bond angle, folding or other similar phenomena). Due to the similarity between the size of the fluorescein and the size of the cavities of the Y zeolite, it is possible that the molecule, in order to enter into the inorganic structure, is forced to bend or distort. The change in the atomic configuration can lead to variations in the energy levels, which might result in the blue shift of the dye.

- *Protonation of fluorescein:* as previously discussed, a similar blue shift in the emission of fluorescein was observed by Martin and Lindqvist <sup>79</sup>. They reported that the shift in their system was due to the formation of the cationic derivative of the dye, as a consequence of the presence of a strong acid environment (10M H<sub>2</sub>SO<sub>4</sub>). Since the zeolite used in this work, contains hydrogen clusters as non-framework ions to stabilise the negative charge of the zeolite framework, we cannot exclude the presence of a reaction between the hydrogen atoms and the dye, which would result in the protonation of the fluorescent molecule. A similar reaction has been already reported by Hashimoto and co-workers <sup>140</sup>, for a fluorescent hybrid system composed of resorufin absorbed into the zeolite. They observed that upon evaporation of the solvent, toluene, from the structure of the zeolite, the emission of the dye increased in intensity. This behaviour was attributed to the deprotonation of the fluorescent molecule as a consequence of its interaction with the non-framework ions present in the zeolite. It is, therefore, plausible to assume that a similar phenomenon, but with opposite chemistry, occurs in our system, leading to the formation of the cationic derivative of fluorescein, and therefore, to a blue emission of the dye.

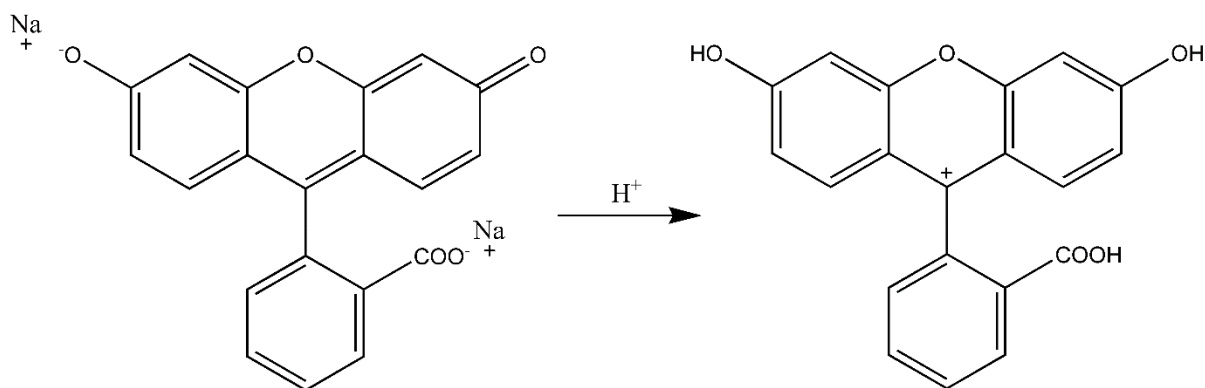


Figure 5.1: Chemical structures of the dianion form of fluorescein (left) and the cationic form (right) resulting from protonation of the dye.

## 5.2 Testing the theories

In order to test if the presence of the blue shift is caused by a chemical reaction between the silicone matrix and the fluorescent molecules, a sample of hybrid material composed only of zeolite and fluorescein was prepared and analysed with the UV-Vis spectrophotometer, and with the fluorimeter. The powder was sandwiched between a microscope slide and a glass coverslip, secured together with transparent tape. The results were compared with the optical properties of the dye in water or ethanol solution as well as with the three component hybrid material (fluorescein-zeolite-silicone).

The absorption spectra of the four samples are depicted in Figure 5.2. The comparison reveals that no difference can be observed in the absorption properties of the dye, as a result of the presence or absence of the silicone matrix. Both the hybrid samples show a single absorbance centred at 445 nm, which differs from the double peaks observed for the ethanol or water solution.

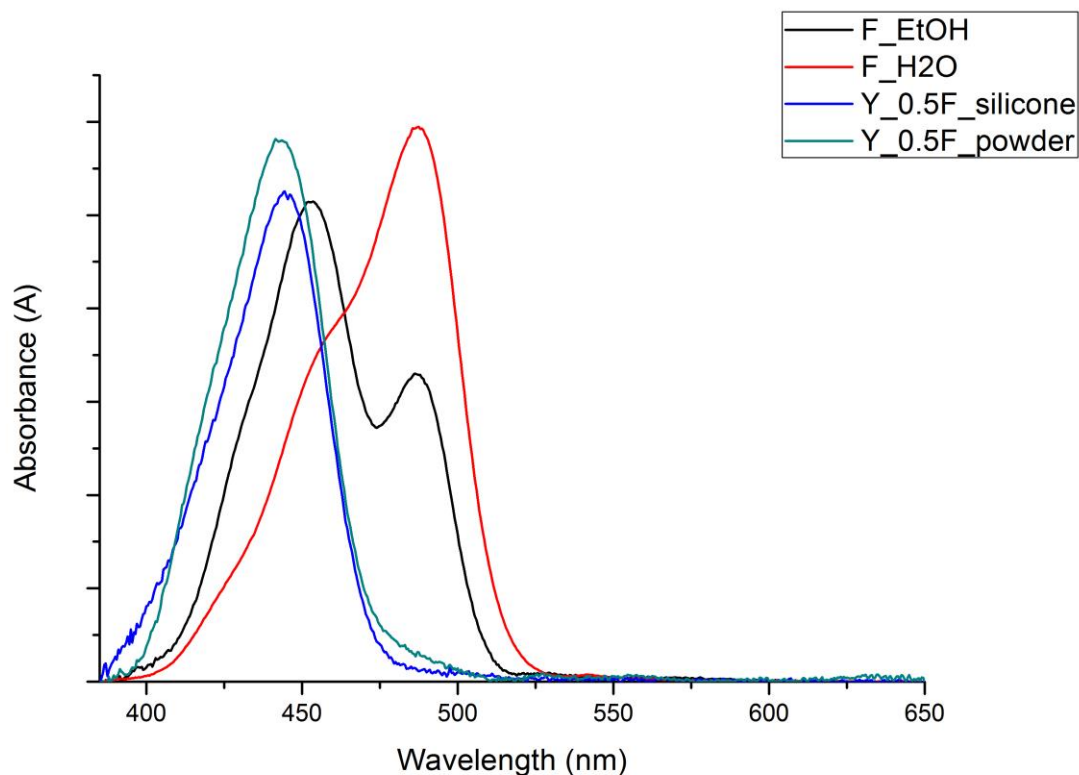


Figure 5.2: Absorption of fluorescein in HY zeolite with and without silicone against the dye in water or ethanol solution.

The similarity between the hybrid samples, however, ceases to exist upon analysis of the emission properties (Figure 5.3). While the hybrid powder embedded in the silicone shows a double emission, with a blue shift compared to the classical green signal of fluorescein, in the absence of the polysiloxane matrix, the emission of fluorescein impregnated into the zeolite is the same as the emission of the dye in water or ethanol, with a single maximum centred at 515 nm.

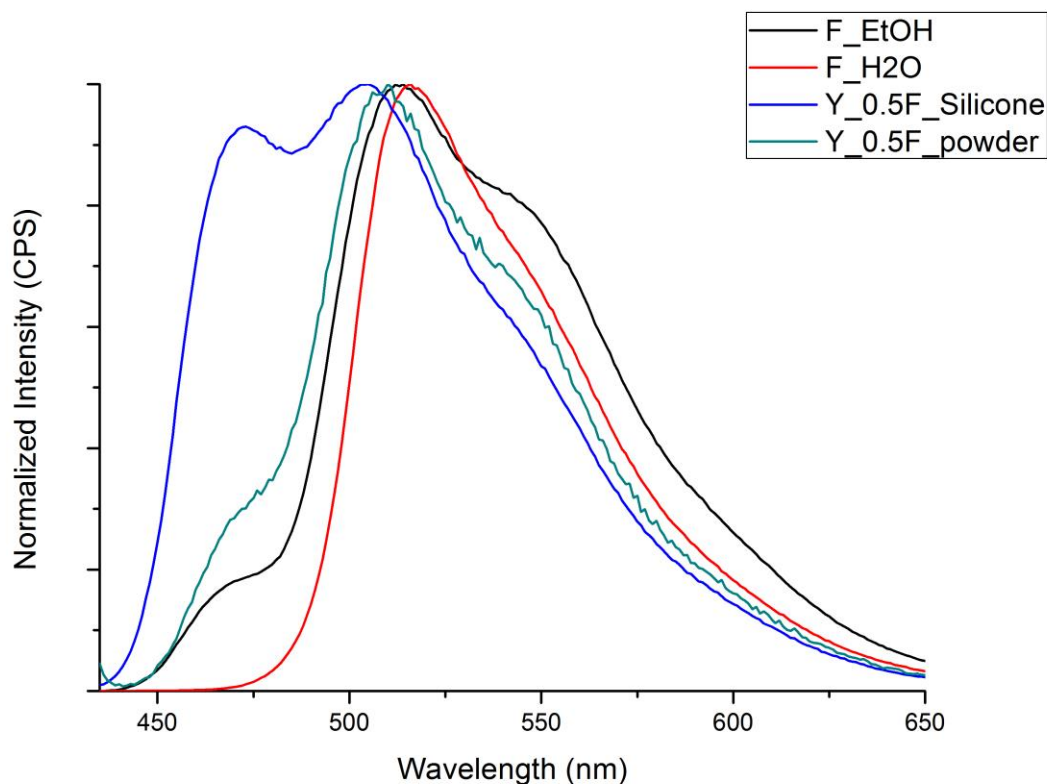


Figure 5.3: Emission of fluorescein impregnated in zeolite before and after the dispersion in the silicone matrix against the dye in ethanol or water solution.

The influence of the polysiloxane matrix on the emission was also confirmed by the successive analysis, where the powder just analysed was recovered and dispersed in the silicone. Such an experiment not only confirmed the presence of the shift, but it also exposed another unexpected phenomenon. Comparing the freshly prepared hybrid sample embedded into the polysiloxane matrix with the sample prepared previously, we observed that the emission signal of the dye, changed overtime.

This behaviour was further investigated by leaving the sample inside the sample chamber of the fluorimeter, and collecting emission at regular intervals (2 days). The results, depicted in Figure 5.4, show that the spectra of the freshly prepared sample showed the double emissions discussed before, with a maximum at 506 nm and a second peak at 470 nm. Day two

measurement showed a lower intensity of the 506 nm peak compared to the signal at 470 nm. Such a behaviour was observed to proceed for 5 days after the sample preparation, and resulted in almost complete disappearance of the 506 nm emission, which became a barely visible shoulder of the 470 nm signal.

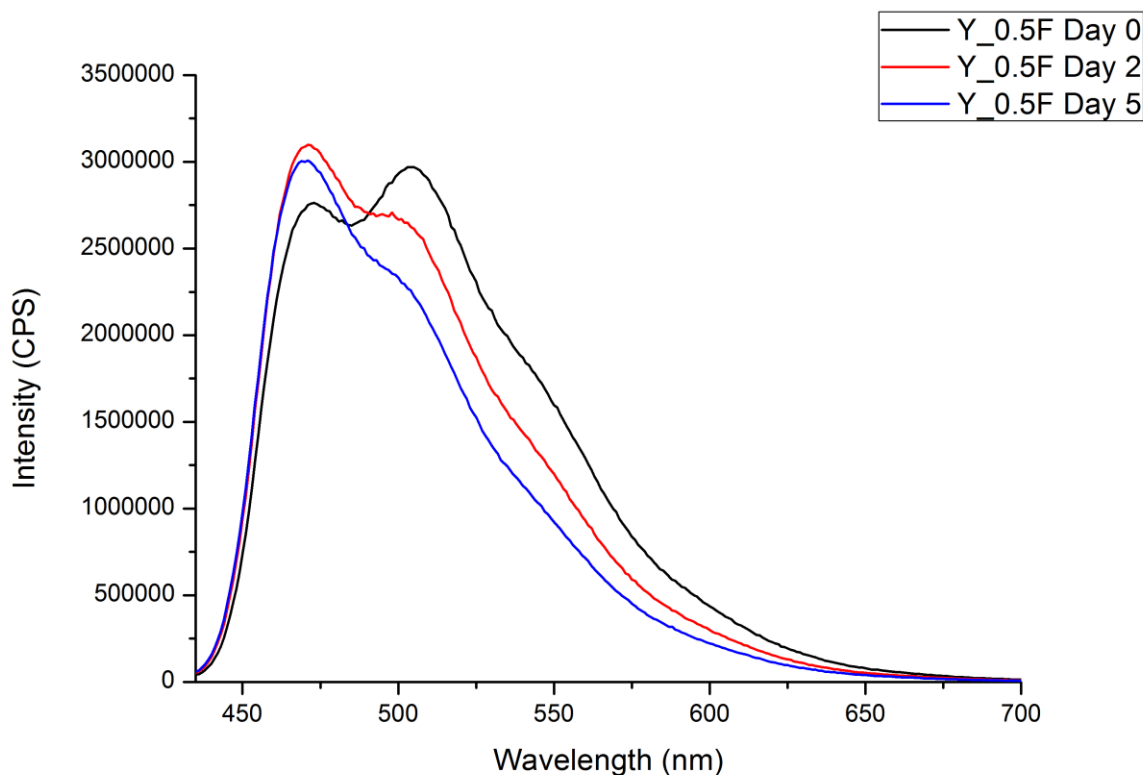


Figure 5.4: Emission of the hybrid material (fluorescein-HY zeolite) dispersed in silicone over a period of 120 hours.

These results seem to suggest that the presence of the silicone plays a fundamental role in the emission of the dye, however, such a hypothesis is partly contrary with the results observed previously. Indeed, if such a reaction between the silicone and the fluorescein is the cause for the peculiar emission, the blue shift should also be present for the samples composed of fluorescein, silica gel and silicone, which did not show any difference when compared to the dye in ethanol or water.

It is more plausible that the reason for the blue emission of fluorescein, when combined with the silicone and the zeolite, arises from the thermal treatment required to cure the polysiloxane matrix. As previously discussed, it has been proved that the presence or absence of the solvent, trapped in the cavities of the zeolite, can have a significant effect on the optical properties of the molecules impregnated into the aluminosilicate.<sup>140</sup>

Before testing such a possibility, a sample of pristine Y zeolite along with a sample of aluminosilicate impregnated with a 0.5% of fluorescein were tested by thermogravimetric analysis. This investigation was aimed to quantify the amount of water or other solvents present in the cavities of the supporting materials, and measure the temperature at which they can be evaporated from the crystals. The results, depicted in Figure 5.5, showed that both the samples lost a significant amount of weight, 12 and 15% for the dye-impregnated zeolite and the pristine sample respectively, at temperatures below 100°C.

This suggested that even the low temperature required to cure the silicone (70° C) is able to remove most of the solvent from the zeolite, and, therefore might have a significant impact on the optical properties of the dye impregnated into the cavities.

To investigate the relationship between the presence/absence of solvent in the zeolite and the optical properties of fluorescein absorbed into the Faujasite, a sample of the fluorescent powder was subjected to the same thermal treatment performed on the system fluorescein-zeolite-silicone.

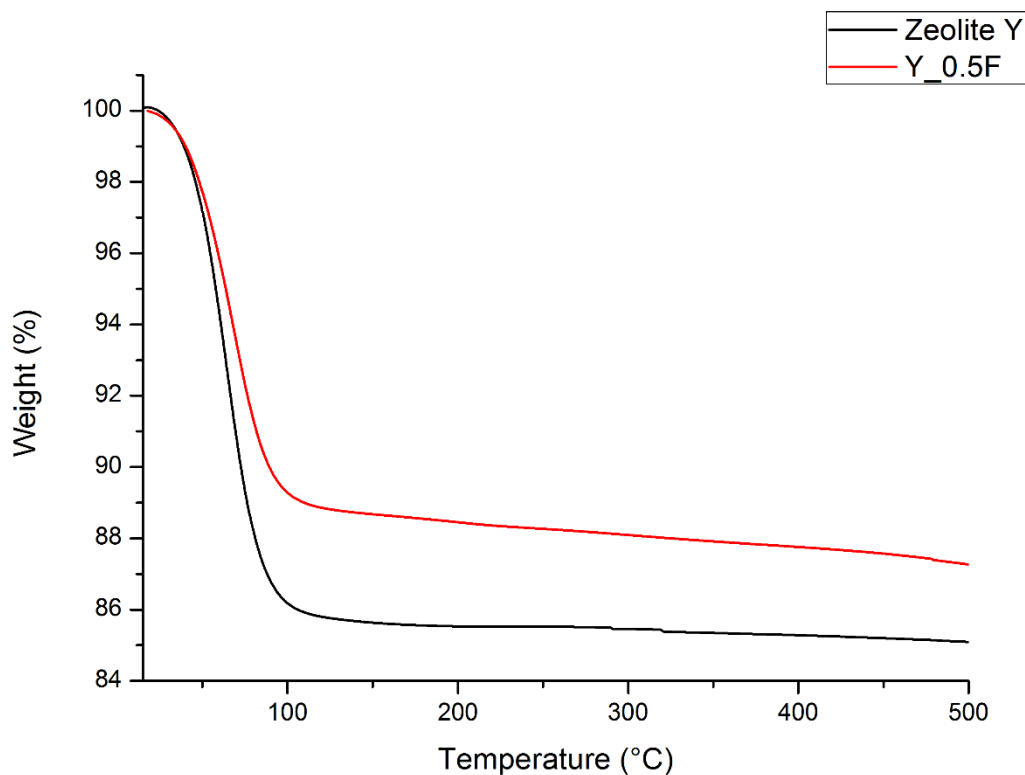


Figure 5.5: Thermogravimetric analysis of a pristine sample of HY zeolite and the aluminosilicate impregnated with fluorescein.

The powder was prepared following the same procedure described above; the fluorescent hybrid was sandwiched between a microscope slide and a coverslip, and heated at 70°C for two hours on a hot plate. The sample was then tested with the fluorimeter, and its emission was compared with that of an untreated sample from the same batch. The results are depicted in the graph in Figure 5.6. The emission spectra for the sample not subjected to the thermal treatment matched the classical green emission of fluorescein, whereas the signal for the heat-treated (HT) sample shows a strong blue shift, which perfectly matches the emission of the dye in the three components system fluorescein-zeolite-silicone.

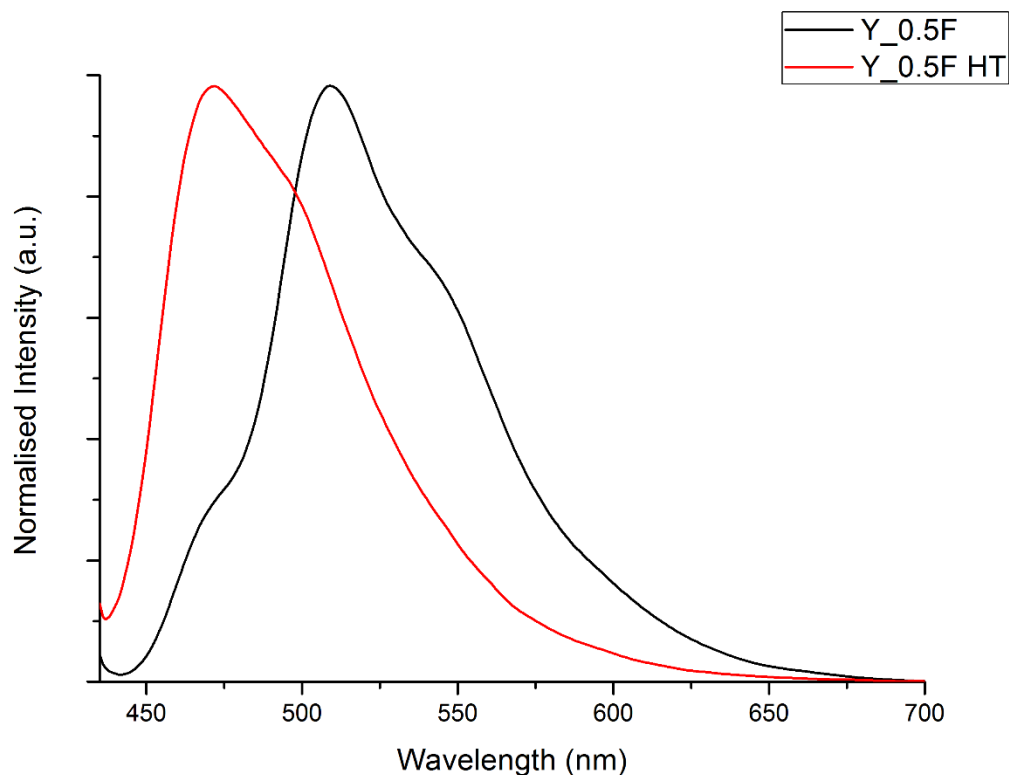


Figure 5.6: Emission of fluorescein in HY zeolite before (black) and after (red) the heat treatment at 70°C.

This comparison clearly demonstrated that the blue shift in the emission of fluorescein is not related to the presence of the silicone matrix, but it is rather a consequence of the solvent evaporation from the supporting material.

Further investigation also revealed that, as a result of the highly absorbent properties of the zeolite, the phenomenon is reversible. Leaving the fluorescent hybrid powder exposed to the moisture in the air for a single night (*ca.* 12 Hours), resulted in the reabsorption of water, which consequently, led to a red shift in emission properties of the dye as represented in Figure 5.7.

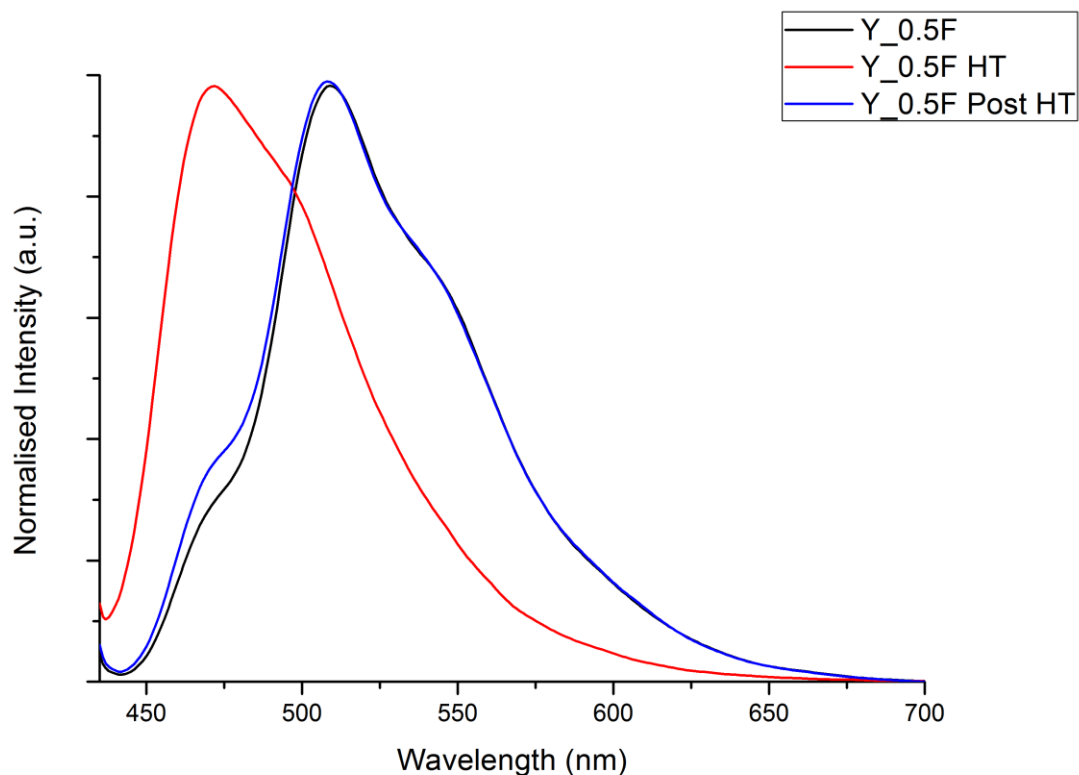


Figure 5.7: Emission spectra of fluorescein into HY zeolite without any treatment (black line), immediately after heating (red line) and one day after the thermal treatment (blue line).

The reversible blue-green emission was also confirmed by the analysis of a freshly prepared sample, heat treated as previously described. Its emission was collected using the automated batch measurement tool provided by the Horiba fluorolog software; the instrument was set to collect an emission spectrum of the sample every 30 minutes for a total time of 18 hours.

The results, depicted in the graph of Figure 5.8 shows the presence of a smooth transition between the initial blue emission, arising from the absence of the solvent, and the final green emission, a consequence of the water reabsorption.

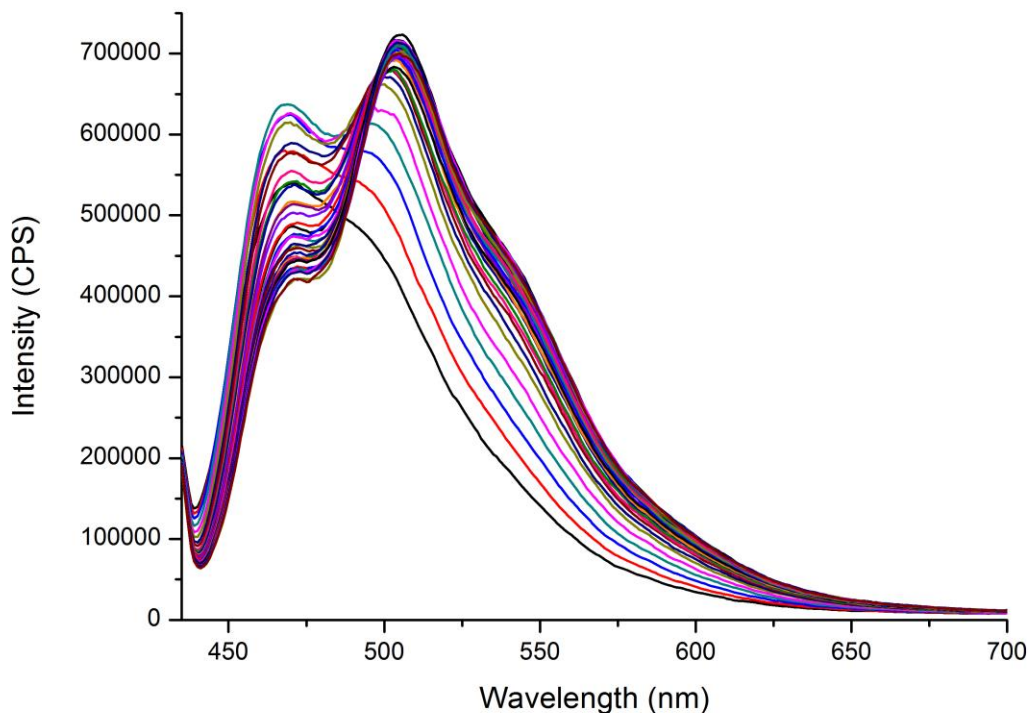


Figure 5.8: Changes in the emission of the HY sample containing a 0.5% w/w of fluorescein within 18 hours after the thermal treatment.

A better overview of the differences in the intensity of the blue and green peaks, within the 18 hour time frame, is given in the graph of Figure 5.9. It is clear that, whether the green emission is constantly gaining intensity over the time, the blue emission, after an initial increase in counts, tends to decrease almost linearly over time. The blue and green signals become equal, but only after nine hours from the thermal treatment. The long time, required for the signal to change, can be taken as an indication that the change in the emission of the dye is not related to the temperature of the sample, but it is rather due to the solvent absorption/desorption.

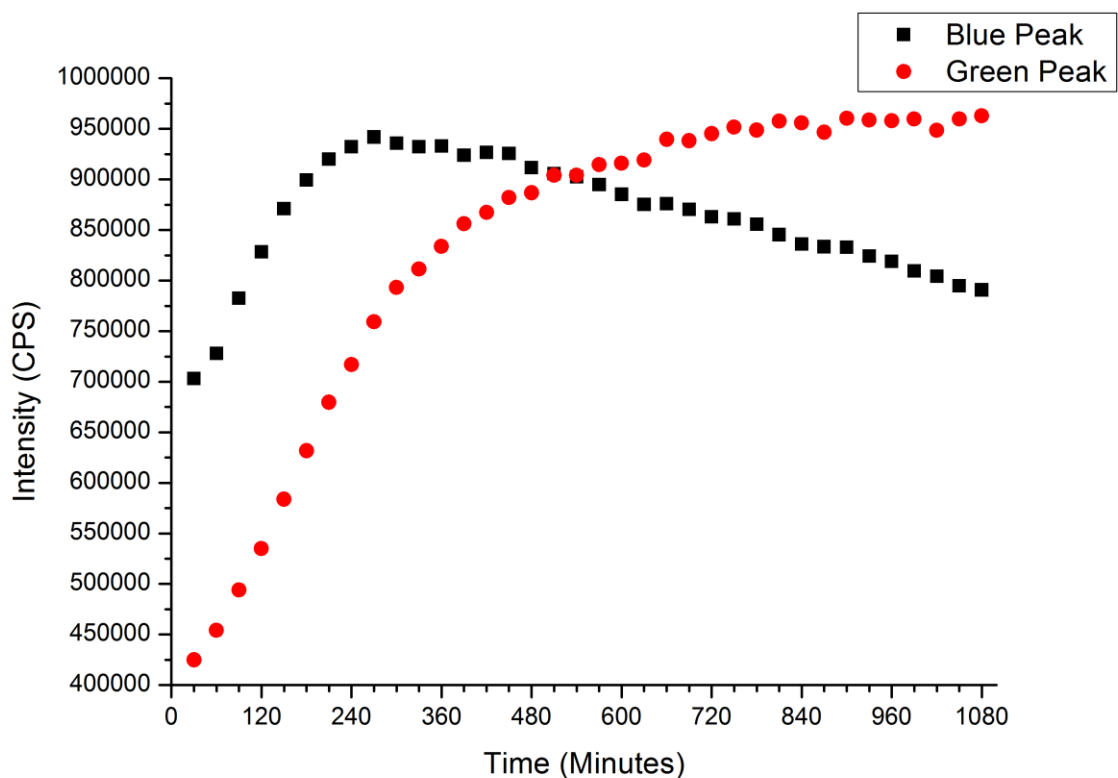


Figure 5.9: Intensity of the blue and green emissions of the sample HY\_0.5F over the course of 18 hours from the thermal treatment.

Although the absorption and desorption of the solvent are key factors in the occurrence of the phenomenon, they do not provide an explanation on the mechanism that regulates the shift in the emission.

From previous research on the subject <sup>79,140</sup> it is possible to attribute the shift to the protonation/deprotonation of the dye's molecules, as a result of their interaction with the hydrogen ions trapped in the zeolite, as non-framework ions. It appears that, when the solvent is removed from the crystals of the supporting material, fluorescein is able to react with the hydrogen cluster generating the cation derivative of the dye. However, in order for this to be possible, the organic molecules of the dye have to be in close proximity with the hydrogen cations, and, therefore, they must migrate within the zeolite structure. This is an argument of

debate in the scientific community.<sup>69,139,141</sup> Owing to the small differences in size between the window of the zeolite supercage, and the size of the organic molecule, contrasting opinions on whether fluorescein can or cannot enter into the cavities of the Faujasite, can be found in the literature.<sup>69,139,141</sup> Some indications on the matter can be obtained from the comparison between the X-ray diffraction patterns of a pristine sample and those of zeolite impregnated with different amounts of fluorescein. Samples with a 0.1, 0.5 and 1% w/w of dye in zeolite were prepared following the procedure described above. The patterns for the four samples were collected using a Bruker D8 Advance powder diffractometer equipped with copper  $\text{CuK}\alpha$ , X-ray source ( $\lambda=1.54178 \text{ \AA}$ ). Identical parameters were set for all the measurements, and, in order to avoid any external variable affecting the measurement, the same sample holder was used for all the samples.

As a result of the low concentration of fluorescein, no difference can be observed, in the patterns in Figure 5.10, between the signals of the pristine sample and those for the dye-functionalised zeolite.

However, a closer observation of the patterns (Figure 5.11) reveals that a shift, toward lower 2 theta values, in the position of the peaks is visible in the pattern as a consequence of the variation of the amount of dye impregnated into the supporting material. This shift is proportional to the amount of dye loaded into the crystals, and it indicates that the unit cell of the zeolite is expanding slightly as a result of the impregnation of the organic molecule. The proportional expansion of the crystals suggests that, despite causing stress in the lattice of the zeolite, fluorescein is able to enter into the supercage of the Faujasite.

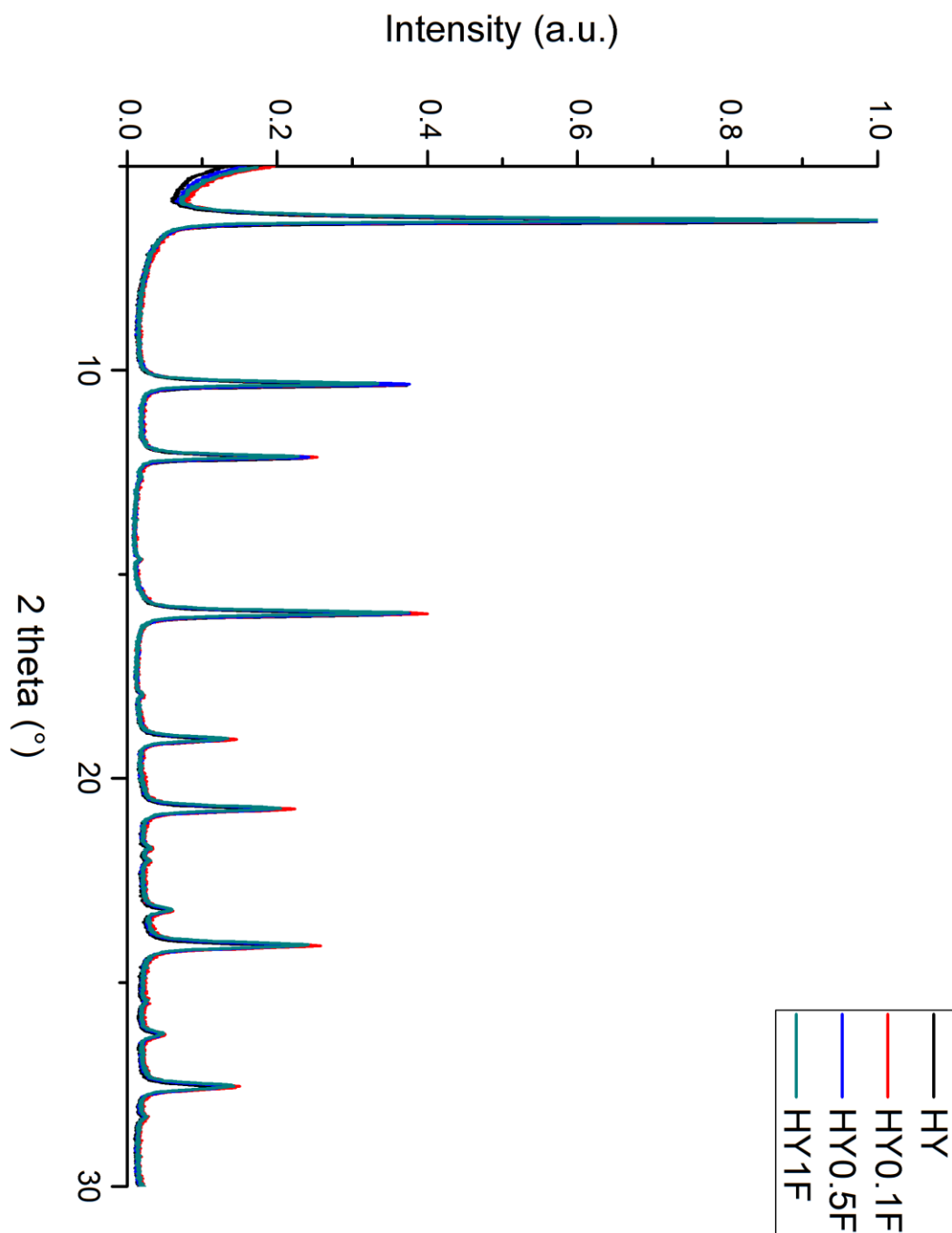


Figure 5.10: XRD patterns of the pure Faujasite sample and the zeolite functionalised with 0.1, 0.5 and 1% w/w of fluorescein.

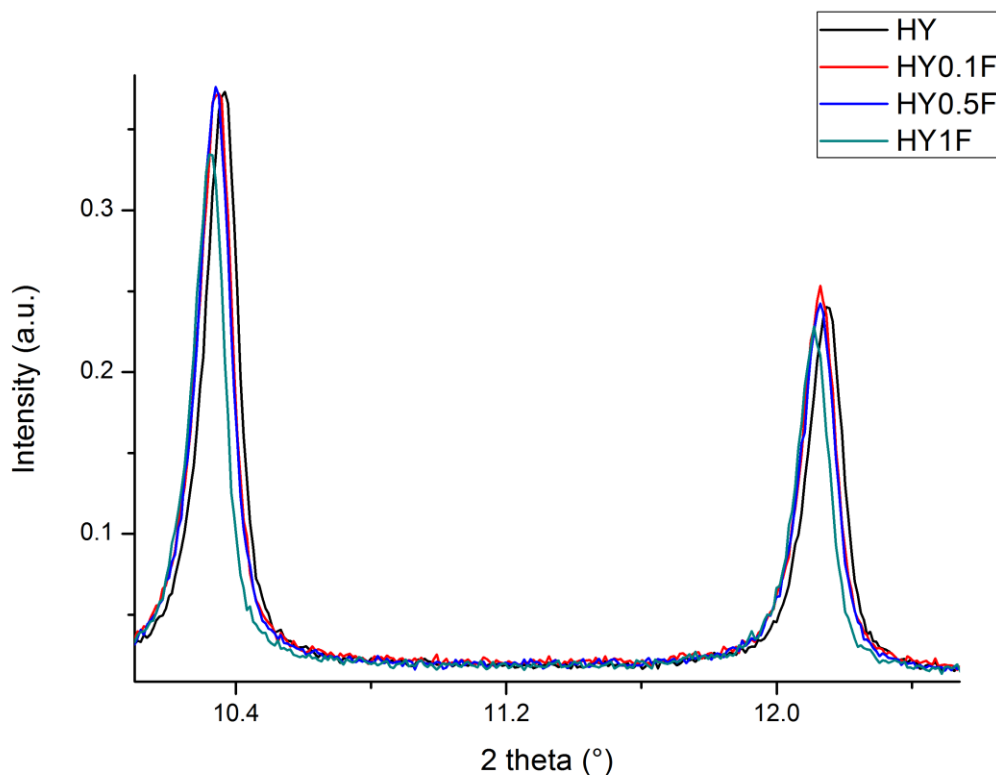


Figure 5.11: Shift in the position of the XRD peak as a consequence of the impregnation of the organic molecule in the zeolite.

Further confirmation on the inclusion of fluorescein into the cavities of the Faujasite, can be obtained from the 3D model of the supporting material and the dye molecule.

The CIF files for the Faujasite and the fluorescein<sup>142</sup> were obtained from the IZA structure database ([www.iza-structure.org/databases](http://www.iza-structure.org/databases)), and the Cambridge Crystallographic Data Centre (CCDC) respectively. Mercury software was used to open the files, isolating the supercell, and merge the structures together.

The final model depicted in Figure 5.12, clearly shows that it is possible for the organic molecule to fit into the main cavities of the Faujasite, and therefore to migrate into the crystals.

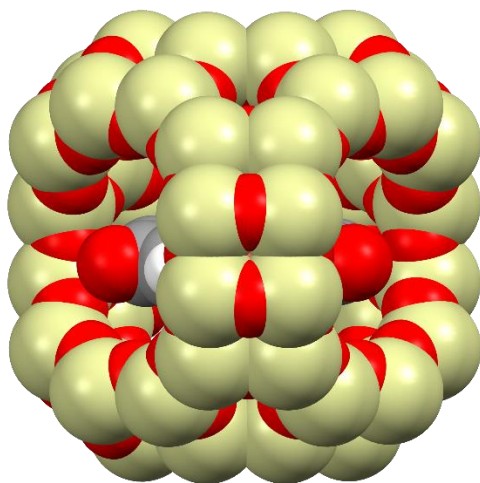


Figure 5.12: 3D model of the zeolite supercage with the molecule of fluorescein.

### 5.2.1 Substitution of the hydrogen ions into zeolite

Confirmation that the peculiar optical behaviour of fluorescein is a consequence of the protonation/deprotonation of the organic dye, can be obtained by substitution of the non-framework hydrogen ions inside the zeolite framework with other cations such as sodium, potassium or calcium. This can be easily done following the well-known ions-exchange procedure reported in the literature.<sup>68,143,144</sup> 325 g of sodium carbonate ( $\text{Na}_2\text{CO}_3$ ) were dissolved in distilled water containing 280 g of HY zeolite; the solution was stirred and kept at room temperature for 24 hours. The sodium exchanged zeolite (NaY) was recovered by filtration and washed with distilled water several times. The zeolite was then impregnated with fluorescein using the impregnation method described previously, and once dry, tested on the UV/Vis spectrophotometer, and the fluorimeter against the hydrogen-containing Faujasite impregnated with fluorescein.

The absorption spectra of the samples clearly evidenced the influence of the cations on the optical properties of the dye (Figure 5.13). The single absorption signal, centred at 440 nm,

characteristic for the HY zeolite, changes to a double signal with a maximum at 490 nm and a shoulder at 465 nm; when the proton clusters into the supporting materials are exchanged with the sodium cations. The absorption spectrum of fluorescein, impregnated into the sodium Faujasite, closely resembles what was already observed for the dye in water solution, indicating that the molecule is trapped in the supporting materials in the dianion form.

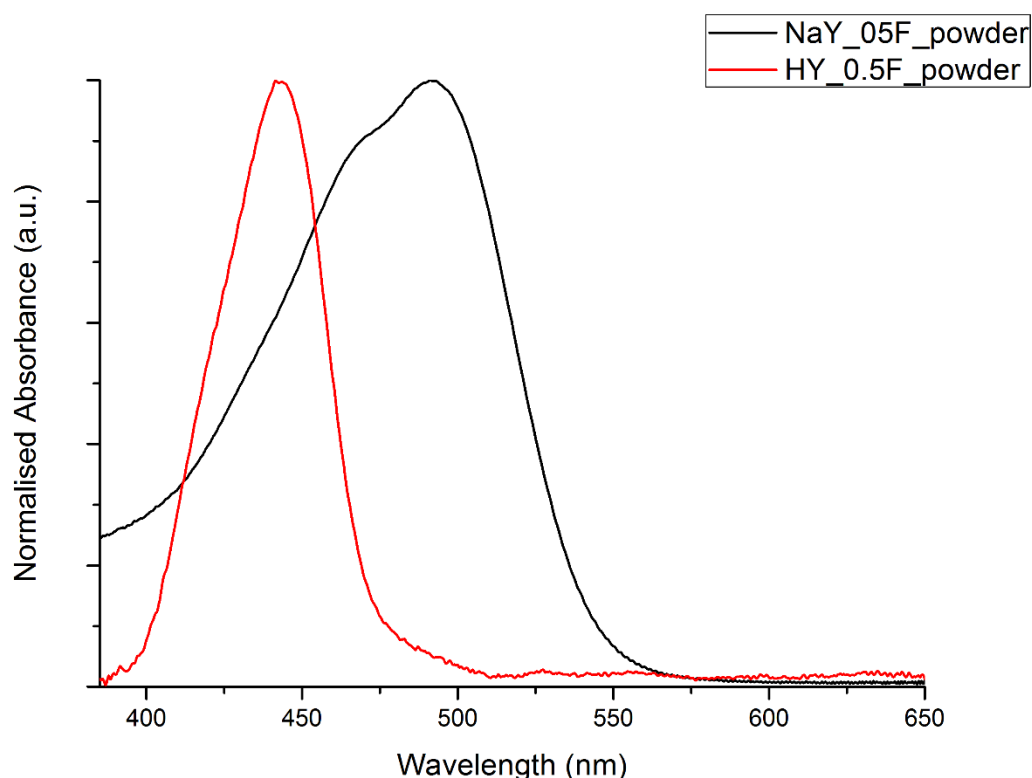


Figure 5.13: Absorption spectra of the HY and NaY zeolite impregnated with fluorescein.

Changes were also observed in the emission of the fluorescent molecule as a result of the different cations (Figure 5.14). Before the heat treatment, the emission spectra of fluorescein into the sodium zeolite resulted in being slightly red-shifted compared to the dye's signal absorbed into the hydrogen Faujasite. The maxima for the NaY sample is centred at 527 nm, and no shoulder is visible in the blue region of the electromagnetic spectrum. More significant differences between the hydrogen and sodium samples can be observed upon heating the hybrid

powders and removing the solvent from the crystals. The substantial shift, leading to the blue emission of fluorescein in the hydrogen containing Faujasite, is not visible when the protons are substituted with sodium ions in the aluminosilicate. The heat treatment of the NaY sample leads only to a slight shift in the dye's emission, which is still located in the green region of the electromagnetic spectrum, and at a higher wavelength than the emission recorded for the HY sample before the heat treatment.

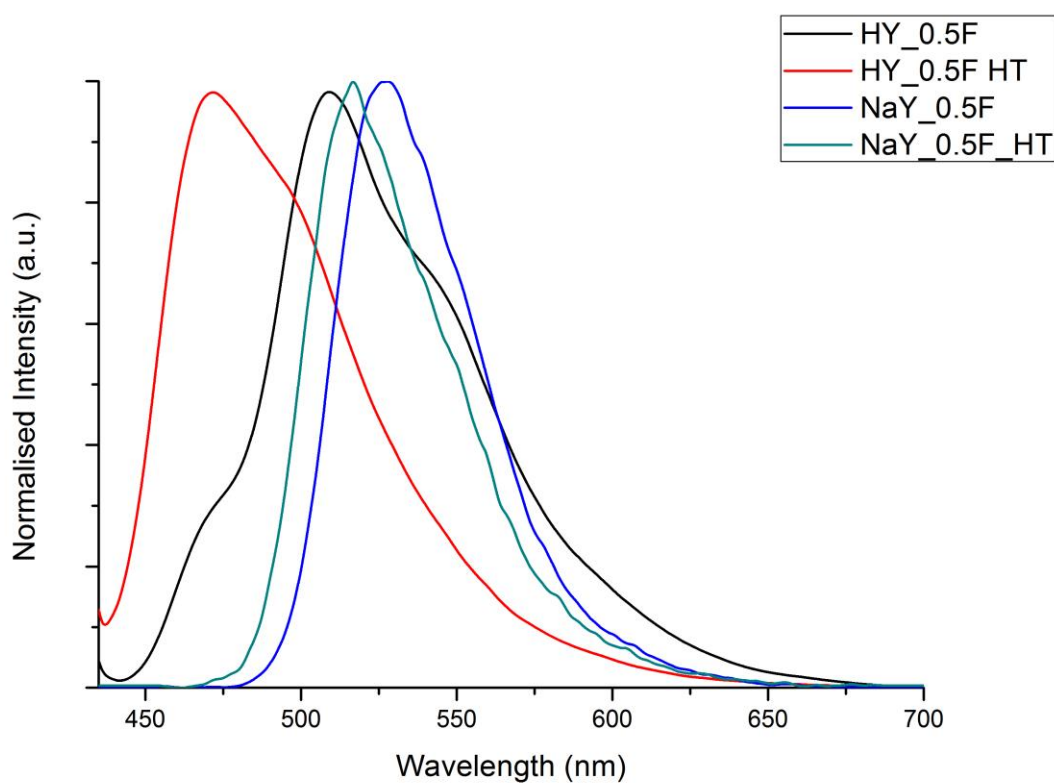


Figure 5.14: Emission spectra of the HY and NaY zeolite before and after the heat treatment.

These results confirmed that the reason for the blue emission in our system is attributable to the protonation of the dye's molecules as a consequence of their interaction with the hydrogen ions trapped into the Faujasite. The cation derivative of fluorescein has only been previously observed in highly acidic solution by Martin and Lindqvist.<sup>79</sup>

Closer observation of the sodium sample also revealed that, upon heating, the dye molecules appear to be ejected from the crystal forming aggregates on the surface of the supporting material. This phenomenon was not observed when hydrogen was present as a non-framework ion. It is plausible that, when sodium has been exchanged in the zeolite, and the water evaporated from the crystals, the fluorescein dianion recrystallised back to the sodium salt, forming aggregates on the surface of the crystals. On the contrary, when hydrogen clusters are present into the Faujasite and water is removed, the protonation of the dye results in a positively charged species which is stabilised within the zeolite crystals by Van der Waals interaction as a consequence of the charge difference between the negative zeolite framework, and the protonated fluorescein.

### **5.3 Impregnation of HPTS into HY Zeolite**

The protonation/deprotonation mechanism responsible for the blue shift in the emission of fluorescein can also be exploited to other kinds of dyes sensitive to the pH, such as 8-Hydroxypyrene-1,3,6-trisulfonic acid trisodium salt (HPTS). The pH sensitivity of HPTS is well-documented, its size is also similar to the molecular dimension of fluorescein, and it has a rigid structure, which prevents any change in the atomic configuration of the molecule which can affect the emission.

The emission of HPTS is known to shift from 511 to 441 nm when the pH of the solution is changed from a basic to an acidic environment.<sup>145-147</sup> The phenomenon is attributed to the protonation of the molecule as represented in Figure 5.15, which results in the transformation of the tetravalent anion, characterised by the 511 nm emission, into the trivalent anion, which emits at 441 nm. The ratio between the tri- and tetravalent forms is related to the pH of the

solution, and only at a proton concentration equal or higher than 6M it is possible to achieve a full conversion, and, consequently, the blue emission from the dye.<sup>145,146</sup>

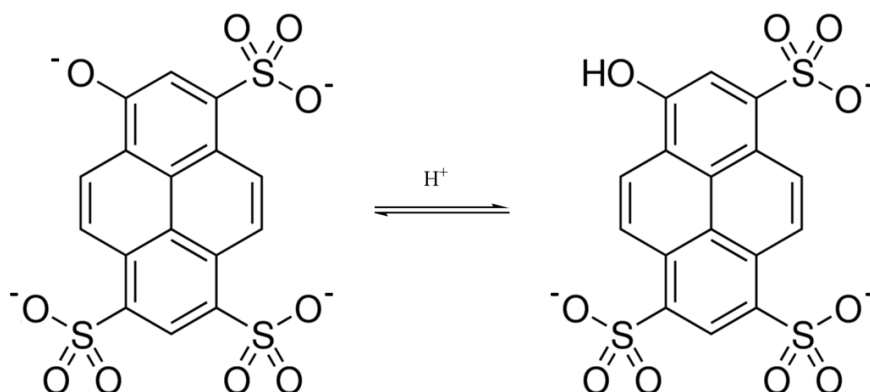


Figure 5.15: Protonation of HPTS leading to the shift in the emission of the molecule.

HPTS was impregnated into the hydrogen containing zeolite using the same procedure describe above. This time, however, the solvent was changed from ethanol to water due to the poor solubility of the HPTS in alcohol. Once the solvent evaporates, the fluorescent hybrid powder (zeolite loaded with a 0.5% of HPTS) was sandwiched between a microscope slide and a coverslip. Two samples were prepared from the same batch, and only one thermally treated at 70° C for two hours before being tested on the fluorimeter. The emissions of the hybrid materials were compared with a water solution of HPTS; samples were excited at 390 nm and the fluorescent signal was collected from 400 to 600 nm. The results of this investigation are reported in Figure 5.16. The analysis of the spectra revealed that no differences can be observed between the emission of the dye dissolved in water, and those of the dye absorbed within the Faujasite cavities not subjected to the thermal treatment. Both the samples presented a main emission at ~ 511 nm accompanied by a shoulder at 411 nm; the only noticeable difference is the relative intensity of the 411 peak, which might indicate a stronger tendency to the protonation of the dye when it is trapped into the zeolite. However, it can also be considered as an artefact generated by the normalisation of the data. More visible and defined variations

in the emission can be seen for the powder sample subjected to the heating process (blue line); in this case, the optical properties differed significantly compared to the signal obtained from the dye in solution. Removing the solvent from the zeolite resulted in a complete protonation of the dye molecules, which as previously reported in the literature<sup>140</sup>, generated a strong shift in the emission of the fluorescent molecule toward the blue region of the electromagnetic spectrum. The heat-treated zeolite-HPTS powder presented a peak centred at 411 nm, and no other noticeable feature, suggesting that all the molecules of the dye have been converted into the protonated derivative.

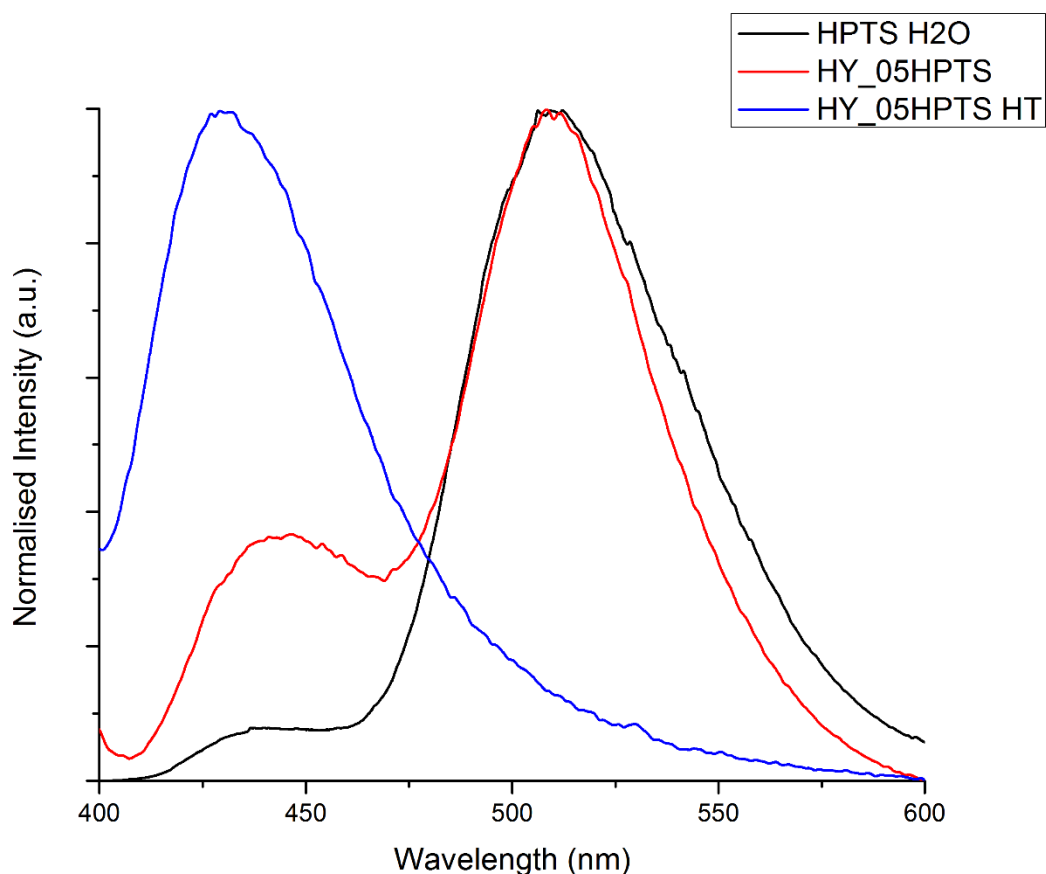


Figure 5.16: Emission of HPTS in water solution and impregnated in HY zeolite before and after the heat treatment.

Similarly, to the fluorescein samples, a time-dependent experiment was set up for the HPTS sample, to monitor the changes in the emission within a period of 18 hours. The spectra,

illustrated in Figure 5.17, show the presence of a smooth transition between the fully protonated molecules and the equilibrium state formed by the coexistence of the tri- and tetravalent form. A slight shift toward shorter wavelength can also be observed in the blue emission for the first four spectra before the blue signal stabilised at 441 nm.

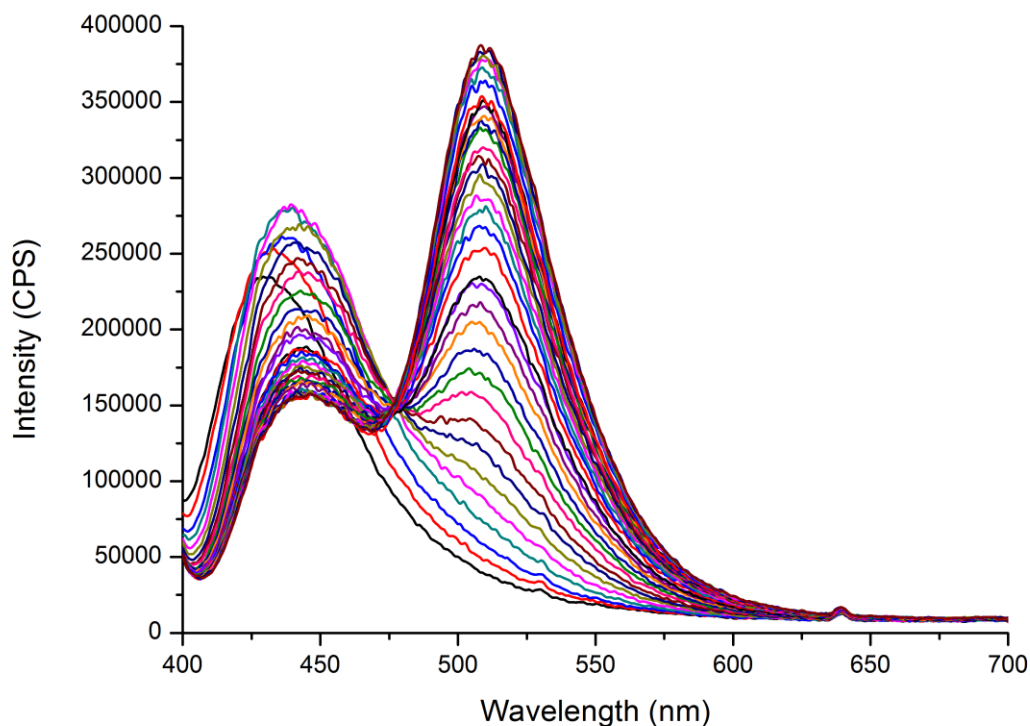


Figure 5.17: Emission of HPTS within a time-frame of 18 hours after the heat treatment.

Analysing the intensity of the blue and green emissions, within a time frame of 18 hours (Figure 5.18), it is possible to note that the initial increase in the intensity of the blue emission is followed by a decrease in the signal, which reached a plateau after 12 hours from the thermal treatment. On the contrary, the green emission appears to steadily increase in an almost linear profile, up until 13 hours from the heating process.

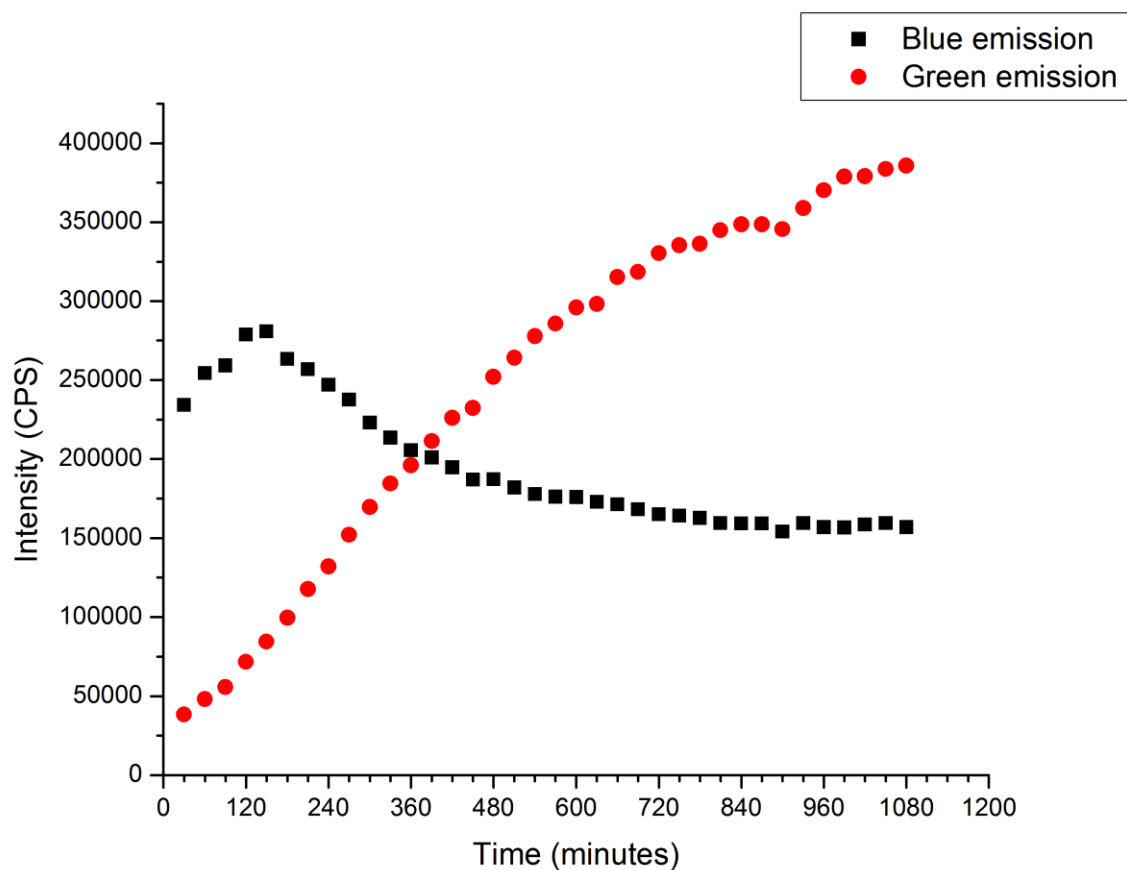


Figure 5.18: Change in the intensity of the blue and green peaks during the 18 hours post the heat treatment.

## 5.4 Recrystallisation of Fluorescein for single crystal analysis

The pH dependence of fluorescein not only affects the optical properties of the dye, but it also has a significant impact on the recrystallisation of the organic molecule. Due to the presence of three neutral forms of fluorescein (Figure 2.14), growing crystals of the dye from a neutral solution, can result in a conformational polymorphism phenomenon such that it is difficult to obtain a single crystal of such a species. Indeed, for a material of such importance it is surprising that no single crystal X-ray structure exists in the literature. The only structure

available is derived from powder X-ray diffraction data.<sup>148</sup> Such an equilibrium can be, however, broken by the use of acid or alkaline environments, which promote the formation of the cation, anion or dianion. The crystal structure of the Sodium dianion has been published as an octahydrate species.<sup>142</sup> Since no structural information was available for the cationic form of fluorescein we attempted to grow suitable crystals from a strong acidic media. Crystals suitable for single crystal X-ray diffraction analysis were prepared from a solution of concentrated trifluoroacetic acid (CAS: 76-05-1) (Sigma Aldrich). A small amount of fluorescein (5 mg) was added to a glass vial containing 1 ml of trifluoroacetic acid. The vial was then hand-shaken before being uncapped and covered with parafilm perforated with a needle. The acid solution was allowed to evaporate slowly and small orange crystals were formed. The crystals were harvested and a suitable specimen was mounted on a microloop sample holder. The single crystal diffraction analysis was performed with a SuperNova, Dualflex, AtlasS2 diffractometer; crystal data, data collection and refinement details are summarised in Table .

Table 6: Experimental Data.

<b>Crystal Data</b>	
Chemical Formula	$C_{20}H_{13}O_5 \cdot C_2F_3O_2$
$M_r$	446.32
Crystal system, space group	Triclinic, $P\bar{1}$
Temperature (K)	120
$a, b, c$ (Å)	8.2511 (14), 10.2200 (11), 12.0793 (14)
$\alpha, \beta, \gamma$ (°)	106.903 (10), 100.898 (13), 95.039 (11)
$V$ (Å <sup>3</sup> )	945.9 (2)
$Z$	2

Radiation type	CuK $\alpha$
$\mu$ (mm <sup>-1</sup> )	1.19
Crystal size (mm)	0.09 x 0.06 x 0.03
<b>Data Collection</b>	
Absorption correction	Gaussian <i>CrysAlis PRO</i> 1.171.38.43a Numerical absorption correction based on gaussian integration over a multifaceted crystal model. Empirical absorption correction using spherical harmonics, implemented in SCALE3 ABSPACK scaling algorithm.
$T_{\min}, T_{\max}$	0.927, 0.975
No. of measured independent and observed [ $I > 2\sigma(I)$ ] reflection	6156, 3322, 2215
$R_{\text{int}}$	0.043
$(\sin\theta/\lambda)_{\text{max}}$ (Å <sup>-1</sup> )	0.595
<b>Refinement</b>	
$R[F^2 > 2\sigma(F^2)], wR(F^2), S$	0.051, 0.153, 1.02
No. of reflection	3322
No. of parameters	329
H-atom Treatment	H atoms treated by a mixture of independent and constrained refinement.
$\Delta\rho_{\text{max}}, \Delta\rho_{\text{min}}$ (e Å <sup>-3</sup> )	0.24, -0.26

Hydrogen bond geometry is reported in Table 7.

Table 7: Hydrogen-bond geometry (Å, °)

$D-H\cdots A$	$D-H$	$H\cdots A$	$D\cdots A$	$D-H\cdots A$
---------------	-------	-------------	-------------	---------------

O1-H1A...O4 <sup>i</sup>	0.98 (4)	1.67 (4)	2.600 (3)	159 (3)
O3-H3b...O7 <sup>ii</sup>	1.02 (5)	1.64 (5)	2.639 (3)	167 (4)
O5-H5B...O6	1.09 (5)	1.47 (5)	2.541 (3)	165 (4)
O6-H5B...O4	1.47 (5)	2.38 (5)	3.459 (3)	126 (2)
Symmetry codes: (i)-x, -y+1, -z-2; (ii) -x+1, -y+1, -z-2				

The crystal structure of the fluorescein-trifluoroacetate is shown in Figure 5.19. The structure clearly demonstrates the presence of the cationic form of the dye, stabilised by the presence of the trifluoroacetic acid anion. The proton transfer between the molecule occurs from the carboxyl group of the trifluoroacetic acid to the hydroxy anion of fluorescein. The single crystal X-ray result also shows the presence of a strong intermolecular hydrogen bond between the O6 oxygen of the acid and the hydrogen of the carboxyl group of the dye.

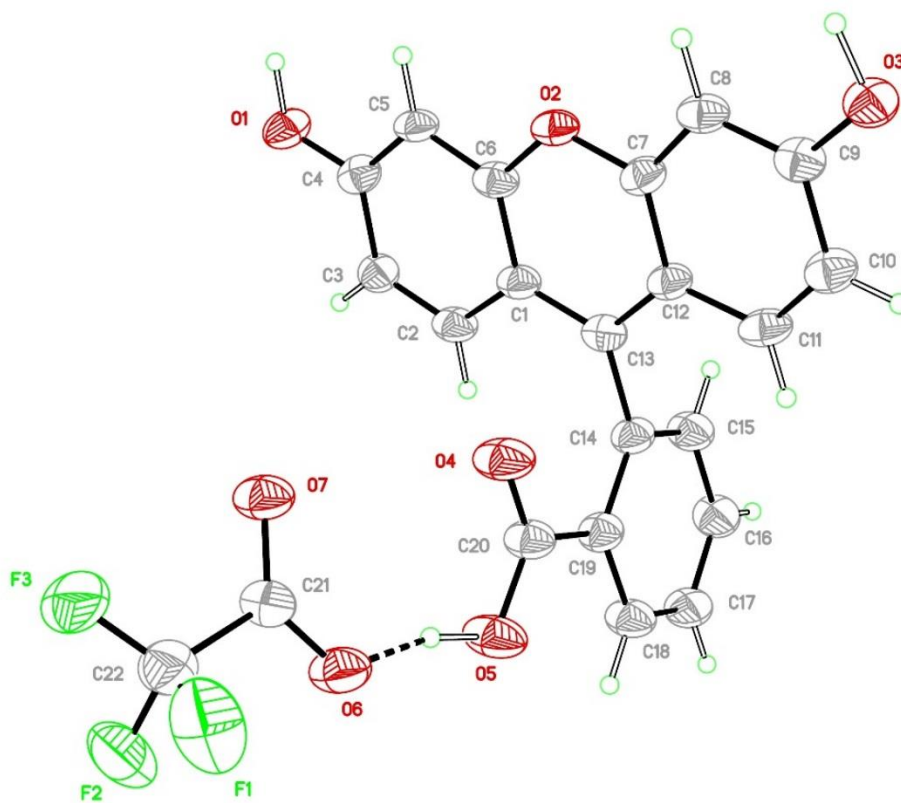


Figure 5.19: Crystal structure of the fluorescein trifluoroacetate salt.

The 3D representation of the unit cell of the co-crystal, down the a, b, and c axis is given in Figure 5.20, whereas the lattice of the fluorescein-trifluoroacetic acid salt form is shown in Figure 5.21.

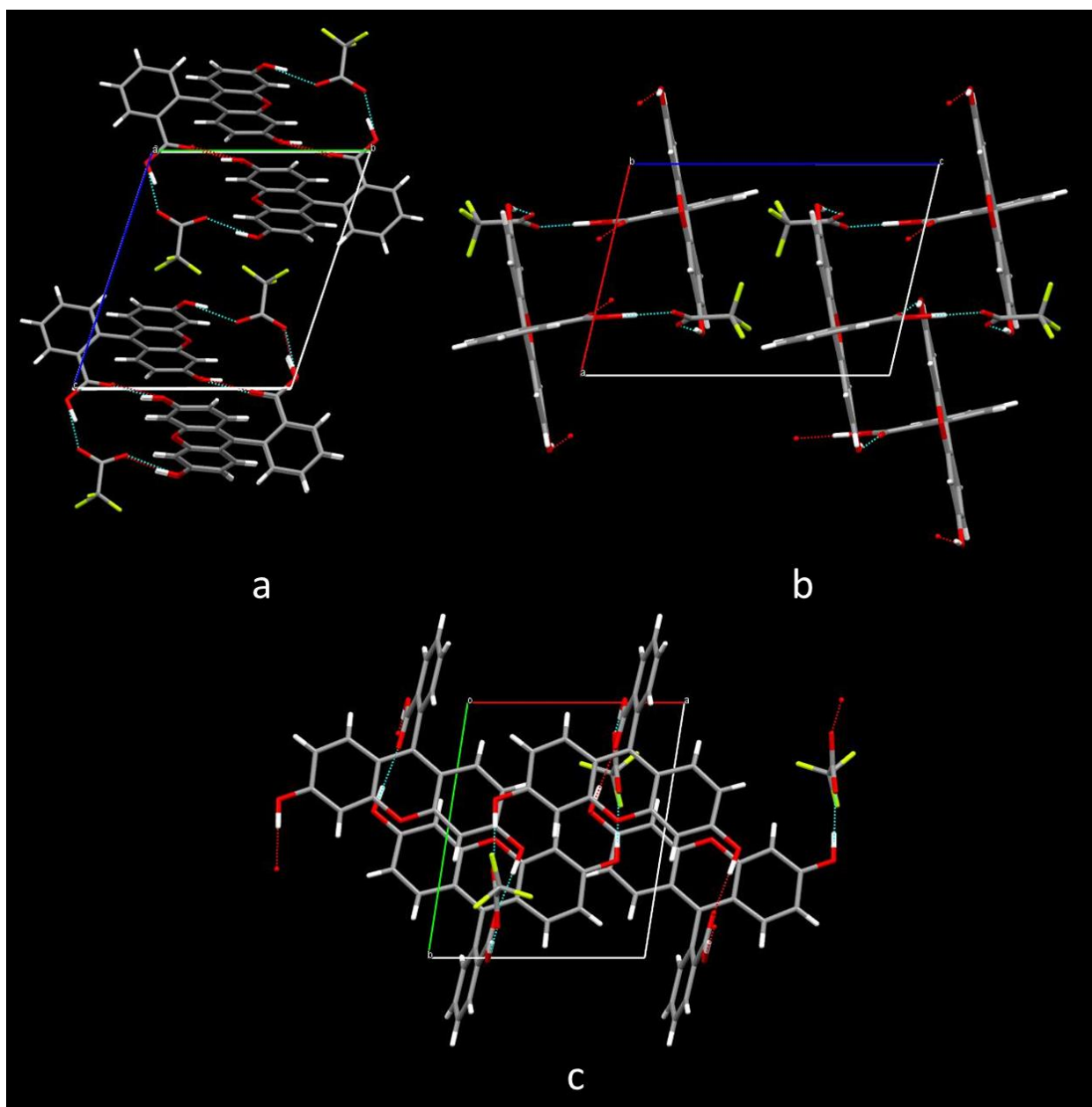


Figure 5.20: Unit cell of the fluorescein-trifluoroacetic acid salt form view down the a (a), b (b) and c (c) axes.

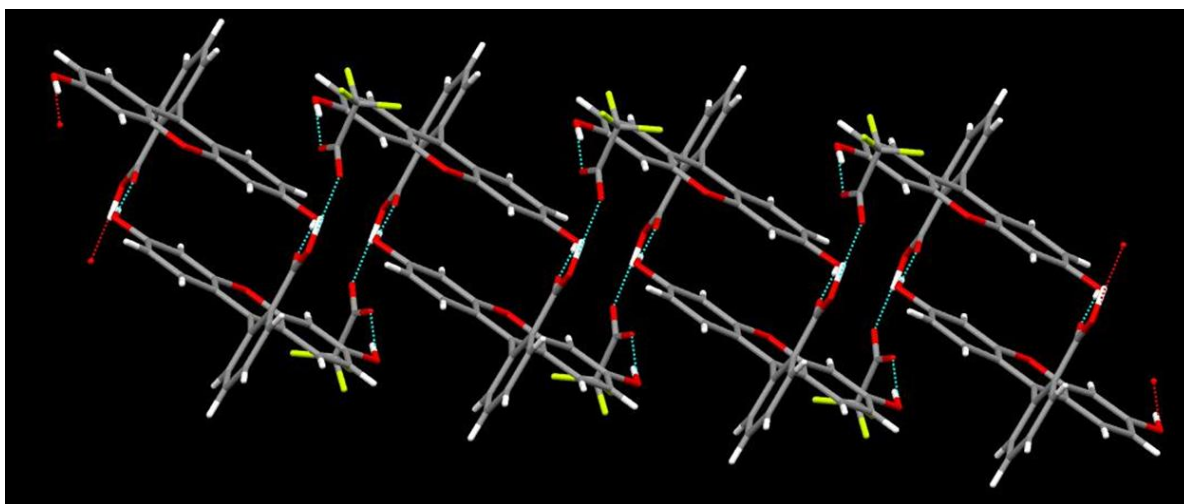


Figure 5.21: Hydrogen bond network of the fluorescein-trifluoroacetic acid salt form.

## 5.5 Synthesis of large Faujasite-fluorescein crystals for single crystal X-ray diffraction

Despite the X-ray powder diffraction analysis and the 3d model of the zeolite-fluorescein, discussed above, seem to indicate the possibility for the organic molecule to migrate within the aluminosilicate framework, they do not give an indication of the location of the fluorescein molecules absorbed into the crystals. The only technique at our disposal that might be able to provide clear information on the matter is a single crystal X-ray diffraction analysis, where the position of the dye's molecule can be visualised by taking into consideration the differences in the electron density between a crystal of zeolite impregnated with fluorescein, and a pristine sample of Faujasite. In order to perform such analysis, however, the synthesis of large Faujasite Y crystals, suitable to be mounted on the diffractometer, had to be carried out since, most of the Y zeolite crystals, that can be acquired commercially, are too small ( $\sim 1 \mu\text{m}$ ) to be utilised.

### 5.5.1 Materials

Fumed silica 99.8% (CAS 112945-52-5), sodium aluminate anhydrous (CAS 11138-49-1), triethanolamine  $\geq 99.0\%$  (TEA) (CAS 102-71-6), sodium hydroxide anhydrous 97% (CAS 1310-73-2) and fluorescein sodium salt 98.5-100.5% (CAS 518-47-8) were purchased from Sigma Aldrich; bis(2-hydroxyethyl) dimethylammonium chloride (TCl) (CAS RN 38402-02-7) was purchased from Acros. All the reagents were used without further purification.

### 5.5.2 Sample preparation

The synthesis of the large faujasite single crystals was performed using the procedure reported by Frechiche *et al.*<sup>149</sup>. A silica slurry, composed by 0.58g of fumed silica dispersed in 10g of deionised water was prepared in a 30ml HDPE bottle. Meanwhile a sodium aluminate solution is prepared by dissolving 6.47g of sodium aluminate powder in a hot solution of 170g of water, which contains 1.51 g of sodium hydroxide; upon cooling, the solution is filtered, and TEA (15.19g for 100g of solution) and TCl (4.19g for 100g of solution) are added to the mixture. The TEA-TCl-sodium aluminate solution is filtered again before being left to react at room temperature for 24 hours. Finally, 16.03g of the stock sodium aluminate solution were added to the silica slurry, and the final mixture was placed in an oven at 95°C for 3 weeks. The obtained powder was filtered and washed repeatedly with deionized water before being dried in air, and impregnated with a 0.5% of fluorescein using the solvent evaporation methods described previously.

### 5.5.3 Results

The morphological and chemical analysis of the large Faujasite crystals, previous to the impregnation of the fluorescein dye, was performed with a Zeiss Supra 35VP scanning Electron

Microscope (SEM). The results, depicted in Figure 5.22, show the presence of impurities in the form of spheres, previously identified by Frechiche *et al.*<sup>149</sup> as gismondine zeolite (GIS), and twinning phenomena, *i.e.* intergrowth of multiple crystals, in the Faujasite zeolite. The average size of the crystals from the SEM analysis was found to be in the order of 130 $\mu$ m.

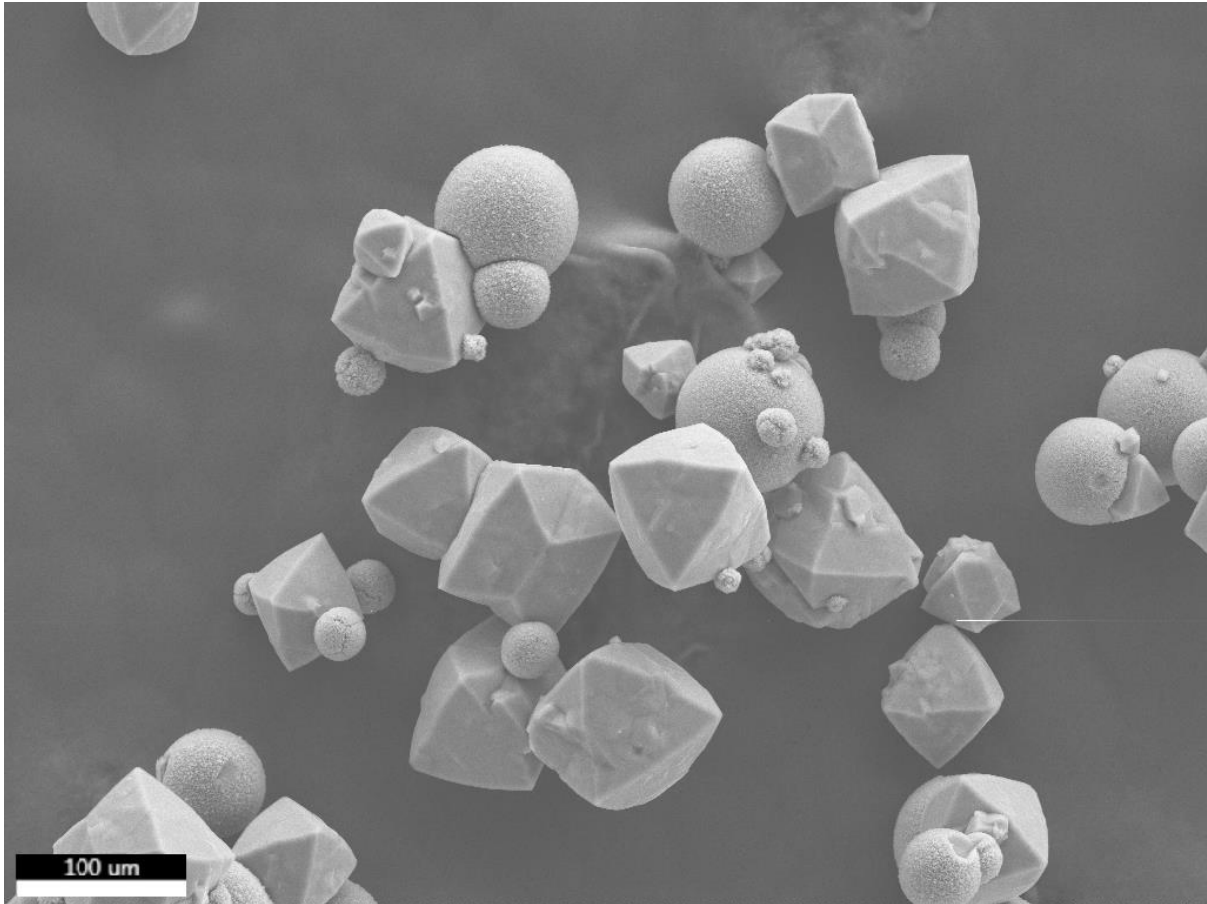


Figure 5.22: SEM micrograph of Faujasite zeolite.

An Energy Dispersive X-ray Analysis (EDX) was performed on the zeolite crystals to gain information about their chemical composition and to investigate the presence of impurities. The result, depicted in Figure 5.23, showed the presence of the typical elements that composed the Faujasite framework (Silicon, Aluminium and Oxygen) along with sodium, probably trapped within the zeolite cavities as non-framework cation for the charge stabilisation, and

minor trace of impurities such as chlorine and carbon. The latter as a consequence of the carbon tape used in the sample preparation.

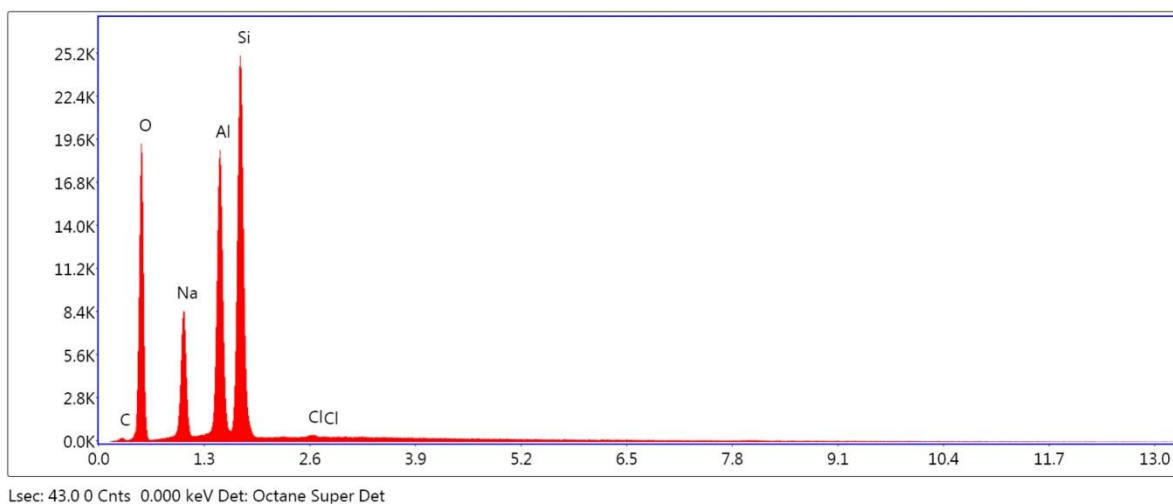


Figure 5.23: EDX analysis of a Faujasite crystal.

Single crystal X-ray diffraction analysis of the pristine zeolite and the zeolite impregnated with fluorescein, did not reveal any information about the location of the organic molecule trapped in the aluminosilicate crystals. The elevated presence of twinning phenomena creates interferences, which made impossible the detection of differences in the electron density between the two samples. The material synthesised was identified as Faujasite type zeolite, with a space group Fd3m.

# Chapter 6 : Fluorescent diamonds

## 6.1 Introduction

Since the discovery of optically active centres in ultra-fine diamonds, this carbon-based material attracted the interest of the scientific community as an alternative to quantum dots, and fluorescent molecules for the new generation of optical probes in biological imaging techniques. Their popularity is attributed to their advantages in terms of low cytotoxicity, high chemical and optical stability, and easy surface functionalisation.<sup>55,88,91–93,150</sup> Optically active diamonds are, however, difficult to produce, as a result of the high energy beams required to promote the formation of structural defects necessary for the generation of colour centres.

In the course of the following chapter the application of fluorescent diamonds, as down-converting material in colour conversion layers (CCLs) for OLEDs, is investigated. The implementation of optically active diamonds into the CCLs not only allow the light output of the OLEDs to be modified, but it can be used to improve the mechanical properties of the matrix in which they are embedded.<sup>88</sup>

In order to generate layers able to completely convert the light generated by the OLEDs, however, a lot of fluorescent diamonds are required. Gamma rays, in virtue of their high penetration depth, represented, therefore, the best candidate for the irradiation and the consequent generation of colour centres. Indeed, being able to penetrate deeply into the structure of the diamond, gamma rays allow for the production of a larger batches of optically active materials compared to the more common electron irradiation. Campbell *et al.*<sup>98</sup> and Iakoubovskii *et al.*<sup>151</sup> investigated the possibility of displacing carbon atoms with gamma rays and described the advantages and disadvantages related to the use of this ionising radiation. No publications, however, were found in the literature concerning the emission behaviour of  $\gamma$  -

irradiated diamonds; we, therefore, performed an optical and structural characterisation of the gamma-treated crystals analysing the samples by photoluminescence and cathodoluminescence spectroscopy, X-ray powder diffraction and electron microscopy.

## **6.2 Materials and methods**

### **6.2.1 Samples Preparation**

Natural diamonds with size in the order of 200 nm were recovered from a commercially available polishing solution (Agar Scientific diamonds slurry 0.25 $\mu$ m). The slurry was treated at 550 °C for two hours to remove the water and the organic solvents; the obtained diamond powder was washed repeatedly with 2-propanol (CAS: 67-63-0) (Sigma Aldrich) and precipitated by centrifugation at 3500 rpm. The sample for the transmission electron microscope was prepared by placing a 5  $\mu$ l drop of a solution of diamonds, dispersed in ethanol, onto carbon-coated TEM grids. The solvent was allowed to evaporate in air before being cleaned by plasma to avoid any contamination.

Gamma irradiated samples were prepared by weighing a small amount of recovered diamonds (50 mg) in glass vials, which were then placed at different distances from the cobalt source, and subsequently annealed at 650 °C for two hours to allow the defects migration.

### **6.2.2 Sample Irradiation**

Samples were irradiated with gamma rays as well as with the electron beam of the transmission electron microscope.

The beam of the TEM was set at the maximum achievable energy (200 KeV), focused on the sample and kept in position for ten minutes. As previously demonstrated elsewhere<sup>152,153</sup> the electron beam of the microscope is capable of creating defects in the crystal structure of diamonds and produce colour centres even in absence of an annealing treatment.<sup>152,153</sup> This

sample was used as a reference, before performing the irradiation of the diamonds with the gamma source.

Gamma irradiation was performed with a  $^{60}\text{Co}$  source able to produce emission line around 1.3 MeV. Since this energy fell in the range of the Compton scattering, the maximum energy transferable from the gamma photon to the ejected electron can be calculated by Equation 2.3 in Chapter 2. Irradiation was performed for 10 minutes with the vials placed at 10 and 100 cm from the source; the  $^{60}\text{Co}$  source activity at the time of the experiment was 274 Ci, which resulted in an absorbed dose of 0.5 and 27 Gy for the sample placed at 100 and 10 cm from the gamma source respectively.

## **6.3 Results**

### **6.3.1 Electron irradiated diamonds**

The morphology, dimension and chemical composition of the powder recovered from the polishing solution were investigated by electron microscopy. Analysis of the sample at the SEM (Zeiss Supra 35VP) reveals the presence of diamonds with a wide distribution in terms of dimension. The average size of the particles resulted in being in the order of 200-300 nm, with most of the crystals showing the presence of twinning phenomena (Figure 6.1).

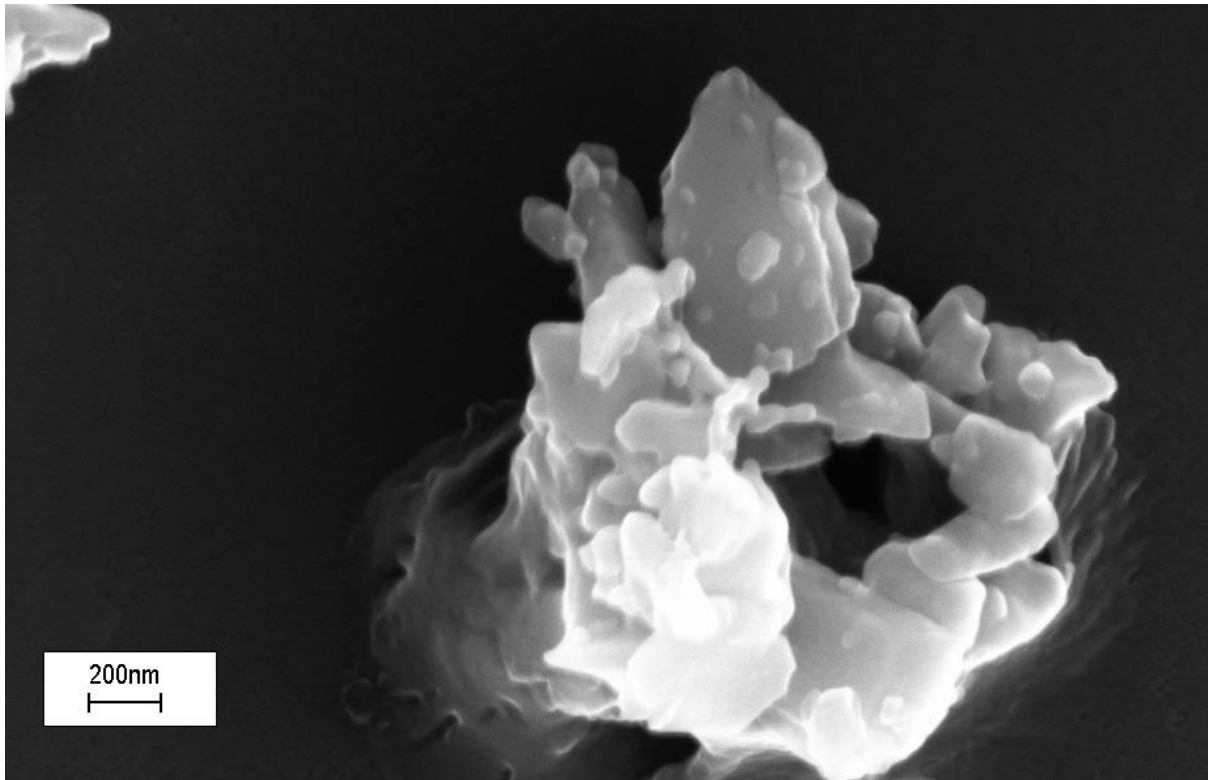


Figure 6.1: SEM micrograph of the diamonds recovered from the polishing slurry.

A JEOL 2100F transmission electron microscope (TEM) was used to irradiate the diamond with electrons, and to perform the analysis of the optical properties of the materials via cathodoluminescence (CL) spectroscopy. The CL images and spectra were recorded with a Gatan Vulcan 465 detector coupled with the microscope, which allows for an in-situ detection of the development of structural defects, leading to the formation of optically active centres. Figure 6.2 depicts the TEM micrograph (left), along with the respective cathodoluminescence image (right), of a twinned crystal exposed to the electron beam of the microscope. The cathodoluminescence image showed evidences of the point nature of the colour centres, shadow and bright areas, representing differences in the intensity of the CL signal, are clearly visible. However, despite the small size of the beam spot used during the irradiation and the analysis, the resolution of a single colour centre was not possible, due to the charge carrier diffusion, which extends the excitation to the entire crystal. <sup>154</sup>

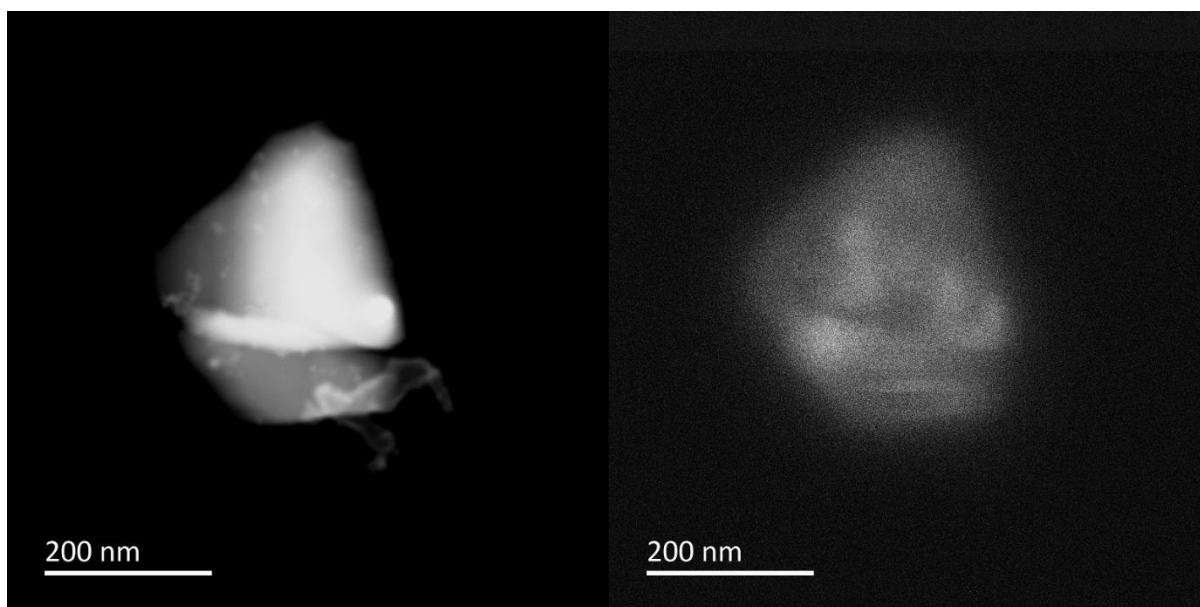


Figure 6.2: Dark field TEM micrograph (left) and CL image (right) of TEM irradiated diamonds.

In addition to the CL image, the emission spectrum of the irradiated crystals was collected in order to identify the type of defects created by the electron irradiation. The characterisation of the luminescent centres in diamonds is generally performed considering the position of the Zero Phonon Line (ZPL) bands. In order for the ZPL peaks to be clearly defined in the emission spectra, low temperatures ( $\sim 70$  K) are required to quench the emission arising from the phonon-assisted bands of the colour centres. Considering the application of fluorescent diamonds as optically active materials for the colour conversion of OLEDs, we analysed the optical properties of our samples at room temperature, to understand their behaviour in a real-life situation.

The cathodoluminescence spectrum of the electron-irradiated sample is presented in Figure 6.3. The emission spread in a wide region, from 400 nm up to 750 nm, with several overlapping features: in order to simplify the peaks interpretation, the complete spectrum was divided into two areas: a UV-green region from 360 to 560 nm, and a red region from 560 to 875 nm. New

baselines were calculated for each area and the recorded signal was fitted with a polynomial curve to easily discern the signal from the noise.

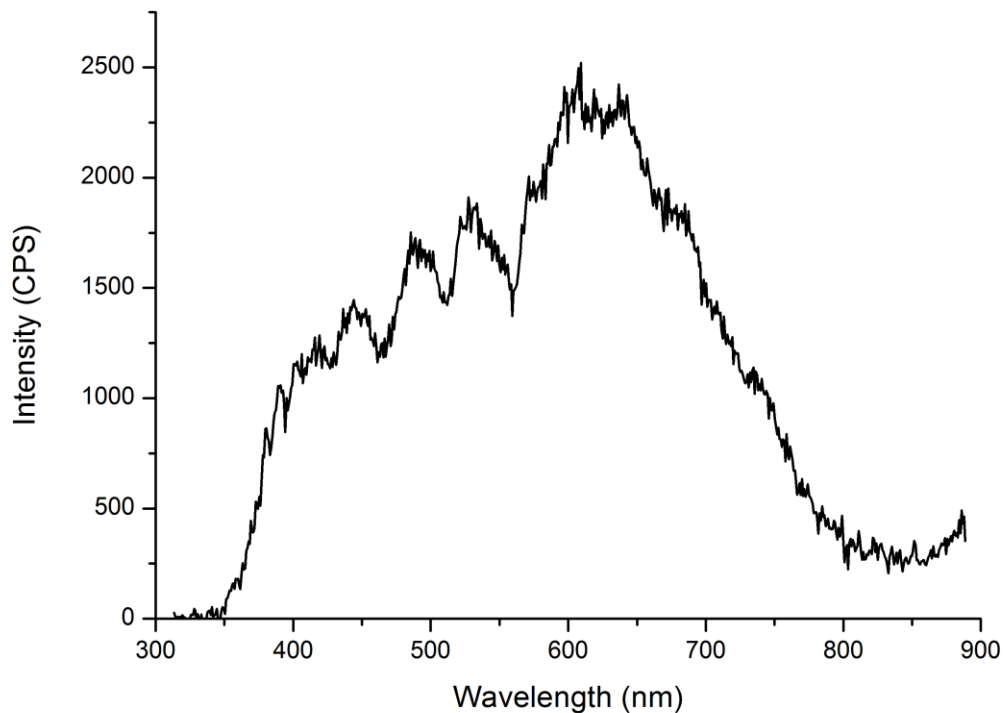


Figure 6.3: Cathodoluminescence spectrum of diamonds collected at the TEM.

The result for the UV-green region is shown in Figure 6.4. The first feature with maxima at 398 nm can be associated with the 3.188 eV centre, a radiation-related optical centre characteristic of all types of diamonds. Its chemical nature is not fully clear and three models have been proposed for its atomic configuration. Zaitsev *et al.*<sup>95</sup> and Collins *et al.*<sup>155</sup> theorized that the centre is formed by an interstitial nitrogen coupled with defects in the lattice, while Collins and Wood<sup>156</sup> correlated the centre with a nitrogen impurity bonded to the nearest carbon in an interstitial position. In the same paper, they also proposed a different configuration consisting of a single substitutional N shifted along the  $\langle 111 \rangle$  axis forming elongated C-N bond.<sup>95</sup> The very same centre is also responsible for the emission at 400 nm, which is generated

by the phonon-assisted decay of the excited state; the 3.188 eV is also known to present a secondary sideband at 410 nm, which in our sample is not visible due to the overlap with the ZPL band of the N3 centre located at 415 nm.<sup>95</sup> The N3 colour centre is common in natural diamond, known for its bright blue emission, which includes sidebands at 435, 440 and 460 nm. The proposed model for this feature consists in a vacancy surrounded by three nitrogen atoms.<sup>83,95,97,154</sup> The origin of the emission at 435 nm is unclear, it can be attributed to the band A centre formed by a double nitrogen impurity or, as reported above, to a phonon-assisted band of the N3 centre. The presence of the emission at 445 nm, however, suggests that the 435 nm signal arises from the band A, since this colour centre is known to have a phonon-assisted at 445 nm, also present in our spectra.<sup>95</sup> The shoulder at 451 nm can be associated with the 2.748 eV centre often reported in the CL of natural diamonds. This centre is originated by the presence of rhombic-I symmetry or A-E transition of a tetragonal centre.<sup>95,157</sup> The broad emission, visible at around 485 nm, can be associated with the formation of slip traces as consequence of the irradiation of type Ia diamonds, or the presence of an intracentre transition at the B1 centres of the A-band.<sup>95</sup> This feature partially overlaps a secondary emission around 500 nm, which can be identified as either the B-line band typical for natural diamonds, or it can be the result of the A<sub>s</sub> band, known to be produced in natural diamonds which have been exposed to a low intensity electron beam.<sup>95</sup> The broad emission between 520 and 535 nm can be associated with the presence of the 3H centre, and it is common for all type of irradiated diamonds. The 3H is characterised by a ZPL at 503 nm and a series of phonon assisted bands. Three models for this centre have been proposed including a combination of carbon atoms and vacancies (V-C-C-V), a vacancy-oxygen pair and, the most plausible of all, a split interstitial <100> crystal plane.<sup>95</sup> The last feature is represented by a shoulder at 540 nm, which has been previously reported by Gucsik *et al.*<sup>157</sup> as the result of dislocation near nitrogen impurities;

similar emission has been reported by Collins<sup>97</sup> and it has been identified as the 2.721 eV centre.

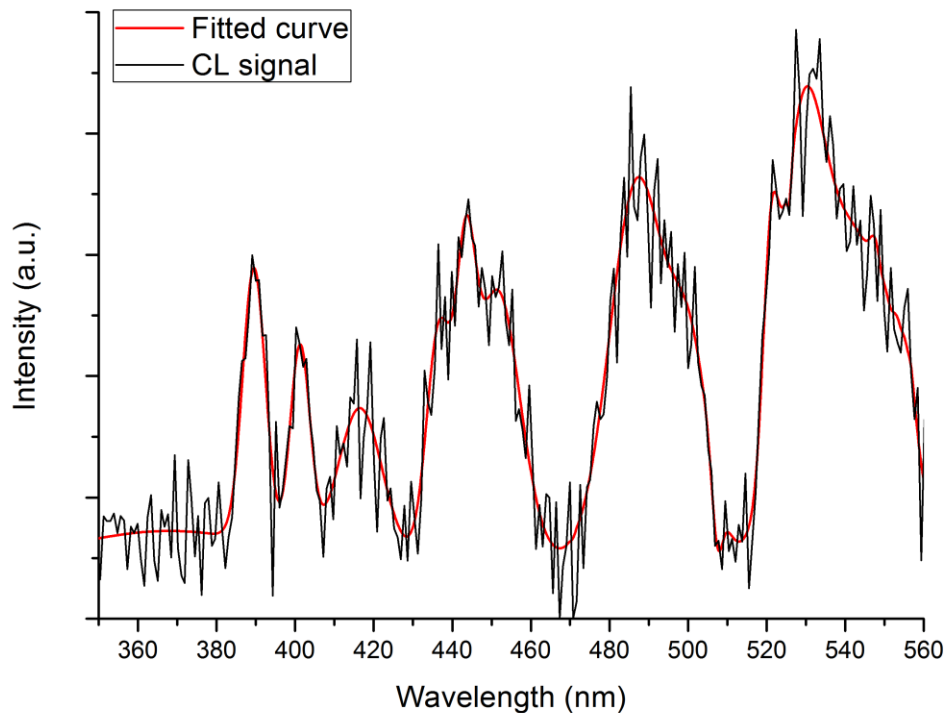


Figure 6.4: UV-green region of the CL spectrum collected at the TEM.

The second part of the cathodoluminescence spectra from 560 to 860 nm is reported in Figure 6.5. The first recognisable feature has been defined as the T1, 2.156 eV or simply the 575 nm centre.<sup>83,95,97</sup> The centre is characteristic in all types of diamonds, and it is generally produced by irradiation followed by annealing at 900-1000 K. However, it has also been detected in natural diamond subjected to low KeV electron irradiation without annealing.<sup>95</sup> The configuration of this feature is uncertain, but the most accepted model, is a nitrogen impurity next to a vacancy ( $NV^0$ ).<sup>93,97</sup> This centre is also known to present phonon assisted bands located around 585nm, 600 nm and 620 nm.<sup>95</sup> Similar optical configuration but with a partial negative charge ( $NV^-$ ) is responsible for the peak at 630 nm and phonon replicas at 700, 721 and 735

nm.<sup>95</sup> The broad emission at 690 nm is due to the B-band characteristic for natural diamonds. The atomic model of this feature is known to be related to the presence of dislocations in the crystals.<sup>95</sup> Finally, the signal at 744 nm can be identified with the GR1 centre; this optical centre generally presents a second peak at 740 nm which in the spectra is not clearly visible due to the partial overlap with the phonon-assisted band of the NV-centre. The GR1 is one of the most studied colour centres in diamonds and it is known to be produced by any kind of irradiation in all types of diamonds. The nature of the centre is attributed to a single vacancy with a neutral charge ( $V^0$ ). Phonon replicas of the GR1 centre are also visible in the spectra at 758 and 773 nm.<sup>95,97,158</sup>

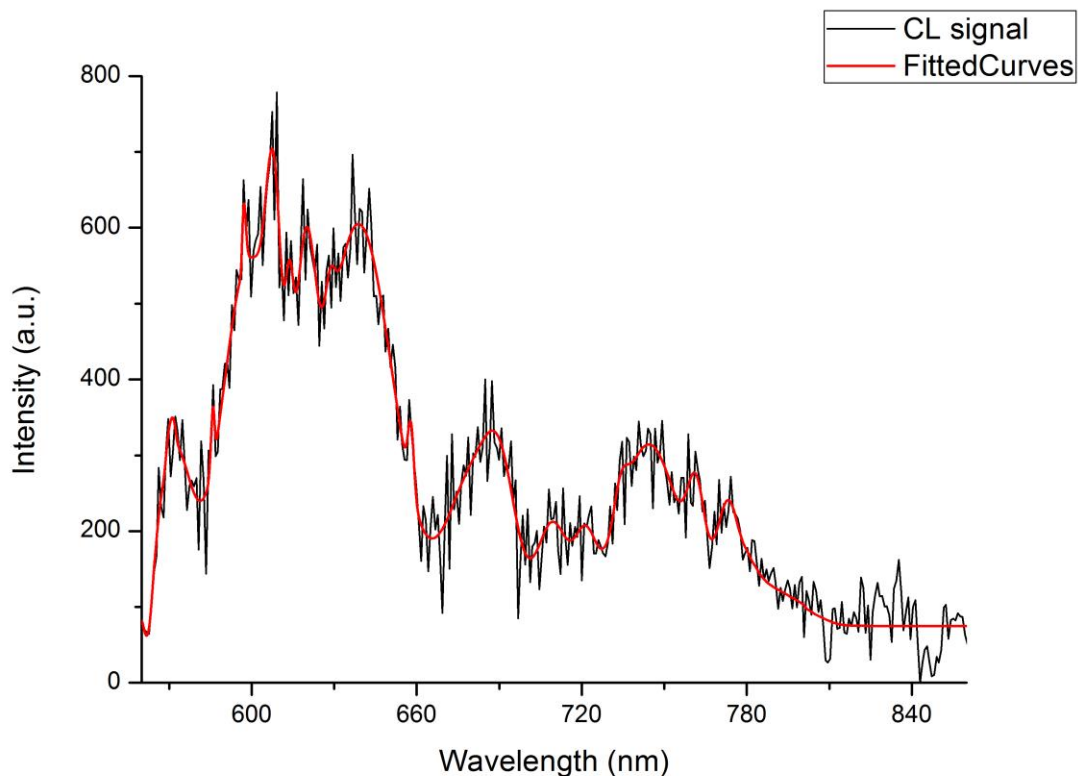


Figure 6.5: CL emission from 560 to 860 nm of TEM irradiated diamonds.

Since the TEM is also equipped with a Gatan Electron Energy Loss Spectroscopy detector, a chemical analysis of the diamonds recovered from the slurry was performed on the same

sample. The high sensitivity of the technique allows the presence of impurities in the crystal lattice to be detected, despite their low concentration (in the order of ppm). Figure 6.6 depicts the EELS spectra obtained from the diamond sample. Clearly discernible from the background is the peak at 403 eV, which can be attributed to the presence of nitrogen.<sup>159</sup>

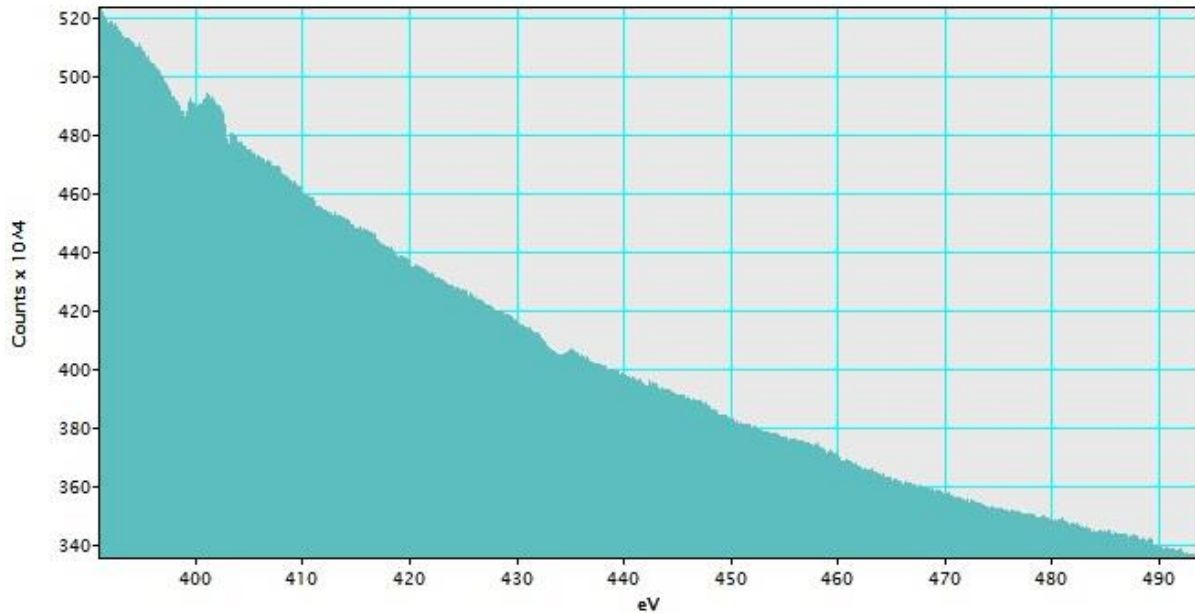


Figure 6.6: EELS spectra of the diamonds recovered from the polishing slurry. The presence of nitrogen is confirmed by the small feature at 403 eV.

### 6.3.2 Gamma irradiated diamonds

The crystallinity of the diamonds recovered from the polishing slurry and of those treated with gamma rays was analysed by synchrotron radiation. The samples were exposed to the X04SA beamline at the Swiss Light Source (SLS). The diamonds were loaded in a 0.1 mm glass capillary and irradiated by an X-Ray beam with an intensity of 20KeV, and a wavelength of 0.622 Å.

The powder diffraction for the pristine and gamma treatment diamonds is shown in Figure 6.7. The analysis revealed an elevated degree of crystallinity, and confirmed the diamond nature of the material recovered from the slurry with the presence of several peaks characteristic for

diamonds at 17.37, 28.55, 33.61, 40.82 and 44.67 degrees, which can be associated with the diffraction from the  $\langle 111 \rangle$ ,  $\langle 220 \rangle$ ,  $\langle 311 \rangle$ ,  $\langle 400 \rangle$  and  $\langle 331 \rangle$  crystal planes. Despite the high resolution of the synchrotron radiation used, however, no discernible differences can be observed comparing the diffraction patterns of the pristine diamonds (black line) with those subjected to a high and low dose gamma irradiation (blue and red line).

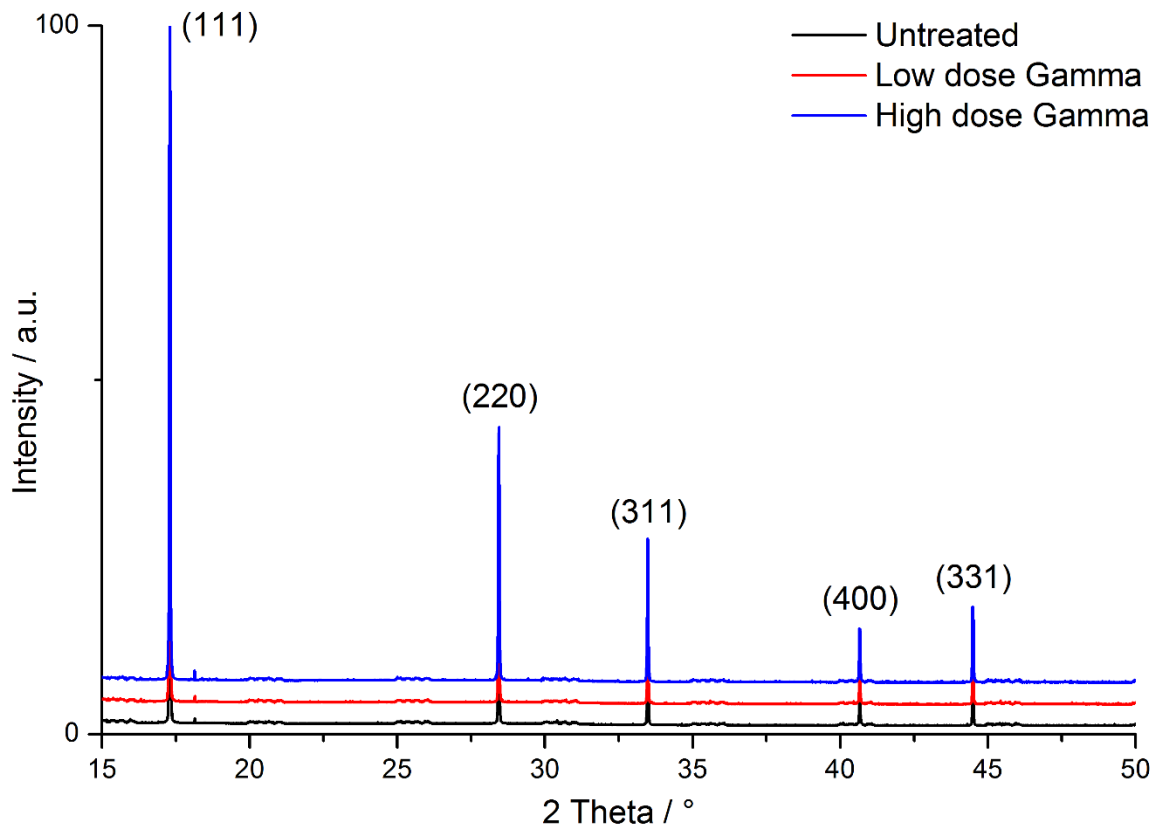


Figure 6.7: XRD pattern of untreated and gamma treated diamonds.

The optical properties of the materials were investigated with a Horiba Fluorolog Jobin Yvon Fluorolog iHR320 operating in front face mode.

Diamonds were dispersed in spectroscopic grade ethanol and excited in the UV at 365 nm, as well as under visible blue light at 480 nm. The emission from the samples was collected from 400 nm to 650 nm for UV, and from 520 nm to 650 nm for visible excitation. Spectra were recorded at room temperature; this along with the large slits values used, required by the low

emission of the samples, resulted in a broadening of signal and prejudiced the detection of the ZPL peaks.

Figure 6.8 shows the normalised fluorescence signal observed from non-irradiated and gamma treated diamonds upon excitation with UV light; the spectra revealed a blue emission for the untreated samples characterised by two peaks at 435 and 458 nm. The nature of these features can be explained as a combination of two separate colour centres, more specifically the A-band, known to present PL at 434 nm and the N3 centre. The presence of the N3, despite being overlapped by the A-band, is recognisable by the shoulder at 458 nm representing a phonon-assisted transition of such optical configuration.<sup>83,95,160</sup>

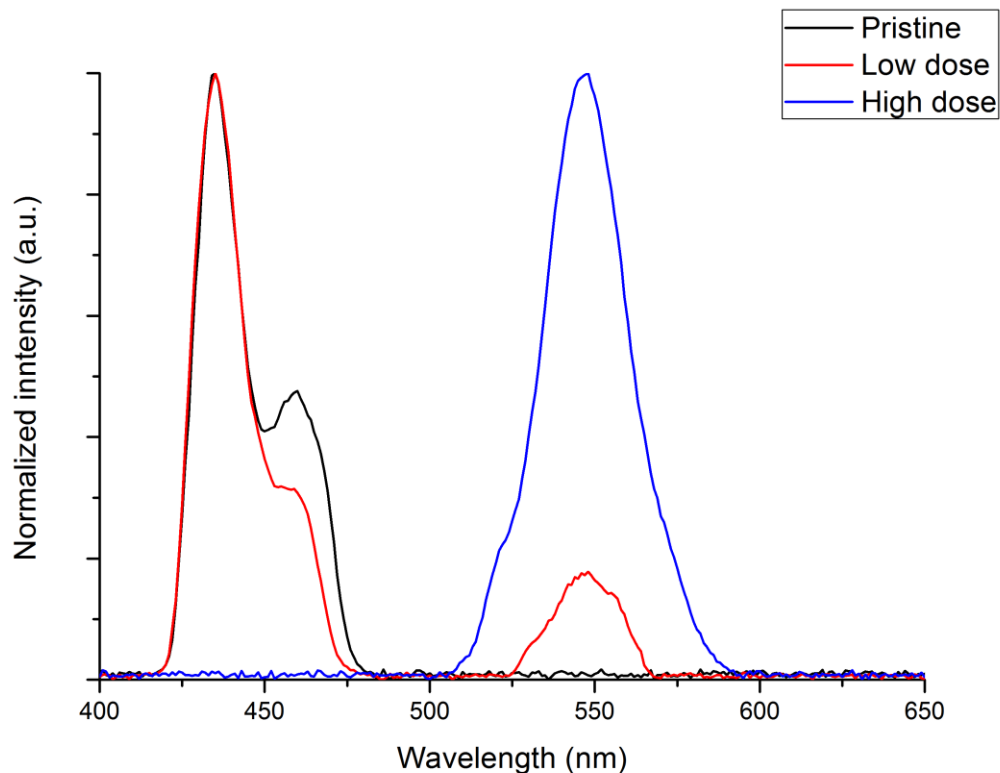


Figure 6.8: Emission of pristine (black), low (red) and high (blue) dose irradiated diamonds upon excitation with UV light (365 nm).

The very same signals are also observable on the sample irradiated with the lowest gamma dose, however, the effect of the ionising radiation on this sample is clearly visible by the presence of a third emission in the green-yellow region of the electromagnetic spectra with a maximum at 545 nm. The fluorescence behaviour of such a signal closely resemble the H3 centre known to be produced in diamond subsequent irradiation and annealing. The optical and chemical characteristic of this configuration are well described by Zaitsev.<sup>95</sup> The atomic model for the H3 is still debated, but all the proposed hypotheses involve the transformation of the diatomic nitrogen inclusions, characteristic for the A band, as a consequence of the newly created defects produced by the ionising radiation. The two most accepted models include a double nitrogen impurity trapped between two vacancies (V-N-N-V) and a pair of nitrogen atoms separated by a vacancy (N-V-N). The possible conversion from the A band to the H3 centre is even more evident in the spectra observed for the sample irradiated with the highest gamma dose. Increasing the amount of radiation will promote the formation of defects within the crystals. As a result of that, the interaction of the vacancies with the double nitrogen impurities will be greater leading to the disappearance of the blue peaks of the A band and the appearance of a strong green-yellow emission of the H3 centre (blue spectrum).

Another singularity present in the spectrum of the sample irradiated with a high  $\gamma$  dose is the absence of the emission at 458 nm, identified with the N3 sideband. A similar quenching, although less evident, is also visible in the low dose sample; such phenomenon can be attributed to the creation of the H3 centre, which might promote an internal energy transfer, where the blue light emitted from the N3 is captured by the H3, and reconverted in the green-yellow radiation.

In order to visualise the effect of a blue light irradiation on the emission of the H3 centre, the gamma irradiated samples were excited with 480 nm light. This wavelength is comparable to the main emission found in blue OLEDs, and will provide an indication of the possible use of

fluorescent diamonds as optically active materials in the colour conversion layers. The results, depicted in Figure 6.9, reveal that the H3 centre can be stimulated by blue light resulting in a green emission centred at 550 nm.

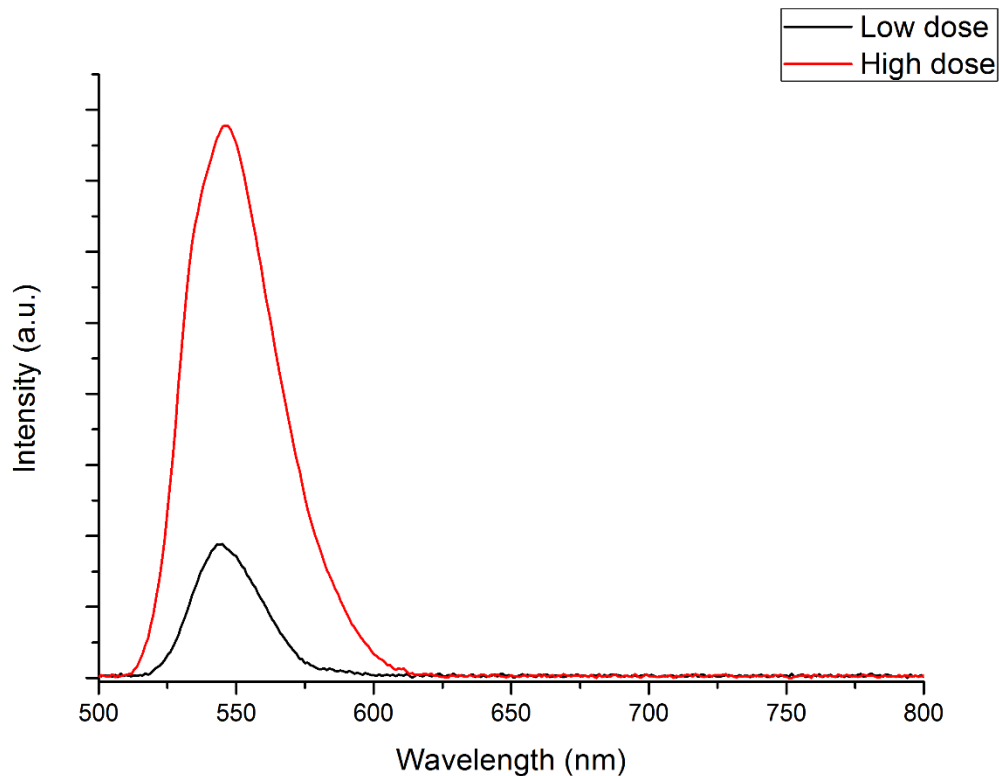


Figure 6.9: Emission of low (black) and high (red) dose irradiated diamonds upon excitation with blue light (480 nm).

A Leica (Leitz DMRB) wide-field fluorescence microscope was used to acquire a fluorescent image of the diamonds irradiated with the lowest dose of gamma radiation. The sample was sandwiched between a microscope slide and a quartz cover slip, and excited with UV and blue light (365 and 488 nm). The results depicted in Figure 6.10 are in agreement with the emissions observed on the fluorimeter; light blue emission can be observed in the crystals upon excitation with UV light, and a green colour can be observed from the diamonds subjected to blue irradiation.

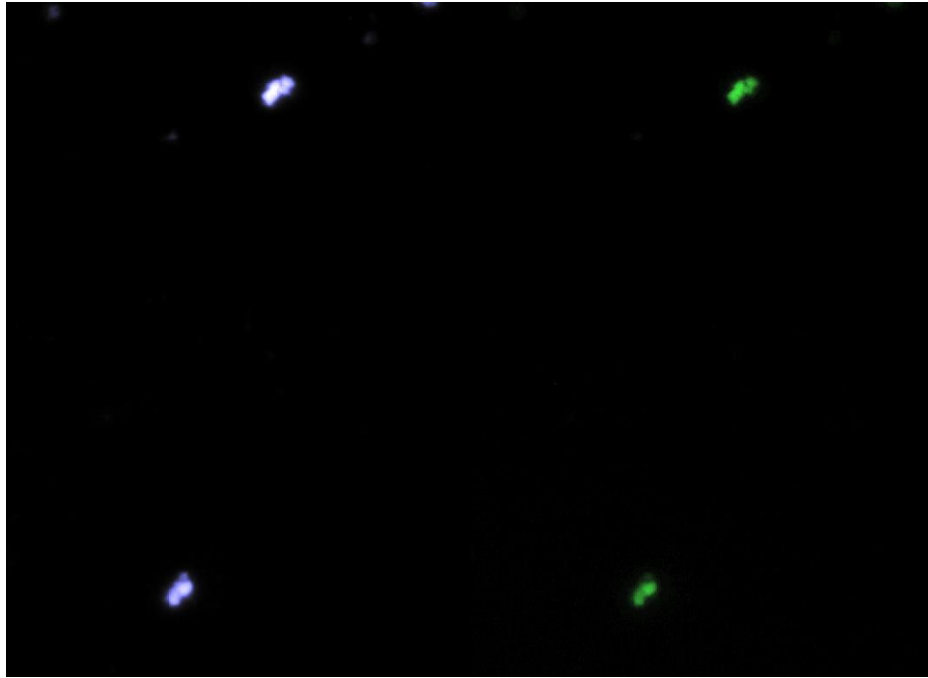


Figure 6.10: Fluorescent microscopy images of diamonds excited by UV (left) and blue light (right).

## 6.4 Discussion

Production of colour centres in natural diamonds, recovered from a commercially available polishing spray, were investigated. The aim of the study was to create fluorescent diamonds by irradiation with gamma rays originated from a  $^{60}\text{Co}$  source, and use the material as an optically active component in the production of colour conversion layers for OLEDs. The results, obtained by gamma irradiation, were compared with those one obtained using the low energy electron beam of the transmission electron microscope. As previously reported by Iakoubovskii *et al.*<sup>151</sup> and Campbell *et al.*<sup>100</sup>, we observed that, gamma rays are capable of creating defects in the diamond's lattice, producing optically active atomic configurations. However, the amount and type of colour centres achieved by gamma rays are less than the colour centres produced by TEM irradiation. Excluding the emission identified with the A band and the N3 centres, which are naturally present in the samples here investigated, treating the diamonds with gamma rays will result in the production of a single optically active configuration

attributed to the H3 colour centre. Although its characteristic emission in the green-yellow region of the electromagnetic spectrum, in response to blue excitation, appears to be promising for the down-conversion of the light emitted by blue OLEDs, its emission resulted in being too low for a practical application of the diamonds as a colour converting materials for the OLEDs.

## **6.5 Conclusions**

Application of fluorescent diamonds as active materials in colour converting layers for thin and flexible OLEDs could lead to promising results in terms of device colour modification in virtue of the multitude of optically active centres, which can be obtained in a single crystal, and their wide spectral response. The physical-chemical properties of diamonds, moreover, have already been demonstrated to be able to significantly improve the wear resistance, as well as the mechanical and thermal properties of polymers and rubbers in which they are dispersed.<sup>88</sup>

We investigated the use of gamma radiation to generate colour centres in diamonds but the approach was not efficient. Due to the small amount of optical configuration that can be generated, and their low fluorescence intensity, gamma irradiated diamonds cannot be used as an alternative down-conversion material for the fabrication of colour conversion layers for OLEDs.

## Chapter 7 : Discussion

In summary, we have presented three solutions for the fabrication of colour conversion layers (CCLs) tailored for flexible blue and green Organic Light Emitting Devices (OLEDs).

The investigation on the solid state processing of organic fluorescent dye dispersed in polymer matrices (Chapter 3.2) demonstrated that is possible to create layers able to convert the light output of the OLEDs. However, this approach brings an important limitation concerning the flexibility of the coating as a result of the poor solubility of the organic molecule in the polymers, which required the fabrication of thick layers. This was particularly problematic for polymethylmethacrylate (PMMA) where the fluorescent dye, rhodamine 6G, remains in a crystalline non-emissive form. Polycarbonate (PC) and polystyrene (PS), despite showing more compatibility with the organic molecule, exhibited of aggregation phenomena. In addition to the mechanical properties, the layers produced with this method presented a problem related to the application of the layers on the OLEDs. Injection moulding and compression moulding techniques were not compatible, due to the high temperature and pressure used, with the delicate nature of the flexible OLEDs. The alternative was found in the solution processed method where the dyes (fluorescein disodium salt and rhodamine 6G) were dispersed in a water-based acrylic varnished (Chapter 3.3). The dyes solubility was found to be sufficient for the conversion of the light output of the OLEDs, and only when the concentration of the organic molecules was increased above 1% w/w, aggregation phenomena were observed. This approach was well received by the design teams involved in the project, since it results in thin, transparent, efficient and extremely flexible layers easy to be applied directly on top of the light emitting devices by screen printing method or paint brushing technique. Varying the method

of application, was possible to fabricate uniform layers or coating with a variable thickness, which resulted in colour gradient effects when applied on the OLEDs.

To explore different tactile perceptions, as required at the beginning of the project, fluorescent silicone layers were developed for the down-conversion of OLEDs; the optical, chemical, physical and mechanical properties of polysiloxanes make this kind of material ideal as a matrix for the fabrication of colour converting layers. Their only drawback concerned the immiscibility of the organic dyes into the silicone. For this reason, we investigate the application of fluorescent particles, specifically luminescent hybrid materials (Chapter 4) and fluorescent nanodiamonds (Chapter 6), as down-converting species for the CCLs.

Nanodiamonds are well-known for their optical and chemical properties, which include a large number of absorption and emission pair, chemical and optical stability, and elevated quantum yield. In addition, their dispersion within the silicone layers can improve the mechanical properties of the final material. Fluorescent centres in diamonds are difficult to produce on a large scale since they are generally obtained by irradiation of the crystals with high energy electron or neutron beams. We, therefore, investigated the use of gamma radiation as an alternative method for the displacement of the carbon atoms in the diamond's lattice. Gamma rays, despite being less effective than electron or neutron radiation, present the advantage of being more available and possess higher penetration depth allowing for the production of larger batches of luminescent diamonds. The obtained result, however, showed that the colour centres generated by gamma irradiation had the suitable absorption-emission pair for the colour conversion of OLEDs, but their intensity was too low for practical application as optically active material in the CCLs.

An alternative to the diamonds was found in the application of hybrid organic-inorganic fluorescent particle constituted by organic dyes absorbed into the pores or cavities of inorganic supporting materials. Such a combination allows for the dispersion of the dye into the otherwise

non-miscible silicone matrix. Silica gel and Faujasite Y zeolite were used as carrier devices for the dyes because of their elevated porosity. The dyes, rhodamine 6G and fluorescein disodium salt, were absorbed into the inorganic scaffolding by solvent evaporation methods, a technique that allowed to avoid the use of complex synthetic and purification procedures. The result we obtained fully satisfied the physicochemical and mechanical requirements and the use of low-temperature curing silicone allowed the direct casting of the polysiloxane layer to the OLED substrate. Moreover, upon encapsulation of fluorescein in the cavities of the zeolite, unexpected and unusual optical properties of the fluorescent molecule were observed. This behaviour was studied (Chapter 5), and it was found to be a consequence of the presence of hydrogen cations in the cavities of the zeolite structure as non-framework ions, which promote the formation of the protonated form of the dye.

## Chapter 8 : Conclusions

In this thesis, several approaches were investigated for the production of colour conversion layers tailored for the down-conversion of blue and green flexible OLEDs. Strict requirements were demanded by the design teams and the industrial partners participating in the Light.Touch.Matter (LTM) project, and had to be taken into consideration. The colour converting layers were required to have specific optical, chemical and mechanical properties in order to match the characteristics of the devices and the prototypes specification. Elevated transparency and flexibility for the matrix had to be coupled with suitable absorption and emission spectra, and high efficiency of the optically active materials. Despite this work was mainly focused on the use of fluorescent organic molecules, in virtue of their wide range of optical characteristics, elevated quantum yield, high availability and low cost; the use of fluorescent particles, such as nanodiamonds, as down-converting materials were also explored. The CCLs developed in the course of this project have been proven to be an effective way to fine tune the emission of OLEDs without affecting their structure, hence keeping the device easy to produce and the cost low. In addition, interesting and particular colour effects, such as gradient or complicate patterns, can be obtained via this approach, as demonstrated by the layers produced by the combination between the water based acrylic varnish with the organic dyes, fluorescein sodium salt and rhodamine 6G, that had been employed by the designer during the fabrication of their prototypes, showcased in conjunction with the last project meeting in Delft. An exception has to be made for the nanodiamonds, where the low emission achieved and the difficulties in the production of these fluorescent particles, resulted in a system characterised by a poor conversion and elevated cost.

The hybrid silicone layer and the fluorescent diamonds described here, represent two novel materials for the fabrication of CCLs. Neither of these materials have never been employed before for the downconversion of the light emitted by the OLEDs. In addition, their development and characterisation led to the discovery of peculiar properties which have not been reported in any scientific publication. Particularly interesting is the reversible shift in the emission of fluorescein which, despite the dye being widely studied, has never been observed before. This phenomenon and the subsequent investigation also resulted in the acquisition of the first single crystals X-Ray structure.

Future research in this area might take into consideration the use of fluorescent metal nano-clusters as down-conversion materials in virtue of their colour tune-ability, stability and efficiency. Also, interesting would be the development of colour conversion layers sensitive to the environment which can provide a direct feedback on environmental conditions such as the level of humidity, temperature or as a consequence of the presence of noxious gases providing the user with a visual response changing the colour of the device or restoring the original OLEDs colour by bleaching out according to the signal received.

# Bibliography

1. Brand, J. C. D. (John C. D. *Lines of light : the sources of dispersive spectroscopy, 1800-1930*. (Gordon and Breach, 1995).
2. Webster, M. Human colour perception and its adaptation. *Netw. Comput. Neural Syst.* **7**, 587–634 (1996).
3. Nathans, J., Thomas, D. & Hogness, D. Molecular genetics of human color vision: the genes encoding blue, green, and red pigments. *Science (80 )*. **232**, 193–202 (1986).
4. Bamfield, P. & Hutchings, M. G. *Chromic Phenomena. RSC Advances* (Royal Society of Chemistry, 2010).
5. Seki, K., Ito, E. & Ishii, H. Energy level alignment at organic/metal interfaces studied by UV photoemission. *Synth. Met.* **91**, 137–142 (1997).
6. Misra, A., Kumar, P., Kamalasanan, M. N. & Chandra, S. White organic LEDs and their recent advancements. *Semicond. Sci. Technol.* **21**, R35–R47 (2006).
7. Kitai, A. *Luminescent materials and applications*. (John Wiley, 2008).
8. Henisch, H. K. Electroluminescence. *Reports Prog. Phys.* **27**, 308 (1964).
9. Kafafi, Z. Organic Electroluminescence. 496 (2005).
10. Lossev, O. V. CII. Luminous carborundum detector and detection effect and oscillations with crystals. *London, Edinburgh, Dublin Philos. Mag. J. Sci.* **6**, 1024–1044 (1928).
11. Destriau, G. Recherches sur les scintillations des sulfures de zinc aux rayons. *J. Chemie Phys.* **33**, 587–625 (1936).
12. Bernanose, A., Comte, M. & Vouaux, P. A New Method of Light Emission by Certain Organic Compounds. *J. Chim. Phys.* **50**, 64 (1953).
13. Shinar, J. Organic Light-Emitting Devices: A Survey. 309 (2004).

14. Thejo Kalyani, N. & Dhoble, S. J. Organic light emitting diodes: Energy saving lighting technology—A review. *Renew. Sustain. Energy Rev.* **16**, 2696–2723 (2012).
15. Geffroy, B., le Roy, P. & Prat, C. Organic light-emitting diode (OLED) technology: materials, devices and display technologies. *Polym. Int.* **55**, 572–582 (2006).
16. Gu, G., Garbuzov, D. Z., Burrows, P. E., Venkatesh, S. & Forrest, S. R. *Organic Light-Emitting Devices.* **22**, (1997).
17. Li, Z. R. & Meng, H. *Organic light-emitting materials and devices.* (2007).
18. Kumar, A., Srivastava, R., Tyagi, P., Mehta, D. S. & Kamalasanan, M. N. Improved light extraction efficiency with angle independent electroluminescence spectrum in nano-phosphor coated white organic light emitting diodes. *Synth. Met.* **161**, 1172–1176 (2011).
19. Sprengard, R. *et al.* OLED devices for signage applications: a review of recent advances and remaining challenges. in *Proceedings of ...* (eds. Kafafi, Z. H. & Lane, P. A.) **5519**, 173 (2004).
20. Adachi, C. *et al.* in *Organic Electronics Materials and Devices* (ed. Ogawa, S.) 43–73 (Springer Japan, 2015).
21. Reineke, S. *et al.* White organic light-emitting diodes with fluorescent tube efficiency. *Nature* **459**, 234–238 (2009).
22. Sasabe, H. & Kido, J. Development of high performance OLEDs for general lighting. *J. Mater. Chem. C* **1**, 1699 (2013).
23. Fernández, M., Casanova, E. & Alonso, I. Review of Display Technologies Focusing on Power Consumption. *Sustainability* **7**, 10854–10875 (2015).
24. Mizukami, M. *et al.* Flexible AM OLED panel driven by bottom-contact OTFTs. *IEEE Electron Device Lett.* **27**, 249–251 (2006).
25. Park, J.-S., Chae, H., Chung, H. K. & Lee, S. I. Thin film encapsulation for flexible AM-

- OLED: a review. *Semicond. Sci. Technol.* **26**, 34001 (2011).
26. Ju, S. *et al.* Fabrication of fully transparent nanowire transistors for transparent and flexible electronics. *Nat. Nanotechnol.* **2**, 378–384 (2007).
  27. Wong, W.-Y., He, Z., So, S.-K., Tong, K.-L. & Lin, Z. A Multifunctional Platinum-Based Triplet Emitter for OLED Applications. *Organometallics* **24**, 4079–4082 (2005).
  28. Guo, Z., Zhu, W. & Tian, H. Dicyanomethylene-4H-pyran chromophores for OLED emitters, logic gates and optical chemosensors. *Chem. Commun.* **48**, 6073 (2012).
  29. Huang, H. *et al.* Novel Deep Blue OLED Emitters with 1,3,5-Tri(anthracen-10-yl)benzene-Centered Starburst Oligofluorenes. *J. Phys. Chem. C* **115**, 4872–4878 (2011).
  30. Yang, C.-H., Tai, C.-C. & Sun, I.-W. Synthesis of a high-efficiency red phosphorescent emitter for organic light-emitting diodes. *J. Mater. Chem.* **14**, 947 (2004).
  31. Duggal, A. R., Shiang, J. J., Heller, C. M. & Foust, D. F. Organic light-emitting devices for illumination quality white light. *Appl. Phys. Lett.* **80**, 3470–3472 (2002).
  32. McKittrick, J. & Shea-Rohwer, L. E. Review: Down Conversion Materials for Solid-State Lighting. *J. Am. Ceram. Soc.* **97**, 1327–1352 (2014).
  33. Kim, C., Park, H.-A., Jang, H. W., Chung, W. J. & Kim, S. Y. All-in-one-type organic light-emitting diodes for color tuning using phosphor in glasses with Pb-free silicate powders. *Curr. Appl. Phys.* **14**, 1677–1681 (2014).
  34. Swanson, S. a. *et al.* Stable and Efficient Fluorescent Red and Green Dyes for External and Internal Conversion of Blue OLED Emission. *Chem. Mater.* **15**, 2305–2312 (2003).
  35. Li, W. X., Jones, R. A., Allen, S. C., Heikenfeld, J. C. & Steckl, A. J. Maximizing Alq<sub>3</sub> OLED Internal and External Efficiencies: Charge Balanced Device Structure and Color Conversion Outcoupling Lenses. *J. Disp. Technol.* **2**, 143–152 (2006).
  36. Krummacher, B., Klein, M., von Malm, N. & Winnacker, A. Optical analysis of down-

- conversion OLEDs. in *Proceedings of SPIE* (eds. Streubel, K. P. & Jeon, H.) **6910**, 691007 (2008).
37. Ji, W. *et al.* Top-emitting white organic light-emitting devices with down-conversion phosphors: Theory and experiment. *Opt. Express* **16**, 15489 (2008).
  38. Qi, Q., Wu, X., Hua, Y., Dong, M. & Yin, S. White organic light emitting devices with a color conversion layer. *Optoelectron. Lett.* **6**, 245–248 (2010).
  39. Bera, D. Optimization of down-conversion phosphor films for high efficiency white organic light-emitting diodes. *J. Photonics Energy* **1**, 11025 (2011).
  40. Gohri, V. *et al.* White top-emitting organic light-emitting diodes employing a heterostructure of down-conversion layers. *Org. Electron.* **12**, 2126–2130 (2011).
  41. Lee, J. *et al.* Down-Conversion White Organic Light-Emitting Diodes Using Microcavity Structure. *Adv. Energy Mater.* **1**, 174–178 (2011).
  42. Ahn, S. D. *et al.* White Organic Light-Emitting Devices Utilizing a Mixed Color-Conversion Phosphor Layer Consisting of CaAl<sub>12</sub>O<sub>19</sub>:Mn and Zn<sub>2</sub>SiO<sub>4</sub>:Mn. *J. Nanosci. Nanotechnol.* **11**, 1770–1773 (2011).
  43. Ho, Y.-H. *et al.* Improve efficiency of white organic light-emitting diodes by using nanosphere arrays in color conversion layers. *Opt. Express* **20**, 3005 (2012).
  44. Koh, T.-W., Cho, H., Yun, C. & Yoo, S. ITO-free down-conversion white organic light-emitting diodes with structured color conversion layers for enhanced optical efficiency and color rendering. *Org. Electron.* **13**, 3145–3153 (2012).
  45. Kwon, W. J. *et al.* Color Stability of White Organic Light Emitting Devices with a Color Conversion Layer Utilizing CdSe/ZnS Quantum Dots and Phosphors Dispersed in Polymethylmethacrylate. *J. Nanosci. Nanotechnol.* **13**, 4390–4393 (2013).
  46. Lee, J. *et al.* Transparent organic light-emitting diodes with different bi-directional emission colors using color-conversion capping layers. *J. Lumin.* **162**, 180–184 (2015).

47. Sabnis, R. W. *Handbook of Fluorescent Dyes and Probes. Handbook of Fluorescent Dyes and Probes* **25**, (John Wiley & Sons, Inc, 2015).
48. Berlman, I. B. in *Handbook of Fluorescence Spectra of Aromatic Molecules* 107–415 (Elsevier, 1971). doi:10.1016/B978-0-12-092656-5.50011-3
49. Steckel, J. S. *et al.* Quantum dots: The ultimate down-conversion material for LCD displays. *J. Soc. Inf. Disp.* **23**, 294–305 (2015).
50. Koole, R., Groeneveld, E. & Vanmaekelbergh, D. *Nanoparticles*. (Springer Berlin Heidelberg, 2014). doi:10.1007/978-3-662-44823-6
51. Babapour, a, Akhavan, O., Azimirad, R. & Moshfegh, a Z. Physical characteristics of heat-treated nano-silvers dispersed in sol–gel silica matrix. *Nanotechnology* **17**, 763–771 (2006).
52. Baidakova, M. & Vul', A. New prospects and frontiers of nanodiamond clusters. *J. Phys. D. Appl. Phys.* **40**, 6300–6311 (2007).
53. Baker, S. N. & Baker, G. A. Luminescent Carbon Nanodots: Emergent Nanolights. *Angew. Chemie Int. Ed.* **49**, 6726–6744 (2010).
54. Balasubramanian, G., Lazarev, A., Arumugam, S. R. & Duan, D.-W. Nitrogen-Vacancy color center in diamond—emerging nanoscale applications in bioimaging and biosensing. *Curr. Opin. Chem. Biol.* **20**, 69–77 (2014).
55. Chang, B.-M. *et al.* Highly Fluorescent Nanodiamonds Protein-Functionalized for Cell Labeling and Targeting. *Adv. Funct. Mater.* **23**, 5737–5745 (2013).
56. Miranda, T. J. *Surface Coatings. Springer* **1**, (Springer Netherlands, 1993).
57. Saunders, K. J. *Organic Polymer Chemistry*. (Springer Netherlands, 1973).
58. Gooch, J. W. *Analysis and Deformulation of Polymeric Materials: Paints, Plastics, Adhesives, and Inks. Order A Journal On The Theory Of Ordered Sets And Its Applications* (1997).

59. Paul, S. Water-borne acrylic emulsion paints. *Prog. Org. Coatings* **5**, 79–96 (1977).
60. Chiantore, O., Scalarone, D. & Learner, T. Characterization of Artists' Acrylic Emulsion Paints. *Int. J. Polym. Anal. Charact.* **8**, 67–82 (2003).
61. Polmanteer, K. E. Current Perspectives on Silicone Rubber Technology. *Rubber Chem. Technol.* **54**, 1051–1080 (1981).
62. Bergna, H. E. *Colloidal Silica: Fundamentals and Applications*. (CRC Press, 2006).
63. Glasser, L. S. D. The chemistry of silica. *Endeavour* **4**, 126 (1980).
64. Davis, M. E. & Lobo, R. F. Zeolite and molecular sieve synthesis. *Chem. Mater.* **4**, 756–768 (1992).
65. Breck, D. W. Crystalline molecular sieves. *J. Chem. Educ.* **41**, 678 (1964).
66. Gates, B. C. Supported Metal Clusters: Synthesis, Structure, and Catalysis. *Chem. Rev.* **95**, 511–522 (1995).
67. Sun, T. & Seff, K. Silver clusters and chemistry in zeolites. *Chem. Rev.* **94**, 857–870 (1994).
68. Kaduk, J. A. & Faber, J. Crystal Structure of Zeolite Y As a Function of Ion Exchange. *Rigaku J.* **12**, 14–34 (1995).
69. Chrétien, M. N., Shen, B., García, H., English, A. M. & Scaiano, J. C. Ship-in-a-Bottle Synthesis of Fluorescence-labeled Nanoparticles: Applications in Cellular Imaging. *Photochem. Photobiol.* **80**, 434 (2004).
70. Álvaro, M., Carbonell, E., Atienzar, P. & Garcia, H. A novel concept for photovoltaic cells: clusters of titanium dioxide encapsulated within zeolites as photoactive semiconductors. *ChemPhysChem* **7**, 1996–2002 (2006).
71. Liu, X., Iu, K.-K. & Kerry Thomas, J. Encapsulation of TiO<sub>2</sub> in zeolite Y. *Chem. Phys. Lett.* **195**, 163–168 (1992).
72. Ozin, G. A., Kuperman, A. & Stein, A. Advanced Zeolite, Materials Science. *Angew.*

- Chemie Int. Ed. English* **28**, 359–376 (1989).
73. Valeur, B. & Berberan-Santos, M. N. *Molecular Fluorescence: principles and applications*. (Wiley-VCH, 2013).
  74. Khan M. G., M., Yoshioka, T., Mottaleb, M. A. & Davide, V. *Photobiogeochemistry of Organic Matter. Environmental Science and Engineering* **3**, (Springer Berlin Heidelberg, 2013).
  75. Wight, P. in *Kirk-Othmer Encyclopedia of Chemical Technology* (John Wiley & Sons, Inc., 2000).
  76. Colles, M. *Dye Lasers. Optics* **1**, (Springer Berlin Heidelberg, 1973).
  77. Beija, M., Afonso, C. A. M. & Martinho, J. M. G. Synthesis and applications of Rhodamine derivatives as fluorescent probes. *Chem. Soc. Rev.* **38**, 2410 (2009).
  78. Diehl, H. & Markuszewski, R. Studies on fluorescein—VIIThe fluorescence of fluorescein as a function of pH. *Talanta* **36**, 416–418 (1989).
  79. Martin, M. M. & Lindqvist, L. The pH dependence of fluorescein fluorescence. *J. Lumin.* **10**, 381–390 (1975).
  80. Tietze, E. & Bayer, O. Die Sulfosäuren des Pyrens und ihre Abkömmlinge. *Justus Liebig's Ann. der Chemie* **540**, 189–210 (1939).
  81. von Bültzingslöwen, C. *et al.* Sol–gel based optical carbon dioxide sensor employing dual luminophore referencing for application in food packaging technology. *Analyst* **127**, 1478–1483 (2002).
  82. Berman, R., Hudson, P. R. W. & Martinez, M. Nitrogen in diamond: evidence from thermal conductivity. *J. Phys. C Solid State Phys.* **8**, L430–L434 (1975).
  83. Walker, J. Optical absorption and luminescence in diamond. *Reports Prog. Phys.* **1605**, (1979).
  84. Bundy, F. P., Hall, H. T., Strong, H. M. & Wentorf, R. H. Man-Made Diamonds. *Nature*

- 176**, 51–55 (1955).
85. Bovenkerk, H. P., Bundy, F. P., Hall, H. T., Strong, H. M. & Wentorf, R. H. Preparation of Diamond. *Nature* **184**, 1094–1098 (1959).
  86. Danilenko, V. V. On the history of the discovery of nanodiamond synthesis. *Phys. Solid State* **46**, 595–599 (2004).
  87. Dolmatov, V. Y. Detonation synthesis ultradispersed diamonds: properties and applications. *Russ. Chem. Rev.* **70**, 607–626 (2001).
  88. Mochalin, V. N., Shenderova, O., Ho, D. & Gogotsi, Y. The properties and applications of nanodiamonds. *Nat. Nanotechnol.* **7**, 11–23 (2011).
  89. Angus, J. C., Will, H. A. & Stanko, W. S. Growth of Diamond Seed Crystals by Vapor Deposition. *J. Appl. Phys.* **39**, 2915–2922 (1968).
  90. Yu, S.-J., Kang, M.-W., Chang, H.-C., Chen, K.-M. & Yu, Y.-C. Bright Fluorescent Nanodiamonds: No Photobleaching and Low Cytotoxicity. *J. Am. Chem. Soc.* **127**, 17604–17605 (2005).
  91. Fu, C.-C. *et al.* Characterization and application of single fluorescent nanodiamonds as cellular biomarkers. *Proc. Natl. Acad. Sci.* **104**, 727–732 (2007).
  92. Hegyi, A. & Yablonovitch, E. Nanodiamond molecular imaging with enhanced contrast and expanded field of view. *J. Biomed. Opt.* **19**, 11015 (2013).
  93. Hui, Y. Y., Cheng, C.-L. & Chang, H.-C. Nanodiamonds for optical bioimaging. *J. Phys. D. Appl. Phys.* **43**, 374021 (2010).
  94. Aharonovich, I. *et al.* Diamond-based single-photon emitters. *Reports Prog. Phys.* **74**, 76501 (2011).
  95. Zaitsev, A. M. *Optical Properties of Diamond. Physical Review B* (Springer Berlin Heidelberg, 2001). doi:10.1007/978-3-662-04548-0
  96. Wang, C., Kurtsiefer, C., Weinfurter, H. & Burchard, B. Single photon emission from

- SiV centres in diamond produced by ion implantation. *J. Phys. B At. Mol. Opt. Phys.* **39**, 37–41 (2006).
97. Collins, A. T. The characterisation of point defects in diamond by luminescence spectroscopy. *Diam. Relat. Mater.* **1**, 457–469 (1992).
98. Campbell, B. & Mainwood, A. Radiation Damage of Diamond by Electron and Gamma Irradiation. *Phys. status solidi* **181**, 99–107 (2000).
99. Poulin, F. & Bourgoïn, J. C. Threshold energy for atomic displacement in electron irradiated germanium. *Rev. Phys. Appliquée* **15**, 15–19 (1980).
100. Campbell, B., Choudhury, W., Mainwood, A., Newton, M. & Davies, G. Lattice damage caused by the irradiation of diamond. *Nucl. Instruments Methods Phys. Res. Sect. A Accel. Spectrometers, Detect. Assoc. Equip.* **476**, 680–685 (2002).
101. Koike, J., Parkin, D. M. & Mitchell, T. E. Displacement threshold energy for type IIa diamond. *Appl. Phys. Lett.* **60**, 1450–1452 (1992).
102. Goland, A. N. Atomic Displacements in Solids by Nuclear Radiation. *Annu. Rev. Nucl. Sci.* **12**, 243–284 (1962).
103. Kwon, J. & Motta, A. T. Gamma displacement cross-sections in various materials. *Ann. Nucl. Energy* **27**, 1627–1642 (2000).
104. Oen, O. S. & Holmes, D. K. Cross Sections for Atomic Displacements in Solids by Gamma Rays. *J. Appl. Phys.* **30**, 1289–1295 (1959).
105. Vinet, L. & Zhedanov, A. A ‘missing’ family of classical orthogonal polynomials. *Vasa* **1**, 1–136 (2010).
106. Lakowicz, J. R. *Principles of Fluorescence Spectroscopy. Principles of fluorescence spectroscopy, Springer, New York, USA, 3rd edn, 2006.* (Springer US, 2006). doi:10.1007/978-0-387-46312-4
107. Crosby, G. a. & Demas, J. N. Measurement of photoluminescence quantum yields.

- Review. *J. Phys. Chem.* **75**, 991–1024 (1971).
108. Porrès, L. *et al.* Absolute measurements of photoluminescence quantum yields of solutions using an integrating sphere. *J. Fluoresc.* **16**, 267–272 (2006).
109. Clearfield, A., Reibenspies, J. & Bruvanesh, N. *Principles and Applications of Powder Diffraction.* (2008).
110. Pecharsky, V. & Zavalij, P. *Fundamentals of Powder Diffraction and Structural Characterization of Materials.* (Springer US, 2009). doi:10.1007/978-0-387-09579-0
111. Egerton, R. F. *Physical Principles of Electron Microscopy. Physical Principles of Electron Microscopy: An Introduction to TEM, SEM, and AEM* (Springer US, 2005). doi:10.1007/b136495
112. Williams, D. B. & Carter, C. B. The Transmission Electron Microscope. *Transm. Electron Microsc.* 3–22 (2009).
113. Ozawa, L. *Cathodoluminescence and Photoluminescence. Cathodoluminescence and Photoluminescence* (CRC Press, 2007).
114. Redfern, J. P. & Coats, A. P. Thermogravimetric Analysis. *Nature* **173**, 1011–1012 (1954).
115. Resch-Genger, U., Grabolle, M., Cavaliere-Jaricot, S., Nitschke, R. & Nann, T. Quantum dots versus organic dyes as fluorescent labels. *Nat. Methods* **5**, 763–775 (2008).
116. Somasundaram, G. & Ramalingam, A. Gain studies of Rhodamine 6G dye doped polymer laser. *J. Photochem. Photobiol. A Chem.* **125**, 93–98 (1999).
117. Tagaya, a & Teramoto, S. Theoretical and experimental investigation of rhodamine B-doped polymer optical fiber amplifiers. *IEEE J.* **31**, 2215–2220 (1995).
118. Zhang, Y. & Yang, J. Design strategies for fluorescent biodegradable polymeric biomaterials. *J. Mater. Chem. B* **1**, 132–148 (2013).

119. Anedda, a. *et al.* Rhodamine 6G–SiO<sub>2</sub> hybrids: A photoluminescence study. *J. Non. Cryst. Solids* **351**, 1850–1854 (2005).
120. Cheng, Y.-J., Yang, S.-H. & Hsu, C.-S. Synthesis of Conjugated Polymers for Organic Solar Cell Applications. *Chem. Rev.* **109**, 5868–5923 (2009).
121. Monte, F. Del, Mackenzie, J. & Levy, D. Rhodamine fluorescent dimers adsorbed on the porous surface of silica gels. *Langmuir* 7377–7382 (2000).
122. Farha, O. K. *et al.* De novo synthesis of a metal–organic framework material featuring ultrahigh surface area and gas storage capacities. *Nat. Chem.* **2**, 944–948 (2010).
123. Cho, E.-B., Volkov, D. O. & Sokolov, I. Ultrabright Fluorescent Mesoporous Silica Nanoparticles. *Small* **6**, 2314–2319 (2010).
124. Schulz-Ekloff, G., Wöhrle, D., van Duffel, B. & Schoonheydt, R. a. Chromophores in porous silicas and minerals: preparation and optical properties. *Microporous Mesoporous Mater.* **51**, 91–138 (2002).
125. Lewkowicz, A., Synak, A., Grobelna, B., Kułak, L. & Bojarski, P. Spectroscopic properties of Rhodamine B entrapped in hybrid porous nanolayers at high dye concentration. *Chem. Phys.* **439**, 121–127 (2014).
126. Nicolet, O. *et al.* Quantum Yield Measurement of Fluorescent Zeolite Nanopigments. *Adv. Funct. Mater.* **19**, 1877–1883 (2009).
127. Zhao, X., Bagwe, R. P. & Tan, W. Development of Organic-Dye-Doped Silica Nanoparticles in a Reverse Microemulsion. *Adv. Mater.* **16**, 173–176 (2004).
128. Bonacchi, S. *et al.* Luminescent Silica Nanoparticles: Extending the Frontiers of Brightness. *Angew. Chemie Int. Ed.* **50**, 4056–4066 (2011).
129. Hungerford, G., Suhling, K. & Ferreira, J. a. Comparison of the fluorescence behaviour of rhodamine 6G in bulk and thin film tetraethylorthosilicate derived sol–gel matrices. *J. Photochem. Photobiol. A Chem.* **129**, 71–80 (1999).

130. Carbonaro, C. M. *et al.* Photostability of porous silica – rhodamine 6G hybrid samples. *Mater. Sci. Eng. C* **26**, 1038–1043 (2006).
131. Reisfeld, R. *et al.* Fluorescence intensification of Rhodamine 6G in Zirconia-Glymo glasses. *Opt. Mater. (Amst)*. **34**, 2021–2024 (2012).
132. Martínez Martínez, V., López Arbeloa, F., Bañuelos Prieto, J. & López Arbeloa, I. Characterization of Rhodamine 6G Aggregates Intercalated in Solid Thin Films of Laponite Clay. 2 Fluorescence Spectroscopy. *J. Phys. Chem. B* **109**, 7443–7450 (2005).
133. Scott, B. J., Wirnsberger, G. & Stucky, G. D. Mesoporous and Mesostructured Materials for Optical Applications. *Chem. Mater.* **13**, 3140–3150 (2001).
134. Pérez-Bueno, J. J. *et al.* Optical Processes in PMMA, SiO<sub>2</sub>, and Hybrid Organic–Inorganic Sol–Gel Films Colored with Rhodamine 6GDN. *J. Phys. Chem. B* **106**, 1550–1556 (2002).
135. Bojarski, P. Concentration quenching and depolarization of rhodamine 6G in the presence of fluorescent dimers in polyvinyl alcohol films. *Chem. Phys. Lett.* **278**, 225–232 (1997).
136. Lu, Y. & Penzkofer, A. Absorption behaviour of methanolic rhodamine 6G solutions at high concentration. *Chem. Phys.* **107**, 175–184 (1986).
137. Magde, D., Wong, R. & Seybold, P. G. Fluorescence Quantum Yields and Their Relation to Lifetimes of Rhodamine 6G and Fluorescein in Nine Solvents: Improved Absolute Standards for Quantum Yields. *Photochem. Photobiol.* **75**, 327–334 (2007).
138. Klonis, N., Clayton, A. H. A., Voss, E. W. & Sawyer, W. H. Spectral Properties of Fluorescein in Solvent-Water Mixtures: Applications as a Probe of Hydrogen Bonding Environments in Biological Systems. *Photochem. Photobiol.* **67**, 500–510 (1998).
139. Łukarska, M. *et al.* Synthesis and encapsulation of fluorescein in zeolite Y. *Microporous Mesoporous Mater.* **236**, 79–84 (2016).

140. Hashimoto, S., Moon, H. R. & Yoon, K. B. Optical microscopy study of zeolite-dye composite materials. *Microporous Mesoporous Mater.* **101**, 10–18 (2007).
141. Kataoka, T., Mozer, A. J., Tsukahara, Y., Yamauchi, T. & Wada, Y. Evidence for Encaging Luminescent Guest Molecules in the Inner Cages of Zeolite Host. *Bull. Chem. Soc. Jpn.* **80**, 2303–2312 (2007).
142. Yamaguchi, K., Tamura, Z. & Maeda, M. Disodium Fluorescein Octahydrate. *Acta Crystallogr. Sect. C Cryst. Struct. Commun.* **53**, 284–285 (1997).
143. Ćurković, L., Cerjan-Stefanović, Š. & Filipan, T. Metal ion exchange by natural and modified zeolites. *Water Res.* **31**, 1379–1382 (1997).
144. Rakoczy, R. A. & Traa, Y. Nanocrystalline zeolite A: synthesis, ion exchange and dealumination. *Microporous Mesoporous Mater.* **60**, 69–78 (2003).
145. Dsouza, R. N., Pischel, U. & Nau, W. M. Fluorescent Dyes and Their Supramolecular Host/Guest Complexes with Macrocycles in Aqueous Solution. *Chem. Rev.* **111**, 7941–7980 (2011).
146. Barnadas-Rodríguez, R. & Estelrich, J. Effect of salts on the excited state of pyranine as determined by steady-state fluorescence. *J. Photochem. Photobiol. A Chem.* **198**, 262–267 (2008).
147. Spry, D. B. & Fayer, M. D. Proton Transfer and Proton Concentrations in Protonated Nafion Fuel Cell Membranes. *J. Phys. Chem. B* **113**, 10210–10221 (2009).
148. Tremayne, M., Kariuki, B. M. & Harris, K. D. M. Structure Determination of a Complex Organic Solid from X-Ray Powder Diffraction Data by a Generalized Monte Carlo Method: The Crystal Structure of Red Fluorescein. *Angew. Chemie Int. Ed. English* **36**, 770–772 (1997).
149. Ferchiche, S., Valcheva-Traykova, M., Vaughan, D. E. W., Warzywoda, J. & Sacco, A. Synthesis of large single crystals of templated Y faujasite. *J. Cryst. Growth* **222**, 801–

- 805 (2001).
150. Krueger, A. New Carbon Materials: Biological Applications of Functionalized Nanodiamond Materials. *Chem. - A Eur. J.* **14**, 1382–1390 (2008).
  151. Iakoubovskii, K., Dannefaer, S. & Stesmans, A. Evidence for vacancy-interstitial pairs in Ib-type diamond. *Phys. Rev. B* **71**, 233201 (2005).
  152. Wotherspoon, a., Steeds, J. W., Catmull, B. & Butler, J. Photoluminescence and positron annihilation measurements of nitrogen doped CVD diamond. *Diam. Relat. Mater.* **12**, 652–657 (2003).
  153. Tizei, L. H. G. & Kociak, M. Spatially Resolved Quantum Nano-Optics of Single Photons Using an Electron Microscope. *Phys. Rev. Lett.* **110**, 153604 (2013).
  154. Tizei, L. H. G. & Kociak, M. Spectrally and spatially resolved cathodoluminescence of nanodiamonds: local variations of the NV 0 emission properties. *Nanotechnology* **23**, 175702 (2012).
  155. Collins, a T., Kamo, M. & Sato, Y. Optical centres related to nitrogen, vacancies and interstitials in polycrystalline diamond films grown by plasma-assisted chemical vapour deposition. *J. Phys. D. Appl. Phys.* **22**, 1402–1405 (1989).
  156. Collins, A. T. & Woods, G. S. Isotope shifts of nitrogen-related localised mode vibrations in diamond. *J. Phys. C Solid State Phys.* **20**, L797–L801 (1987).
  157. Gucsik, A. *et al.* Cathodoluminescence Microscopy and Spectroscopy of Micro- and Nanodiamonds: An Implication for Laboratory Astrophysics. *Microsc. Microanal.* **18**, 1285–1291 (2012).
  158. Steeds, J. W., Charles, S. J., Davies, J. & Griffin, I. Photoluminescence microscopy of TEM irradiated diamond. *Diam. Relat. Mater.* **9**, 397–403 (2000).
  159. Turner, S. *et al.* Determination of Size, Morphology, and Nitrogen Impurity Location in Treated Detonation Nanodiamond by Transmission Electron Microscopy. *Adv. Funct.*

*Mater.* **19**, 2116–2124 (2009).

160. Himics, L., Tóth, S., Veres, M., Balogh, Z. & Koós, M. Creation of deep blue light emitting nitrogen-vacancy center in nanosized diamond. *Appl. Phys. Lett.* **104**, 93101 (2014).